



Supplement of

Quantification of primary and secondary organic aerosol sources by combined factor analysis of extractive electrospray ionisation and aerosol mass spectrometer measurements (EESI-TOF and AMS)

Yandong Tong et al.

Correspondence to: Jay Gates Slowik (jay.slowik@psi.ch)

The copyright of individual parts of the supplement might differ from the article licence.

Text S1. Profile construction for factors to which the EESI-TOF is insensitive

In the Sect. 2.3.3, Eq. (11) proposes a generalised strategy for constructing reference factor profiles, that can be applied regardless of differences in the measurement units between instruments. Here we discuss the special case of a factor measured by the AMS but to which the EESI-TOF is insensitive, In this case, all variables in the EESI-TOF component of the profile are set to a low value based on an assumed $AS_k = 0.01 \text{ cps (ug m}^{-3}\text{)}^{-1}$, which is orders of magnitude lower than the AS_k of detectable factors. This approach is preferred to simply setting the EESI-TOF variables to zero, as this was empirically observed to create instabilities in the ME-2 solver. The full profile is then calculated as follows:

$$\frac{(f_{k,j})_{j=all,ref}}{1 \mu\text{g m}^{-3}} = \begin{cases} \frac{(f_{k,j})_j}{\sum_j (f_{k,j})_j}, & j \in AMS,ref \\ AS_k \cdot \frac{1/n_{EESI}}{\sum_j (f_{k,j})_j}, & j \in EESI,ref \end{cases} \quad (\text{S1})$$

Here n_{EESI} denotes the number of ions in the EESI-TOF dataset and as noted above we assume $AS_k = 0.01 \text{ cps (ug m}^{-3}\text{)}^{-1}$.

Text S2. Method validation and solution selection

Text S2.1 PMF analysis of single-instrument datasets

Single-instrument AMS and EESI-TOF PMF analysis was previously conducted and validated for both the summer and winter datasets (Qi et al., 2019; Stefenelli et al., 2019). To determine the F_{overlap}^* , the EESI-TOF-only PMF was re-run on only the period when both AMS and EESI-TOF were operating based on the same configuration and mass spectra in Stefenelli et al. (2019) and Qi et al. (2019). In addition, the AMS PMF analysis was re-run on the same period, but with the NO^+ and NO_2^+ ions included. As discussed above, these ions contain a large fraction of the AMS signal deriving from organonitrates. For EESI-TOF-only PMF analysis in both datasets, we used the same constraints as in the referenced studies, that is, cooking-influenced OA ($\text{COA}_{\text{S,E}}$) was constrained for the summer dataset and cigarette-smoking OA ($\text{CSOA}_{\text{W,E}}$) was constrained for the winter dataset. For AMS-only PMF analysis, the only constrained factor in the original studies was hydrocarbon-like OA during winter ($\text{HOA}_{\text{W,A}}$). We additionally constrained inorganic nitrate (InorgNit) in both the summer and winter datasets, by including 1) the $\text{CO}_2^+(\text{NO}^+ + \text{NO}_2^+)$ ratio, where the CO_2^+ signal was produced by reaction of nitrate on the vaporiser (Pieber et al., 2016), as well as minor organic contaminants, and 2) $\text{NO}^+/\text{NO}_2^+$ ratio. In summer, we took the mass spectrum acquired from the NH_4NO_3 calibration period during the campaign to calculate the ratios in 1) and 2), whereas in winter, we constructed the reference using the two ratios from the ambient measurements ($\text{NO}^+/\text{NO}_2^+=2.54$) during periods of high nitrate to organic ratios.

Fig. S1 and Fig. S2 show the results from these single-instrument AMS and EESI-TOF PMF analyses for summer and winter, respectively, as well as a comparison with the factor time series from the original studies. Because the results are very similar to the single-instrument studies, they are discussed only briefly here. The AMS-only PMF yielded five OA factors consistent with those of Stefenelli et al. (2019), namely hydrocarbon-like OA ($\text{HOA}_{\text{S,A}}$), cooking-influenced OA ($\text{COA}_{\text{S,A}}$), cigarette-smoking OA ($\text{CSOA}_{\text{S,A}}$), more oxygenated OA, MO- $\text{OOA}_{\text{S,A}}$, and less oxygenated OA (LO- $\text{OOA}_{\text{S,A}}$), and additionally a factor dominated by NO^+ and NO_2^+ in a ratio consistent with that of ammonium nitrate, denoted InorgNits_{S,A}. The main difference between these results and those reported by Stefenelli et al. (2019) is some exchange of signal between MO- $\text{OOA}_{\text{S,A}}$ and LO- $\text{OOA}_{\text{S,A}}$. In addition, the contribution from NO^+ and NO_2^+ is not solely apportioned to InorgNits_{S,A} but also to factors such as LO- $\text{OOA}_{\text{S,A}}$; however, this does not affect the identity and interpretation of these factors.

Similarly, for the winter dataset, seven factors were resolved consistent with the OA factors determined by Qi et al. (2019), namely $\text{HOA}_{\text{W,A}}$, $\text{COA}_{\text{W,A}}$, LO- $\text{OOA}_{\text{W,A}}$, MO- $\text{OOA}_{\text{W,A}}$, biomass burning OA ($\text{BBOA}_{\text{W,A}}$), event-specific OA ($\text{EVENT}_{\text{W,A}}$) and nitrogen-rich OA (Nitrogen $\text{OA}_{\text{W,A}}$), as well as a new factor consistent with InorgNit_{W,A}. Apart from being apportioned to InorgNit, NO^+ and NO_2^+ were also apportioned to non-InorgNit factors, indicating organonitrate content and/or imperfect attribution of inorganic NO^+ and NO_2^+ to these factors. Although the NO^+ and NO_2^+ contributions in some non-InorgNit factors are significant, causing some changes in the factor time series compared to those in Qi et al. (2019), the main features of the spectra from other OA components (i.e., ions other than NO^+ and NO_2^+) in these factors are retained.

As discussed in Sect. 2.3.4, scaled residual probability distributions, i.e., $P(e_{ij}/s_{ij})$, for the selected single-instrument solutions were calculated and are shown in Fig. S3. As discussed in Eq. (14), this yields values for F_{overlap}^* , which are calculated to be 0.769 in summer and 0.899 in winter.

Text S2.2 Construction of reference profiles

In the cPMF analysis, the factor profiles for HOA, COA, and InorgNit were constrained in both the summer and winter datasets, while CSOA was constrained in winter only. All reference profiles were constructed according to Eq. (11). Here we discuss the methods used to determine $(f_{k,j})_{j=AMS,ref}$, $(f_{k,j})_{j=EESI,ref}$, and the estimated AS_k used to synthesise the reference profile. Note that COA and CSOA are retrieved by both AMS and EESI-TOF, while HOA and InorgNit are not retrieved by the EESI-TOF in the configuration used for these campaigns. Specifically, no HOA-sensitive EESI-TOF extraction/ionisation scheme has yet been developed, while the measurable ion corresponding to inorganic nitrate, $[\text{NaNO}_3]\text{Na}^+$, has been detected in other studies (Tong et al., 2021) but falls below the m/z transmission window used here.

For summer $\text{COA}_{S,C}$, $(f_{k,j})_{j=AMS,ref}$ and $(f_{k,j})_{j=EESI,ref}$ were taken from the factor profiles for $\text{COA}_{S,A}$ and $\text{COA}_{S,E}$, respectively. AS_{COA_S} was calculated as the ratio of the mean signals of $\text{COA}_{S,E}$ (cps) to $\text{COA}_{S,A}$ ($\mu\text{g m}^{-3}$). For $\text{HOA}_{S,C}$, $(f_{k,j})_{j=AMS,ref}$ the HOA profile of Crippa et al. (2013b) was used, and for $\text{InorgNits}_{S,C}$, it was taken to be the mass spectrum acquired from the NH_4NO_3 calibration period during the campaign. The latter included the CO_2^+ signal produced by reaction of nitrate on the vaporiser (Pieber et al., 2016), here observed with a $\text{CO}_2^+/(\text{NO}^+ + \text{NO}_2^+)$ ratio of 0.0345, as well as minor organic contaminants. For both $\text{HOA}_{S,C}$ and $\text{InorgNits}_{S,C}$ all ions in $(f_{k,j})_{j=EESI,ref}$ were set at the same intensity, and AS_k was selected to be $0.01 \text{ cps } (\mu\text{g m}^{-3})^{-1}$.

The $\text{COA}_{W,C}$ reference profile was constructed using the identical method as for $\text{COA}_{S,C}$, with $\text{COA}_{W,A}$ and $\text{COA}_{W,E}$ as references. For $\text{CSOA}_{W,C}$, $(f_{k,j})_{j=EESI,ref}$ was taken to be the $\text{CSOA}_{W,E}$ profile. However, because the AMS did not resolve CSOA in the winter, we used the $\text{CSOA}_{S,A}$ profile for $(f_{k,j})_{j=AMS,ref}$ and estimated AS_{CSOA_W} as follows:

$$AS_{\text{CSOA}_W} = \frac{AS_{\text{COA}_W}}{AS_{\text{COA}_S}} \cdot AS_{\text{CSOA}_S} \quad (\text{S2})$$

where AS_{COA_S} , AS_{CSOA_S} , and AS_{COA_W} are the EESI-TOF apparent sensitivities of the corresponding factors, calculated assuming direct correspondence between the AMS and EESI-TOF factors sharing the same name (Stefenelli et al., 2019; Qi et al., 2019).

The reference profile for $\text{HOA}_{W,C}$ is identical to $\text{HOA}_{S,C}$, and constructed in the same way using the same profile as in the summer dataset. Unlike summer, the calibration mass spectrum of NH_4NO_3 was not used as the reference profile for $\text{InorgNit}_{W,C}$, because the $\text{NO}^+/\text{NO}_2^+$ in the NH_4NO_3 calibration period (1.58) was not consistent with that observed from ambient measurements (2.54) during periods of high nitrate to organic ratios, possibly indicating contributions from non- NH_4^+ cations. Instead, the InorgNit reference profile of AMS ions was constructed based on these features: 1) the $\text{NO}^+/\text{NO}_2^+$ ratio (2.54) from 26 Jan 2016 to 31 Jan 2016, when the instrument remained stable and the ratio of nitrate to OA was high, suggesting the contribution from organonitrates to NO^+ and NO_2^+ was low, 2) the $\text{CO}_2^+/(\text{NO}^+ + \text{NO}_2^+)$ ratio (0.00026) was assumed to be the same as during the calibration period in the Zurich winter campaign and 3) the ratio of intensity of each organic ion to CO_2^+ was kept the same as

during the calibration period in the Zurich winter campaign. Then $(f_{k,j})_{j=EESI,ref}$ and $AS_{InorgNit,w}$ were determined using the same method as in summer. All reference factor profiles constructed using this method are presented in Figure S5.

Text S2.3 Determination of C_{EESI} and number of solutions

Because F_{overlap} depends on both the weighting factor C_{EESI} and the number of factors p , an exploration of this two-dimensional space is required. As discussed earlier, for computational efficiency the a values of all constrained factor profiles were set to zero during this initial exploration. Anchor profiles for the constrained factors are shown in Fig. S5. For the summer dataset, in which both the AMS-only and EESI-TOF-only PMF analyses yielded 6 factors, the cPMF was explored from 5 to 12 factors with $\text{HOA}_{\text{S,C}}$, $\text{COA}_{\text{S,C}}$ and $\text{InorgNit}_{\text{S,C}}$ constrained. For the winter dataset, in which the AMS-only and EESI-TOF-only PMF analyses yielded 8 and 11 factors, respectively, the cPMF was explored from 7 to 15 factors with $\text{HOA}_{\text{W,C}}$, $\text{COA}_{\text{W,C}}$, $\text{CSOA}_{\text{W,C}}$ and $\text{InorgNit}_{\text{W,C}}$ constrained. For the summer dataset, C_{EESI} was explored from 0.1 to 100, and in winter from 0.001 to 50. The results of this exploration are shown in Fig. S6a and Fig. S6b, which present $|F_{\text{overlap}} - F_{\text{overlap}}^*|$ as a function of C_{EESI} and p for the summer and winter datasets, respectively.

The Zurich summer dataset displays the expected trend of $|F_{\text{overlap}} - F_{\text{overlap}}^*|$ with respect to C_{EESI} . Balanced solutions are found at intermediate values of C_{EESI} , with lower and higher values yielding solutions in which the AMS and EESI-TOF, respectively, are overweighted. Examples of scaled residual distributions for these three cases (AMS overweighted, balanced, and EESI-TOF overweighted) are shown in Fig. S4. The black box in Fig. S6a denotes a set of solutions satisfying the criterion in Eq. (14), which are selected for further inspection. The value of β is selected empirically to yield a practical number of solutions for manual inspection, with 0.02 chosen for summer and 0.005 for winter. Factor profiles and time series for solutions satisfying the β criterion, comprising solutions with 6 to 9 factors (black box in the figure) are shown in Figs S7 to Fig. S16. An 8-factor solution was chosen as the best representation of the data, and included $\text{HOA}_{\text{S,C}}$, $\text{COA}_{\text{S,C}}$, $\text{CSOA}_{\text{S,C}}$, $\text{InorgNit}_{\text{S,C}}$, two daytime SOAs ($\text{DaySOA1}_{\text{S,C}}$ and $\text{DaySOA2}_{\text{S,C}}$) and two nighttime SOAs ($\text{NightSOA1}_{\text{S,C}}$ and $\text{NightSOA2}_{\text{S,C}}$), discussed in detail in Sect. 3.1.1. Solutions with higher numbers of factors yielded uninterpretable splits in the SOA or CSOA factors. Among the balanced 8-factor solutions, we selected the solution with $C_{\text{EESI}} = 2$, which has the minimum value of $|F_{\text{overlap}} - F_{\text{overlap}}^*|$. This solution serves as the base case for further analysis. The other 8-factor solutions exhibit time series and profiles that are similar to the selected solutions. Therefore, we simply select the 8-factor solution with minimum $|F_{\text{overlap}} - F_{\text{overlap}}^*|$.

For the winter dataset, solutions with 12 or more factors are similar to the summer in which balanced solutions (i.e., $\beta < 0.005$) are clustered narrowly around a single value of C_{EESI} (in this case 0.05), as shown in the right black box in Fig. S6b. However, in addition, solutions with 10 to 11 factors show balanced solutions over a relatively broad range, $C_{\text{EESI}} = 0.001$ to 0.01, as shown in the left black box in Fig. S6b. This complex behaviour highlights the importance of fully exploring the two-dimensional space. Solutions from the left black box (e.g., a 10-factor solution with $C_{\text{EESI}} = 0.01$, and 11-factor solutions with $C_{\text{EESI}} = 0.001$, 0.005, and 0.01 which are shown in Fig. S17 to Fig S20) exhibited mixed factors, in which biomass burning was not clearly separable from other sources. In contrast, the 12-factor solution (see Fig. S21) and 13-factor solution (see Fig. S22) in the narrow band successfully resolves these factors. The 12-factor and 13-factor solutions differ in that the 13-factor solution includes uninterpretable splitting of biomass-burning-related factors. Similarly, higher-order solutions also result in uninterpretable factor splitting. Therefore, the 12-factor solution with C_{EESI} of 0.05 is selected as the best representation of the combined dataset.

Text S2.4 Acceptance criteria and factor-specific a value boundaries

As discussed in Sect. 2.3.5, the combined bootstrap/ a -value randomisation analysis requires (1) a set of criteria for solution acceptance/rejection and (2) factor-specific boundaries for randomised a value selection to maintain computational efficiency. The final set of acceptance criteria and a -value boundaries are presented in Table 2. Here we discuss their selection, which is determined synergistically by consideration of 1) unique correlations of factor time series with the base case (see Sect. 2.3.4), 2) factor-based acceptance criteria, which are here based on selected key mass spectral features (see Sect. 3.1.1 and Sect. 3.1.2 for a complete discussion of factor characteristics). Both (1) and (2) are evaluated as a function of changing a values within the multi-2D scanning algorithm (see Sect. 2.3.5). For assessing the solution/base case correlations, we utilise a confidence level of 0, meaning that the only requirement is the ability to construct a correlation matrix with the values on the diagonal being higher than any vertical or horizontal transect. This accepts the largest possible number of solutions while requiring an unambiguous relationship between base case and bootstrapped factors. Recall that the multi-2D algorithm consists of two-dimensional a -value scans in which the a values of constrained factors are scanned from 0 to 1 with a step size of 0.1, the a values of other constrained factors are set to zero, and the remaining factors are left free.

Here we describe the general steps to determine acceptance criteria and a value boundaries. A factor-based acceptance criterion is defined by the combination of a diagnostic quantity relating to one or more factors and a corresponding acceptance/rejection threshold (θ). Solutions that fulfil all criteria simultaneously are classified as accepted solutions. We calculate the acceptance probability as a function of a value for a given factor (this is calculated independently for each factor). For a given factor, the acceptance probability is defined as the ratio of the number of accepted solutions to the total number of solutions, for which the factor has the selected a value and the a value of at most one other constrained factor is non-zero (that is, we consider only multi-2D runs where the factor in question is being scanned against a single other factor, while discarding runs for which the factor in question is fixed at $a=0$ while two other factors are scanned; this is relevant only for analyses with at least 3 constrained factors). The acceptance probability is not only a function of the a value of the target constraint but also a function of the threshold θ . When an appropriate value of θ cannot be defined *a priori*, it is selected via sensitivity tests. The final selection of the threshold θ and a value ranges is a compromise between (1) maintaining a reasonably high acceptance probability, thereby providing sufficient statistics without an excessive number of bootstrap runs; and (2) ensuring a sufficiently broad exploration of the solution space to encompass most environmentally reasonable solutions and thus accurately assess errors. Therefore, we determine the threshold θ and a value upper limit for each constrained factor at which a steep drop-off from high to low probability of acceptance occurs.

For the summer dataset, three factors are constrained: HOA_{S,C}, COA_{S,C}, and InorgNit_{S,C}, yielding three pairs ($C(3,2) = 3$) of two-dimensional a -value scans. Two factor-based diagnostic quantities with acceptance/rejection thresholds (θ) were selected: 1) the ratio of C₃H₃O⁺ to C₃H₅O⁺ for COA_{S,C} should be higher than the threshold $\theta_{\text{COA}_{S,C}}$ (Mohr et al., 2012), and 2) the ratio of CO₂⁺/(NO⁺+NO₂⁺) for InorgNit_{S,C} should not be higher than $\theta_{\text{InorgNit}_{S,C}}$, because the CO₂⁺ signal in InorgNit_{S,C} should not greatly exceed the CO₂⁺ signal produced by reaction of nitrate on the vaporiser (Pieber et al., 2016); excessively high values would indicate mixing with OA. To explore the sensitivity of the acceptance probability to the threshold θ , we varied $\theta_{\text{COA}_{S,C}}$ from 4.5 to 5.1 with a step of 0.1 (note that 5.0 is the ratio of C₃H₃O⁺ / C₃H₅O⁺ in the reference profile) and $\theta_{\text{InorgNit}_{S,C}}$ from 0.034 to 0.040 with a step of 0.01, (note that 0.0345 is the ratio of CO₂⁺/(NO⁺+NO₂⁺) in the reference profile).

The acceptance probability as a function of a value and the various thresholds (θ 's) for COA_{S,C}, InorgNits_{S,C}, and HOA_{S,C} are shown in Fig. S25. Vertical dashed lines denote the final selected a values, while the thicker traces denote the selected θ values (both of which are also given in Table 2). For $\theta_{\text{COA}_{S,C}} > 5.0$, very few runs are accepted. Within the range $4.5 \leq \theta_{\text{COA}_{S,C}} \leq 5.0$, $\theta_{\text{COA}_{S,C}}$ does not affect the relationship between acceptance probability and a value for InorgNits_{S,C} (Fig. S25b), but has a considerable effect for COA_{S,C} and HOA_{S,C}, with a decreasing $\theta_{\text{COA}_{S,C}}$ leading to the acceptance probability remaining high at larger a values. Visual inspection of the solutions suggests that this is due to increased mixing, mostly between COA_{S,C} and HOA_{S,C}. Therefore, we select a value of $\theta_{\text{COA}_{S,C}} = 5.0$, corresponding to the C₃H₃O₃⁺/C₃H₅O₃⁺ in the factor profile. For $\theta_{\text{InorgNits}_{S,C}}$, values smaller than 0.0345 (i.e., reference profile) result in a very low acceptance probability, whereas choice of $\theta_{\text{InorgNits}_{S,C}}$ results in similar acceptance probabilities as a function of a value. Therefore, we select 0.0345, as the acceptance probability for $\theta_{\text{InorgNits}_{S,C}}$ of 0.035 is not substantially different from 0.0345. Having selected these θ values, we set a value limits at the point where an incremental increase/decrease in a yields a large change in acceptance probability (i.e. transition from high probability to low probability). For the current dataset, constrained factors, and selected θ 's, there is no such transition at low a values, and we therefore select only an upper limit for the a values. For COA_{S,C}, there is a clear decrease for both criteria between $a_{\text{COA}_{S,C}} = 0.1$ and $a_{\text{COA}_{S,C}} = 0.2$, and we therefore set the a value boundaries as $0 \leq a_{\text{COA}_{S,C}} \leq 0.2$. InorgNits_{S,C} maintains an acceptance probability of ~50 % for $a_{\text{InorgNits}_{S,C}} \leq 0.4$, before decreasing to <20 % at $a_{\text{InorgNits}_{S,C}} = 0.5$ and ~0 for $a_{\text{InorgNits}_{S,C}} > 0.5$; therefore the range $0 \leq a_{\text{InorgNits}_{S,C}} \leq 0.5$ is chosen. Finally, for HOA_{S,C}, the acceptance probability decreases from ~55 % at $a_{\text{HOA}_{S,C}} \leq 0.1$ to ~35 % at $a_{\text{HOA}_{S,C}} \leq 0.2$, so the a value range for HOA_{S,C} is selected as $0 \leq a_{\text{HOA}_{S,C}} \leq 0.2$. The a values selected for constraints for the further summer bootstrap analysis are summarised in Table 2. However, we also see that for HOA_{S,C} the acceptance probability increases and stays high again for the a value of 0.4 to 0.8. Therefore, we made an additional bootstrap analysis to explore the result when the a value of HOA_{S,C} randomises from 0 to 0.8, as discussed in the last paragraph in this section.

In the winter dataset, four factors (HOA_{w,c}, COA_{w,c}, CSOA_{w,c}, and InorgNit_{w,c}) are constrained, yielding six pairs ($C(4,2) = 6$) of two-dimensional a -value scans. Compared to the summer dataset, the unique base case/bootstrap correlation requirement yields a much smaller number of accepted solutions, probably due to the more complicated aerosol sources and/or evolution conditions in winter (e.g., multiple biomass burning-related factors). Three factor-based diagnostic quantities were selected: 1) the fraction of the nicotine signal ($[\text{C}_{10}\text{H}_{14}\text{N}_2]\text{H}^+$) apportioned to CSOA_{w,c}, 2) the relative intensity of the AMS primary biomass burning tracer C₂H₄O₂⁺ (Alfarra et al., 2007; Cubison and Jimenez, 2015) in the factor profiles (AMS part) of less-aged biomass burning (LABB_{w,c}) vs. more-aged biomass burning (MABB_{w,c}), and 3) the relative intensity of the EESI-TOF primary biomass burning tracer levoglucosan ($[\text{C}_6\text{H}_{10}\text{O}_5]\text{Na}^+$) (Lopez-Hilfiker et al., 2019; Qi et al., 2019; Stefenelli et al., 2019) in the factor profiles of LABB_{w,c} vs. MABB_{w,c}. For 2) and 3), we require that the contribution of the primary tracer is higher for the profile of LABB_{w,c} than MABB_{w,c} as follows:

$$\frac{\text{LABB}_{w,c,\text{ion}} - \text{MABB}_{w,c,\text{ion}}}{(\text{LABB}_{w,c,\text{ion}} + \text{MABB}_{w,c,\text{ion}})/2} > \theta_{\text{ion}} \quad (\text{S3})$$

where LABB_{w,c,ion} and MABB_{w,c,ion} are the "ion" intensity in the LABB_{w,c} and MABB_{w,c} factor profiles, and "ion" in Eq. (S3) denotes either AMS C₂H₄O₂⁺ (criterion 2) or EESI-TOF levoglucosan ($[\text{C}_6\text{H}_{10}\text{O}_5]\text{Na}^+$) (criterion 3), and θ_{ion} denotes the acceptance threshold.

For criterion 1), we select the threshold $\theta_{\text{CSOA}_{\text{w,c}}}$ from investigation of Fig. S26, which shows the frequency distribution of the fraction of total nicotine signal apportioned to $\text{CSOA}_{\text{w,c}}$, derived from the multi-2D scans used to assess criteria 2 and 3 (see below). The figure shows that for nearly all runs, the fraction of total nicotine mass apportioned to this factor is higher than 0.96. The exceptions are clear outliers, and we therefore select $\theta_{\text{CSOA}_{\text{w,c}}} = 0.96$ which was therefore chosen as the criterion threshold.

The acceptance probability as a function of a value is shown in Fig. S27 for $\text{HOA}_{\text{w,c}}$, $\text{COA}_{\text{w,c}}$, $\text{InorgNit}_{\text{w,c}}$, and $\text{CSOA}_{\text{w,c}}$. For criteria 2 and 3, sensitivity tests are conducted using $\theta_{\text{C}_2\text{H}_4\text{O}_2^+}$ and $\theta_{\text{levoglucosan}}$, which were varied from 0 to 1 with a step of 0.1, and the final selected values are shown as a thicker line. The acceptance probability decreases to near-zero for $\theta_{\text{C}_2\text{H}_4\text{O}_2^+} \geq 0.1$ and $\theta_{\text{levoglucosan}} \geq 0.2$. We select 0 for both thresholds, which is the most permissive value, requiring only that $\text{MABB}_{\text{w,c}}$ appear more aged than $\text{LABB}_{\text{w,c}}$ (i.e., reduced contribution from POA tracers). Similar to the summer dataset, there is no major decrease in acceptance probability at low a values, and we therefore impose only an upper limit. For $\text{HOA}_{\text{w,c}}$, we set the upper a value boundary at 0.9, due to the large decrease in acceptance probability at $a_{\text{HOA}_{\text{w,c}}} = 1.0$. However, for the other constrained factors, the acceptance probability decreases steadily without a steep drop-off. We target an acceptance probability of ~ 0.4 (by considering the unmixing status) as a subjective compromise between exploration and computational efficiency, and select as an upper boundary the largest a value that achieves this. This results in upper a value limits of 0.3 for $\text{COA}_{\text{w,c}}$, and 0.5 for $\text{InorgNit}_{\text{w,c}}$. For $\text{CSOA}_{\text{w,c}}$, the high acceptance probability is kept high from the a value of 0 to 0.6. Therefore, we chose the a value range of $\text{CSOA}_{\text{w,c}}$ to be 0 to 0.6. However, it is also observed that the acceptance probability for this factor dips at 0.7 and stays high again at a values of 0.8 and 0.9, so we made an additional bootstrap analysis with the a value range for $\text{CSOA}_{\text{w,c}}$ of 0 to 0.9 to explore the influence of the a value of this factor on overall result, as discussed in the following paragraph. The a values selected for the four constraints for the further winter bootstrap analysis are summarised in Table 2.

After a -value selection, 1000 bootstrap runs were performed for summer and winter, respectively, and in each bootstrap run, an a value was randomly selected for each constrained factor, with a step size of 0.05 for summer and 0.1 for winter within the corresponding range. The criteria for accepted solutions in the bootstrap analysis are exactly the same as the criteria and θ in Text S1.4 and are given in Table 2. As noted above, accepted solutions must simultaneously satisfy all criteria including the time-series-based mixing status exploration and mass-spectral-based criteria. Note that we also did an additional bootstrap analysis for summer and winter, respectively, as mentioned in previous paragraphs, to explore the bootstrap result with larger a value range of $\text{HOA}_{\text{s,c}}$ and $\text{CSOA}_{\text{w,c}}$. In the additional bootstrap analysis for summer, a value range for $\text{HOA}_{\text{s,c}}$ was set to be $0 \leq a_{\text{HOA}_{\text{s,c}}} \leq 0.8$, while the a value ranges of the other two constraints were kept the same as indicated in Table 2. Likewise, we only changed the a value range of $\text{CSOA}_{\text{w,c}}$ to be $0 \leq a_{\text{CSOA}_{\text{w,c}}} \leq 0.9$, while keeping the a value ranges of the other three constraints the same as in Table 2. Since the results of these additional bootstrap analysis are not qualitatively different from the bootstrap analysis with a value ranges in Table 2, we only present the bootstrap results with a value ranges in Table 2.

Text S3 Organonitrate content estimation

In Sect. 3.1, we present final results from the cPMF analysis of the summer and winter campaigns. The final solutions are reported as the average of all accepted bootstrap/*a*-value randomisation runs (764 for summer, 308 for winter), with uncertainties corresponding to the standard deviation.

A complication in this analysis is that the NO^+ and NO_2^+ signal can result from either organic or inorganic nitrate. Ideally, all inorganic NO^+ and NO_2^+ would apportion to the $\text{InorgNits}_{\text{S,C}}$ and $\text{InorgNit}_{\text{W,C}}$ factors, however inspection of the solutions reveals that this is not the case, as discussed in the factor presentations (Sect. 3.1.1 and Sect. 3.1.2). Therefore, we estimate the organic and inorganic contributions to these ions by the method of Kiendler-Scharr et al. (2016), as follows:

$$\text{frac}_{\text{ON},k} = \frac{(1 + R_{\text{ON}})(R_k - R_{\text{cal}})}{(1 + R_k)(R_{\text{ON}} - R_{\text{cal}})} \quad (\text{S4})$$

Here we apply this analysis on a factor-by-factor basis, where $\text{frac}_{\text{ON},k}$, defined in Eq. (S4), represents the fraction of ON apportioned to the *k*th factor, and R_k denotes the intensity ratio of NO_2^+ to NO^+ in the factor profile. R_{cal} is the reference $\text{NO}_2^+/\text{NO}^+$ ratio for inorganic nitrate, taken as that of the $\text{InorgNit}_{\text{W,C}}$ and $\text{InorgNits}_{\text{S,C}}$ reference profiles for their respective datasets. R_{ON} , defined in Eq. (S5b), is the intensity ratio of NO_2^+ to NO^+ for organonitrate, which ranges from 0.08 to 0.20 (Fry et al., 2009; Rollins et al., 2009; Bruns et al., 2010; Fry et al., 2011; Boyd et al., 2015).

$$\text{frac}_{\text{ON},k} = \frac{(f_{\text{ON},k,\text{NO}^+} + f_{\text{ON},k,\text{NO}_2^+})}{(f_{k,\text{NO}^+} + f_{k,\text{NO}_2^+})} \quad (\text{S5a})$$

$$R_{\text{ON}} = \frac{f_{\text{ON},k,\text{NO}_2^+}}{f_{\text{ON},k,\text{NO}^+}} \quad (\text{S5b})$$

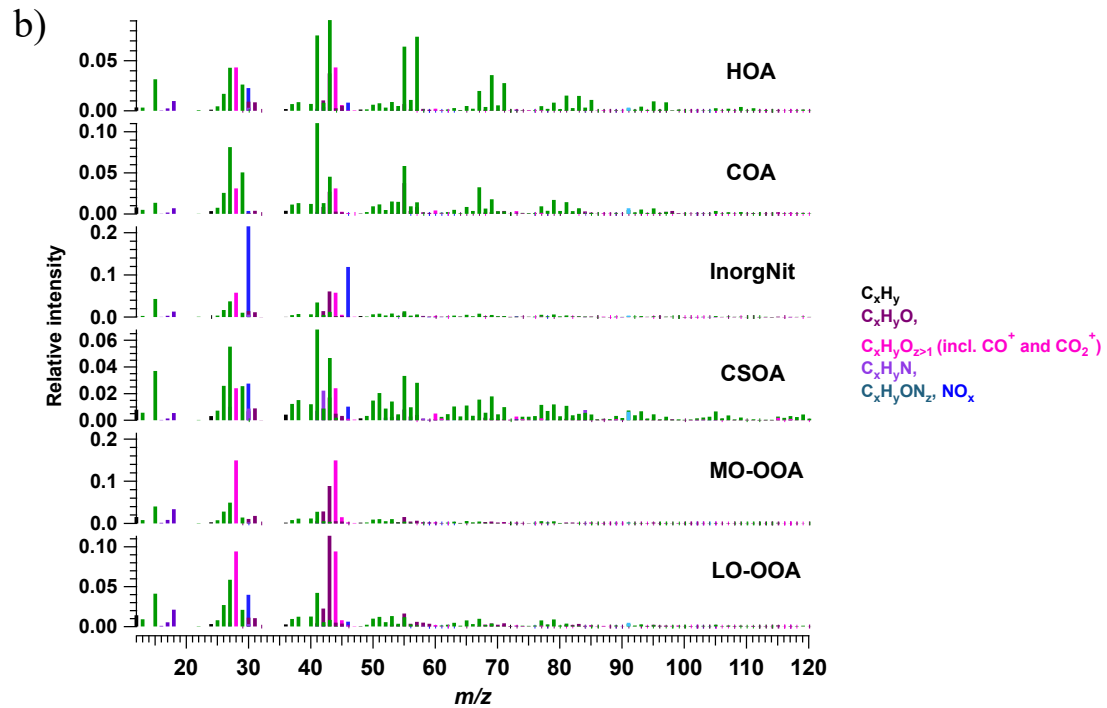
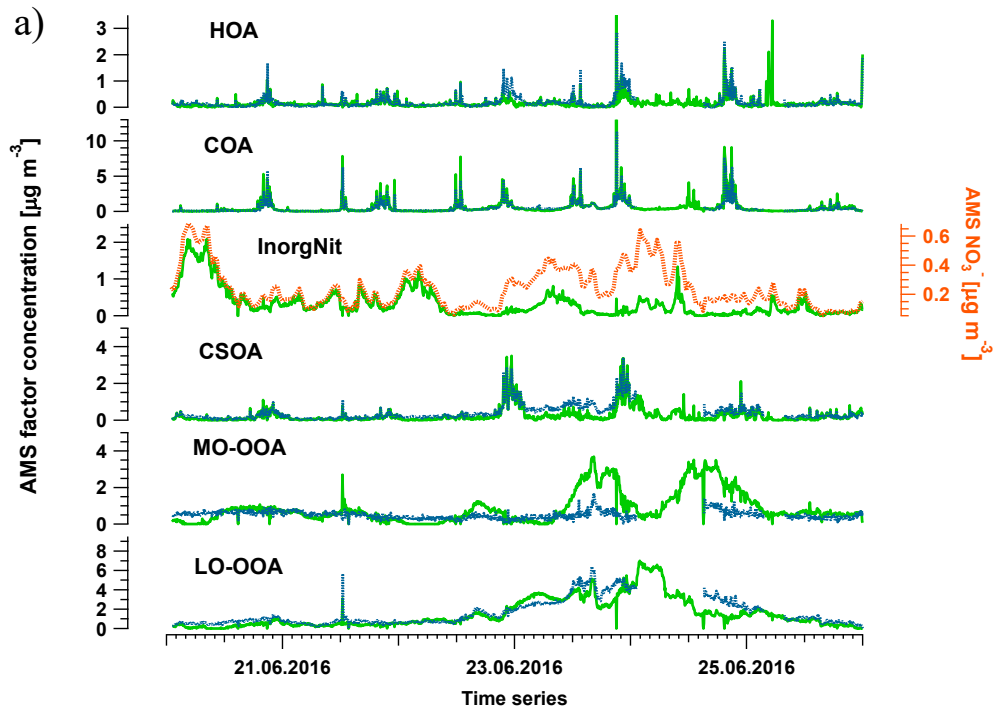
Here f_{k,NO^+} and f_{k,NO_2^+} denote the total NO^+ and NO_2^+ signal, respectively in the *k*th factor profile, while $f_{\text{ON},k,\text{NO}^+}$ and $f_{\text{ON},k,\text{NO}_2^+}$ denote the organonitrate contribution to these ions. Because f_{k,NO^+} and f_{k,NO_2^+} are directly available from the factor profile, $\text{frac}_{\text{ON},k}$ is independently calculated via Eq. (S4), and R_{ON} is assumed, Eqs. (S5a) and (S5b) constitute a system of 2 equations with 2 unknowns, which can be solved algebraically for $f_{\text{ON},k,\text{NO}^+}$ and $f_{\text{ON},k,\text{NO}_2^+}$, yielding:

$$f_{\text{ON},k,\text{NO}^+} = \frac{(R_k - R_{\text{cal}})(f_{k,\text{NO}^+} + f_{k,\text{NO}_2^+})}{(1 + R_k)(R_{\text{ON}} - R_{\text{cal}})} \quad (\text{S6a})$$

$$f_{\text{ON},k,\text{NO}_2^+} = \frac{(R_k - R_{\text{cal}})(f_{k,\text{NO}^+} + f_{k,\text{NO}_2^+})}{(1 + R_k)(R_{\text{ON}} - R_{\text{cal}})} \cdot R_{\text{ON}} \quad (\text{S6b})$$

These calculations are important not only for profile interpretation, but also for quantitative apportionment of OA. Specifically, as noted earlier, calculations of the OA contribution to the factor time series, $(g_{i,k})_{\text{AMS}}$, and the EESI-TOF sensitivity to a given factor, AS_k , should consider only the organic contribution to NO^+ and NO_2^+ . In this study, we estimated the contribution from organonitrates for all factors in summer and winter assuming the midpoint of the R_{ON} range ($R_{\text{ON}} = 0.14$). Organonitrate contributions ($\text{frac}_{\text{ON},k}$) to the total nitrate signal for each factor and the corresponding OA fraction $\sum_j (f_{k,j})_{\text{AMS}}$ are shown in Table S1. We also include the same calculations performed assuming an R_{ON} of 0.08 or 0.20, which as discussed above constitute the lower and upper estimates from previous studies. For $R_{\text{ON}} = 0.14$, the $\text{frac}_{\text{ON},k}$ for all SOAs in summer are higher than 75 %, and for winter, this fraction $\text{frac}_{\text{ON},k}$ varies by factor from 0 to 100 %, with four factors having $\text{frac}_{\text{ON},k} = 100$ % ($\text{SOA1}_{\text{W,C}}$, $\text{MABB}_{\text{W,C}}$, $\text{LABB}_{\text{W,C}}$ and $\text{NitOA1}_{\text{W,C}}$), suggesting the NO^+ and NO_2^+ signals are strongly influenced by ON. If $R_{\text{ON}} = 0.08$ is assumed, the estimated $\text{frac}_{\text{ON},k}$ decreases by ~12 % for

the summer SOA factors and by 10 % to 20 % for the winter SOA factors, whereas assuming $R_{\text{ON}} = 0.20$ increases $\text{frac}_{\text{ON},k}$ by ~15 % in the summer and 16% in the winter OA factors. The effect of this assumption on the factor OA concentration and thus AS_k is much smaller, with all factors below ± 2 % except for one wintertime SOA factor ($\text{SOA1}_{\text{w,c}}$, ± 6 %).



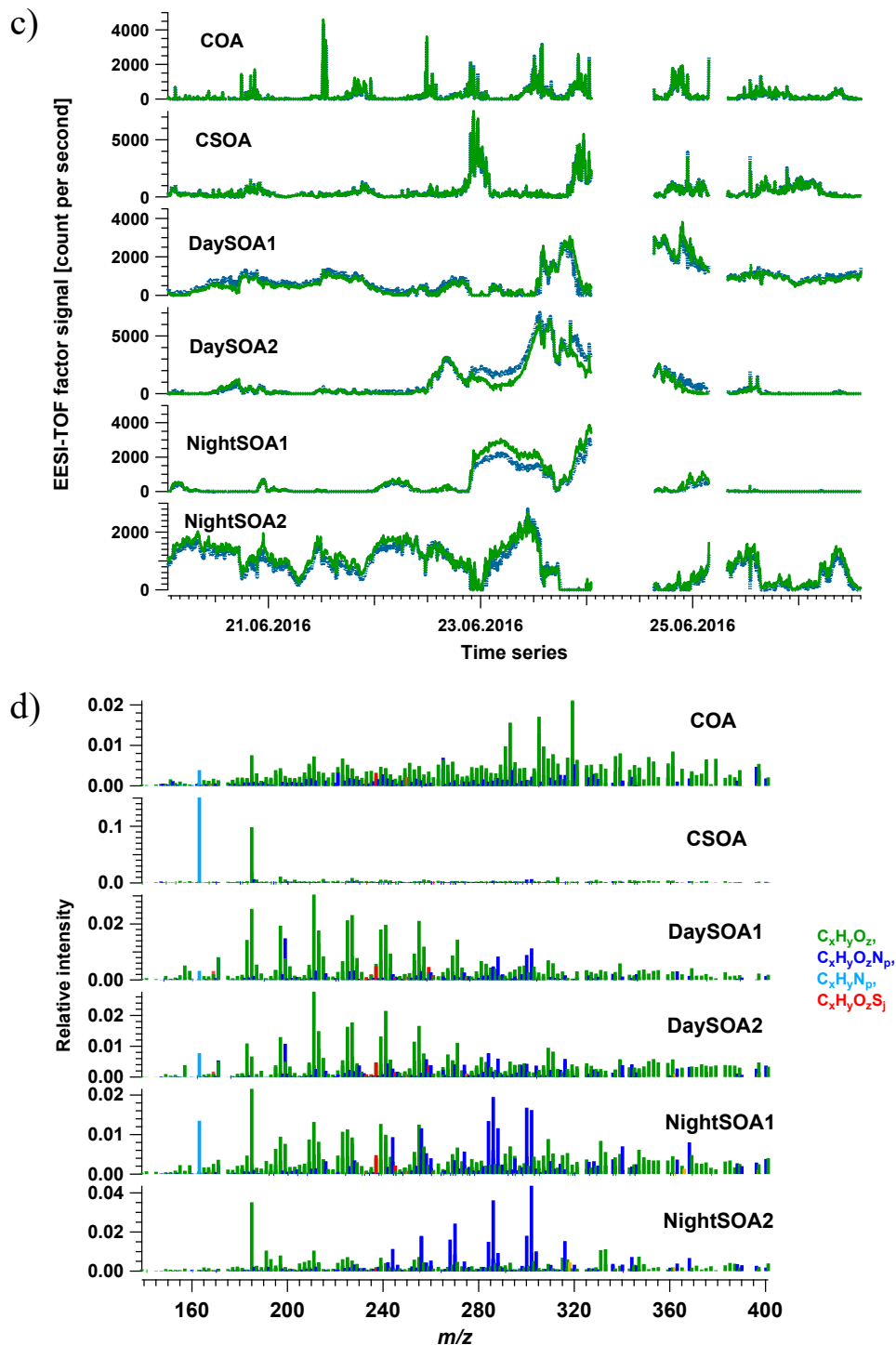
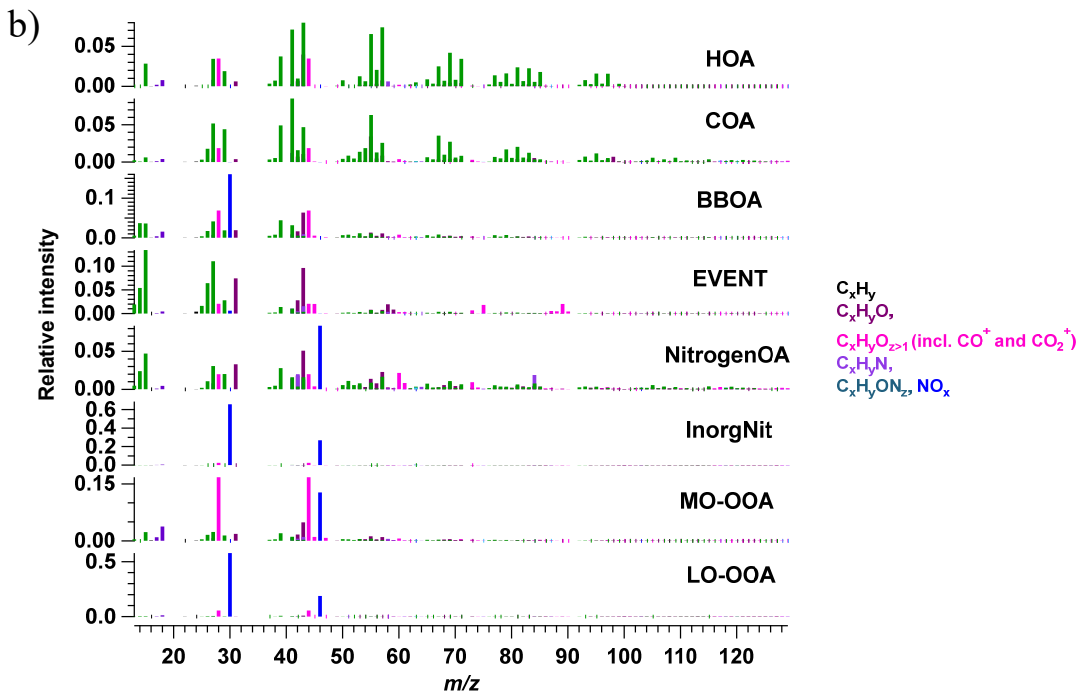
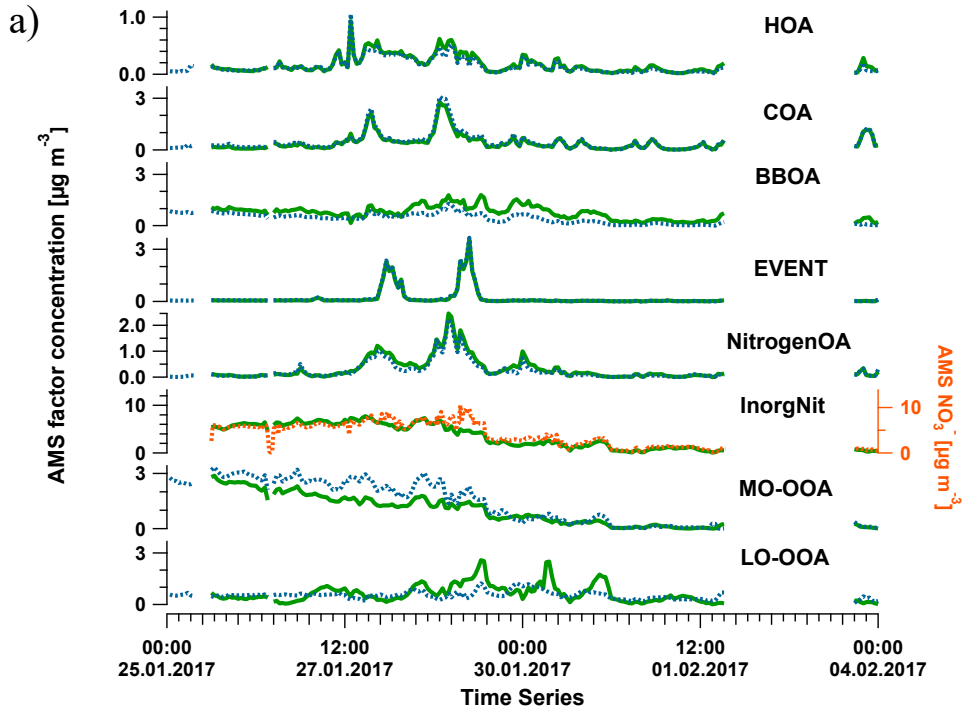


Figure S1. The time series and factor profile of AMS-only PMF solution is shown in a) and b), and the time series and factor profile of EESI-TOF-only PMF solution is shown in c) and d), respectively. Green lines are the factor time series of AMS-only and EESI-TOF-only PMF solution in this study, whereas the blue lines are the factor time series of solution in Stefenelli et al. (2019). Note, in addition to the original AMS PMF solution from Stefenelli et al. (2019), the AMS-only PMF solution from this study yields an inorganic nitrate factor (InorgNit), because NO^+ and NO_2^+ are included in the input matrix.



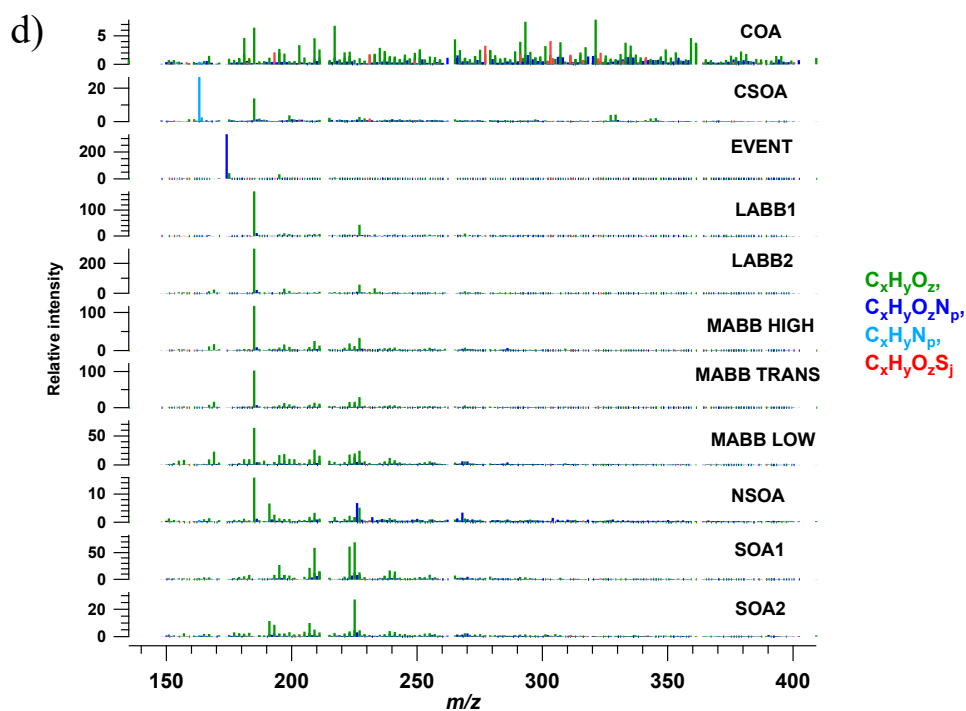
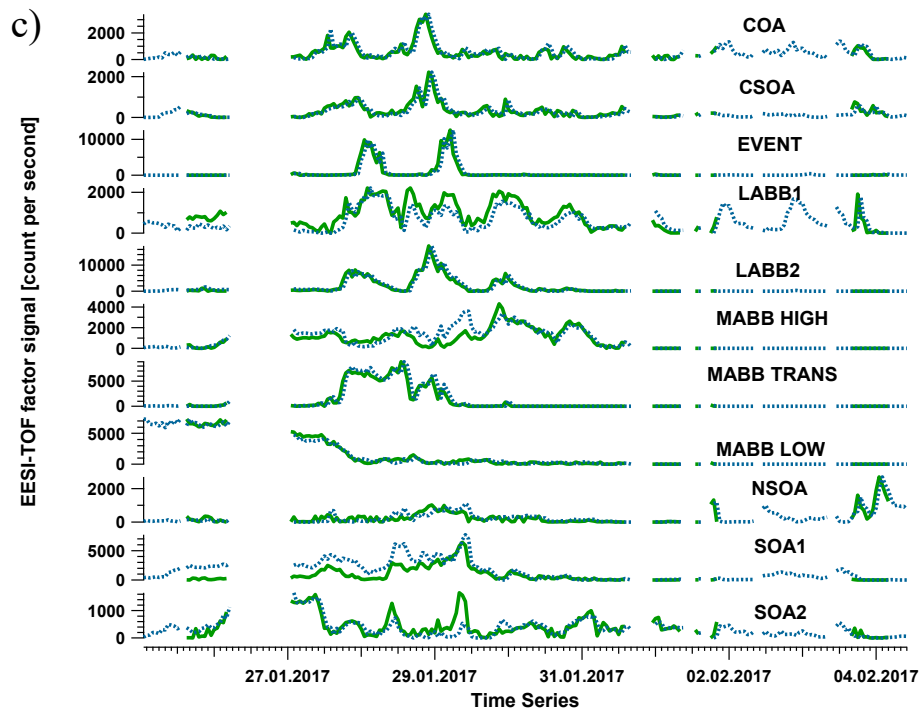


Figure S2. The time series and factor profile of AMS-only PMF solution is shown in a) and b), and the time series and factor profile of EESI-TOF-only PMF solution is shown in c) and d), respectively. Green lines are the factor time series of AMS-only and EESI-TOF-only PMF solution in this study, whereas the blue lines are the factor time series of solution in Qi et al. (2019). Note, in addition to the original AMS PMF solution from Qi et al. (2019), the AMS-only PMF solution in this study yields a inorganic nitrate factor (InorgNit), because NO^+ and NO_2^+ are included in the input matrix.

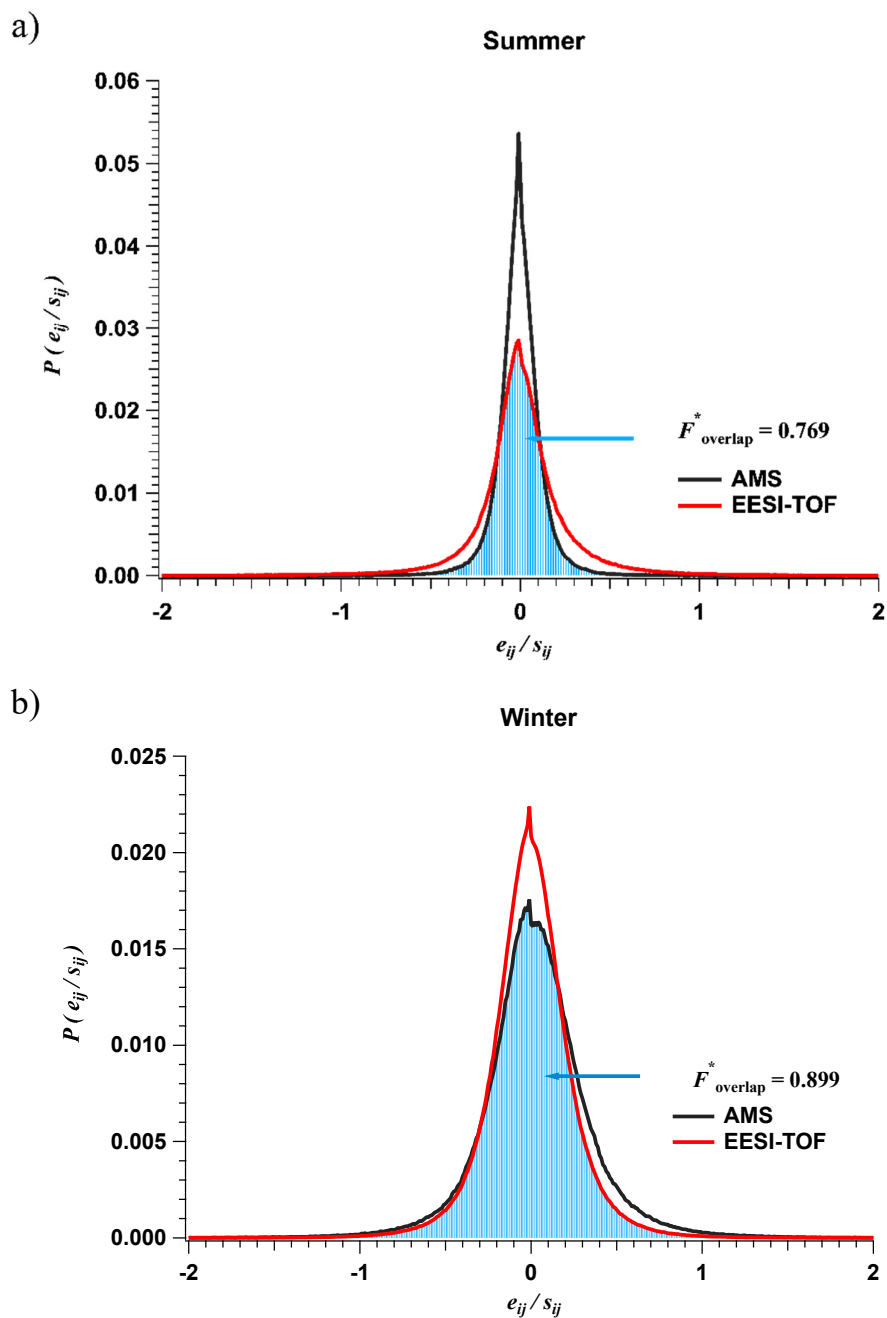
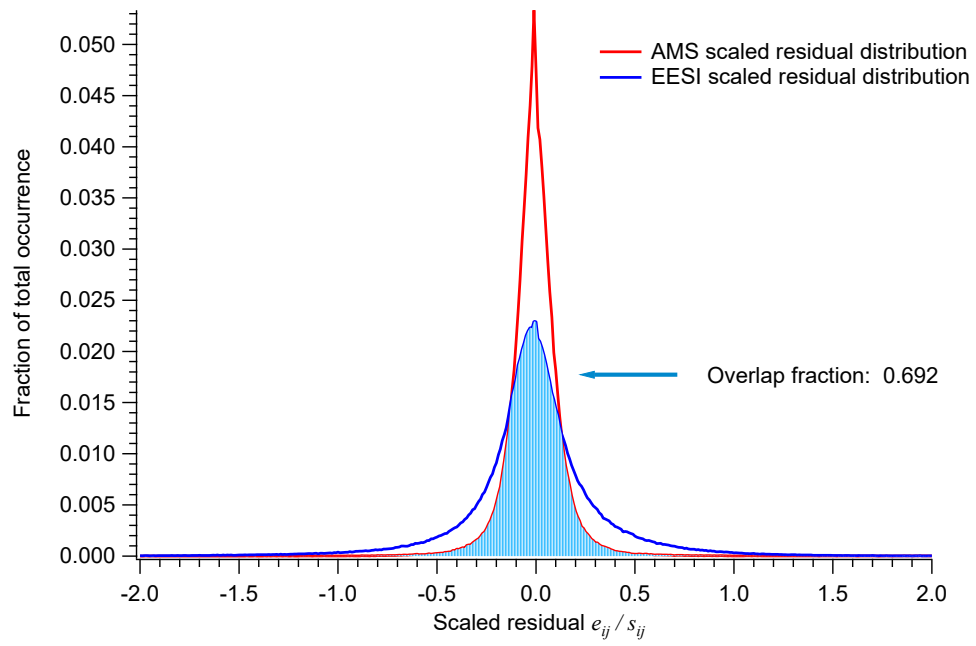


Figure S3. Scaled residual probability distributions and region of overlap from individual AMS PMF solution and EESI-TOF PMF solutions for the summer (a) and winter (b) datasets. Red and black lines show the residual distributions for the EESI-TOF and AMS, respectively; shading denotes the region of overlap.

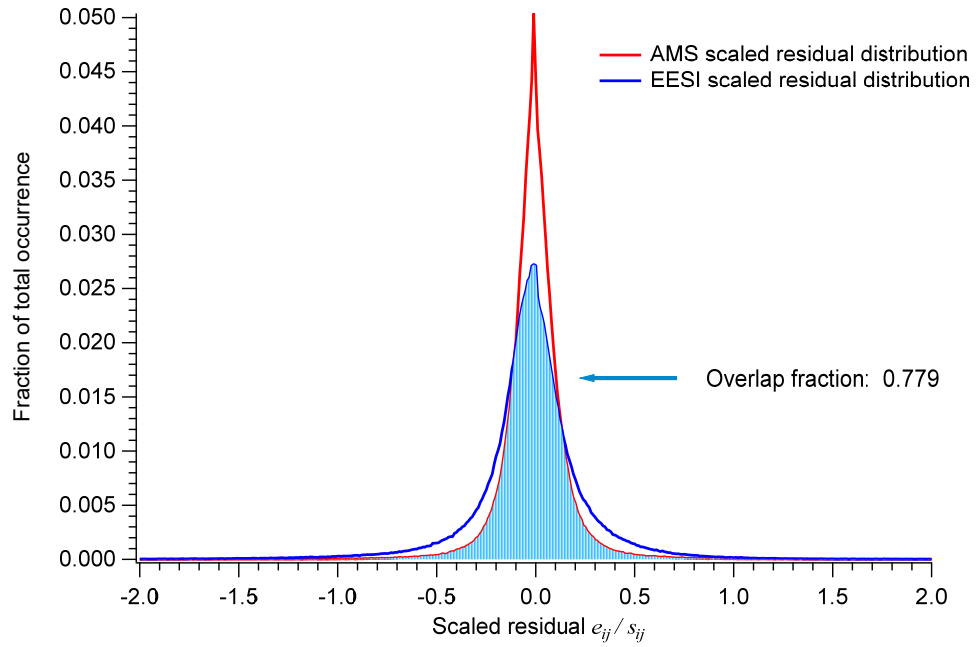
a)

Scaled residual of 8-factor solution with C_{EESI} of 0.1



b)

Scaled residual of 8-factor solution with C_{EESI} of 2



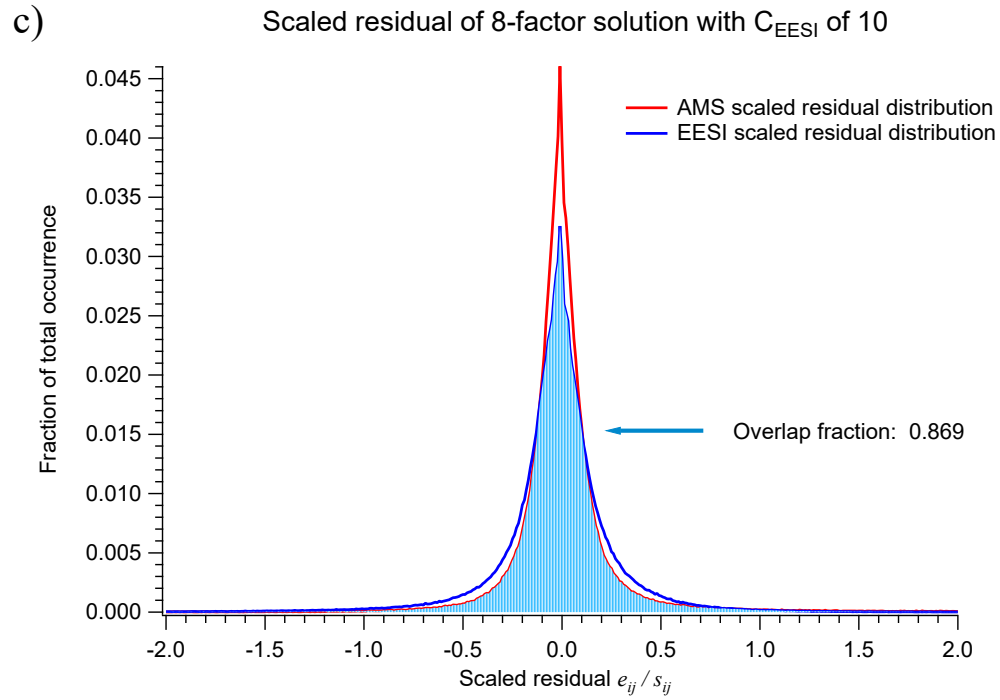


Figure S4. Scaled residual distribution of AMS (red line) and EESI (blue line) in an 8-factor solution from joint dataset in Zurich summer and corresponding overlap fractions when C_{EESI} is equal to 0.1 in a), 2 in b), and 10 in c), respectively. Balanced solution is shown in b), whereas in a) and c), AMS and EESI is overweighted, respectively.

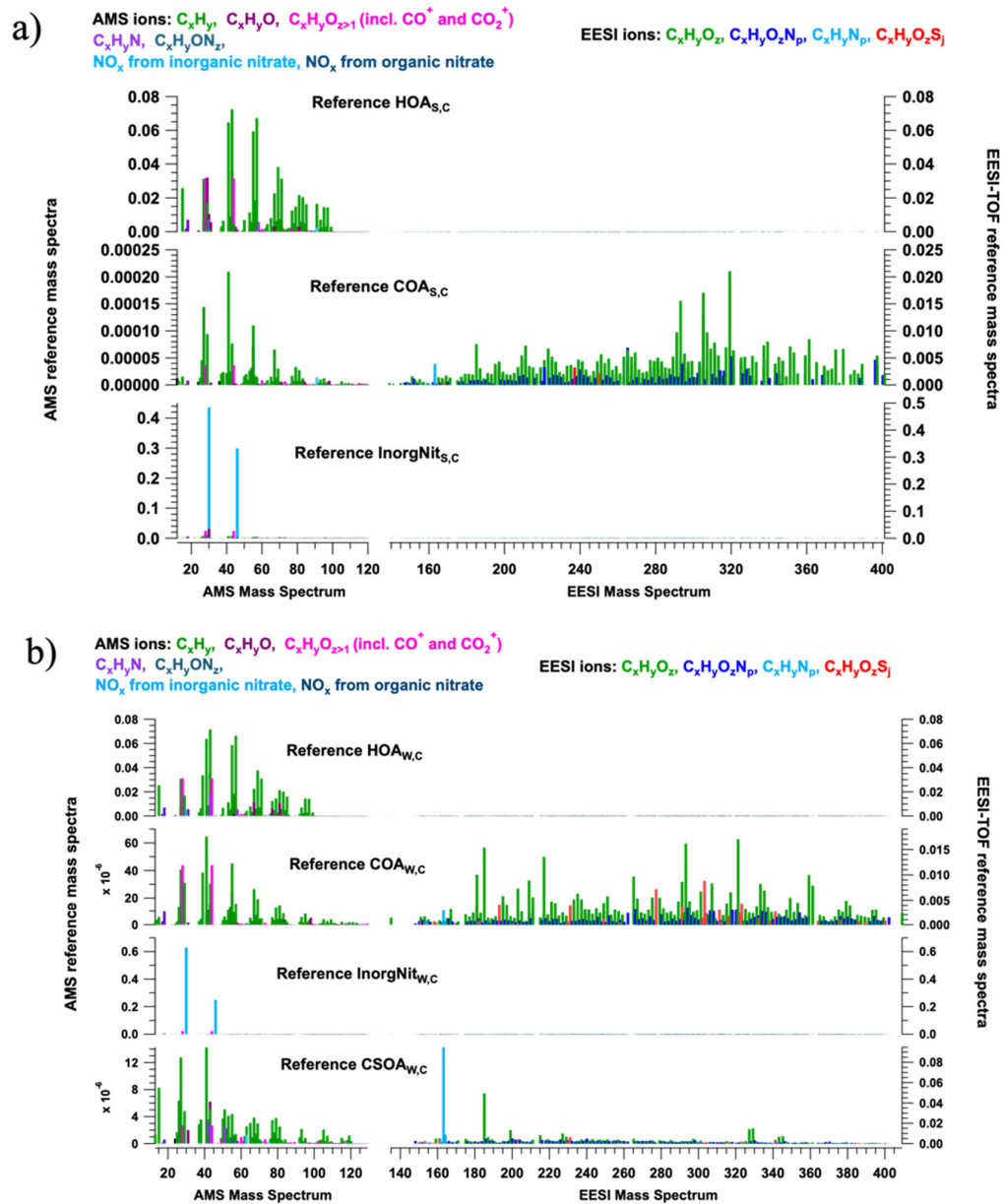


Figure S5. Normalised reference factor profiles for all constrained factors in (a) summer and (b) winter, coloured by different ion families.

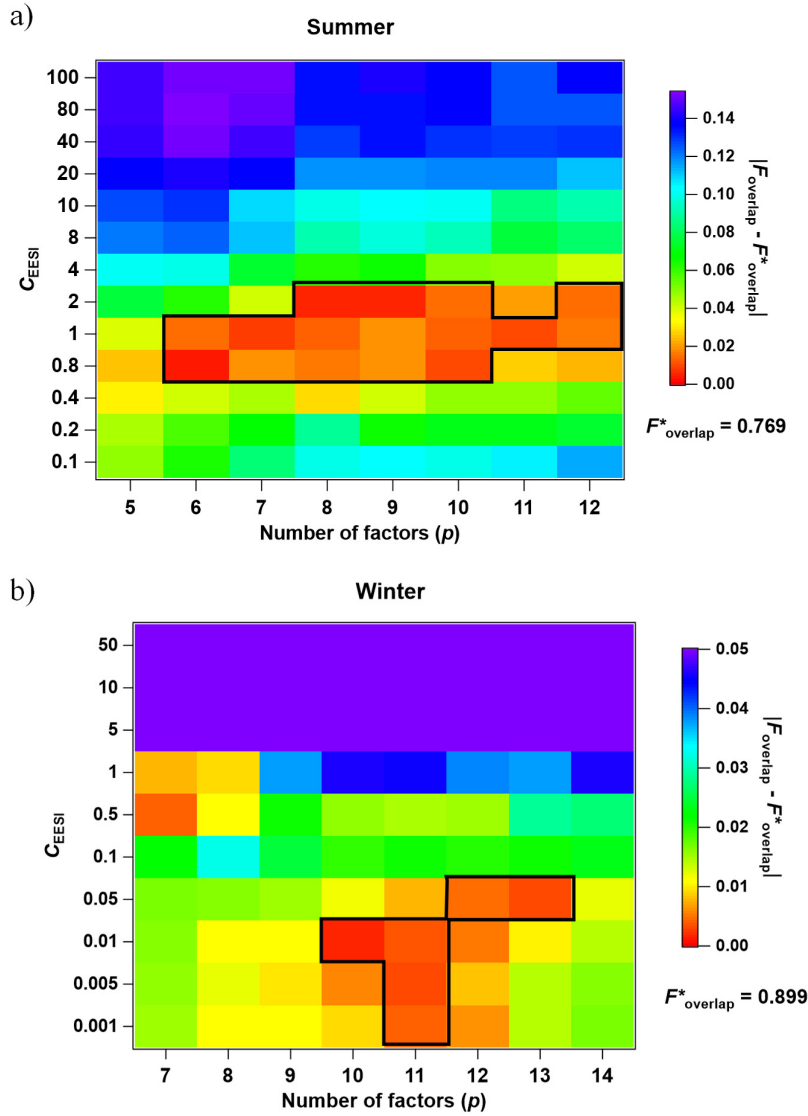


Figure S6. Identification of balanced solutions in the combined dataset (i.e., $|F_{\text{overlap}} - F_{\text{overlap}}^*|$ as a function of C_{EESI} and p) for summer (a) and winter (b) datasets. Note that $|F_{\text{overlap}} - F_{\text{overlap}}^*| = 0$ defines a balanced solution. Solutions within the black box satisfied the $|F_{\text{overlap}} - F_{\text{overlap}}^*| < \beta$ criterion defined in Eq. (14) (β is set to be 0.02 and 0.005 for summer and winter, respectively) and were selected as base case candidates, from which the base case that can best represent the combined data was selected by manual inspection.

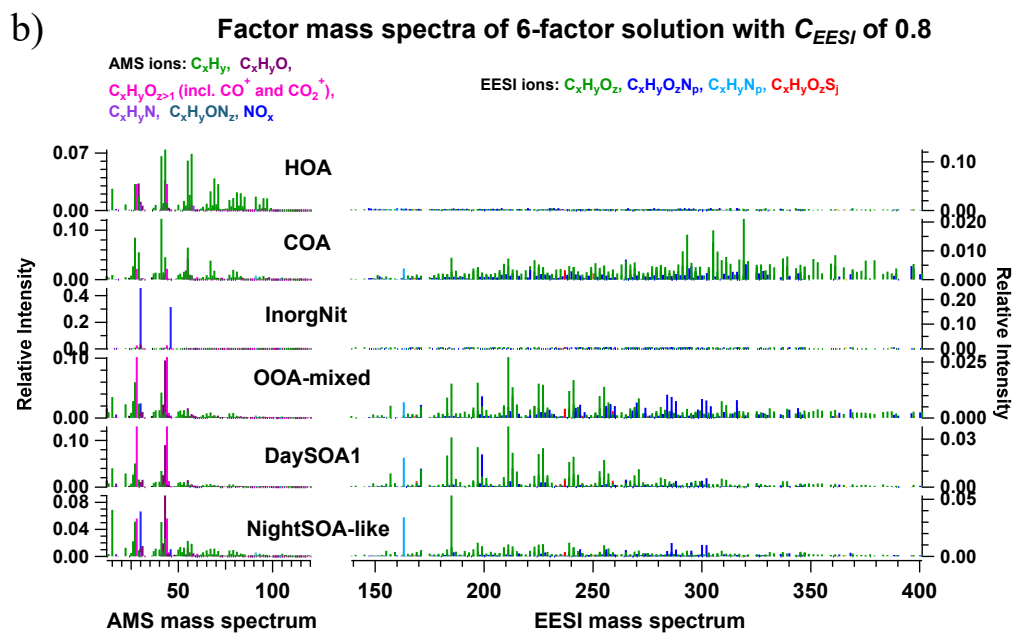
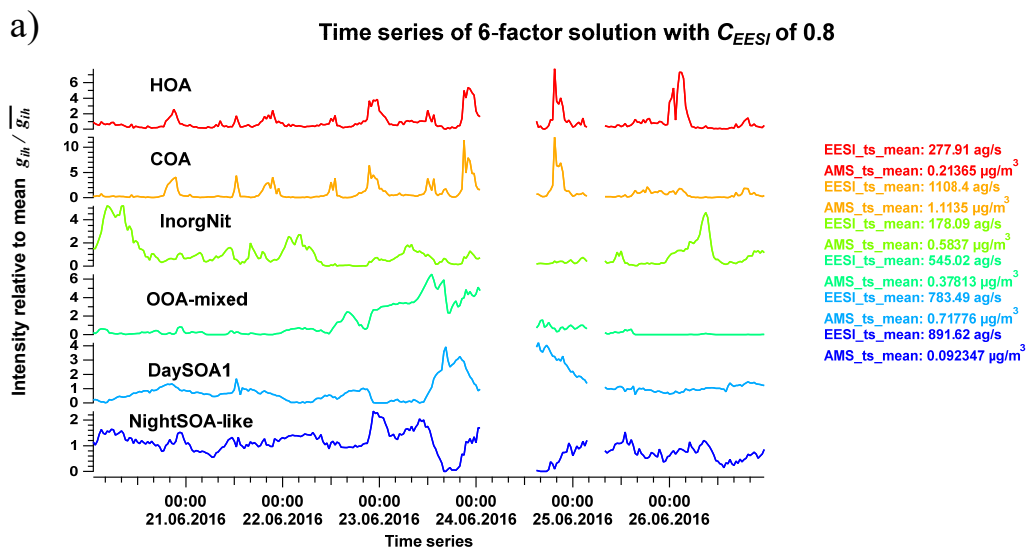


Figure S7. Factor time series in a) and mass spectra in b) for 6-factor solution with C_{EESI} of 0.8 for Zurich summer dataset.

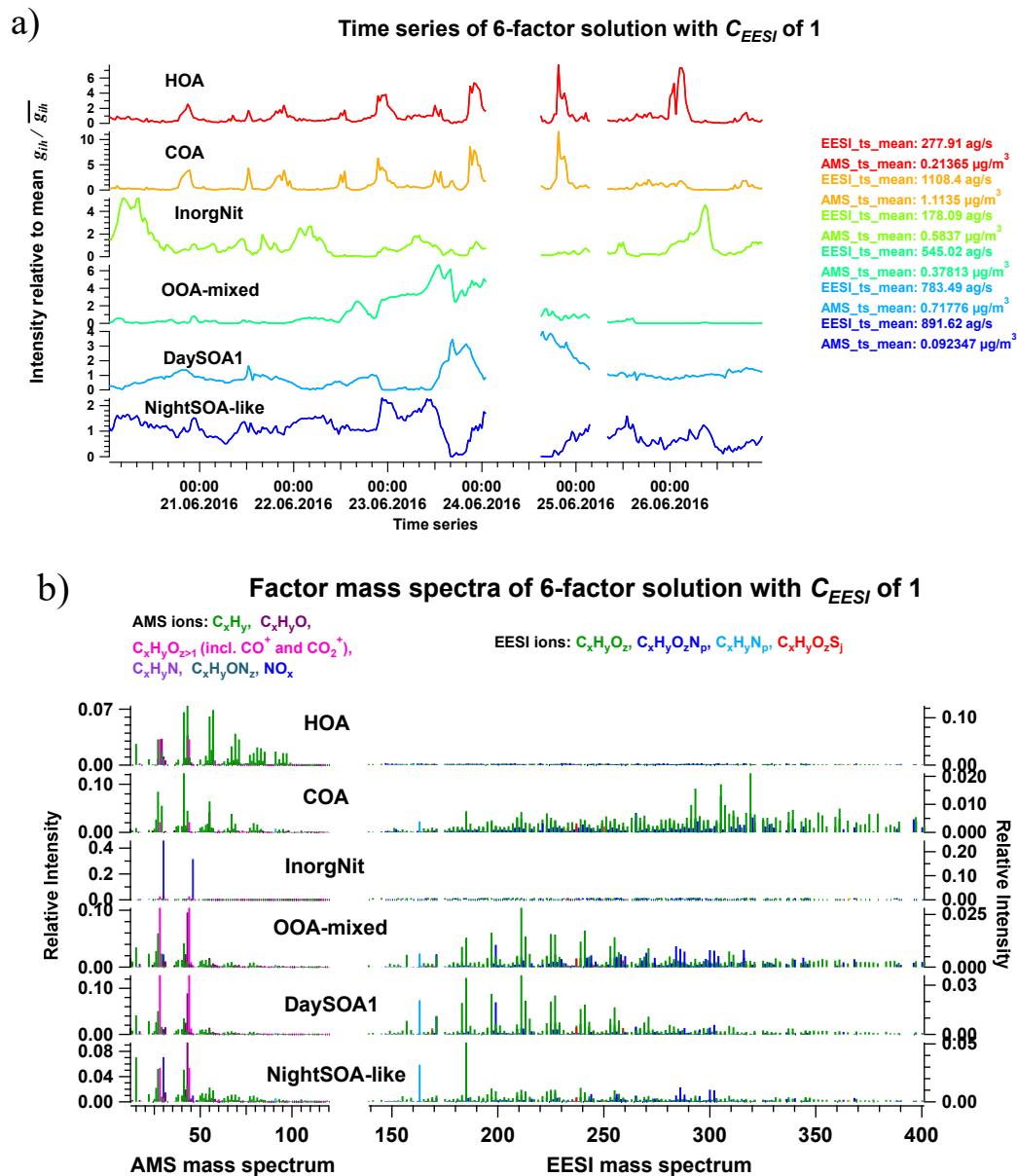


Figure S8. Factor time series in a) and mass spectra in b) for 6-factor solution with C_{EESI} of 1 for Zurich summer dataset.

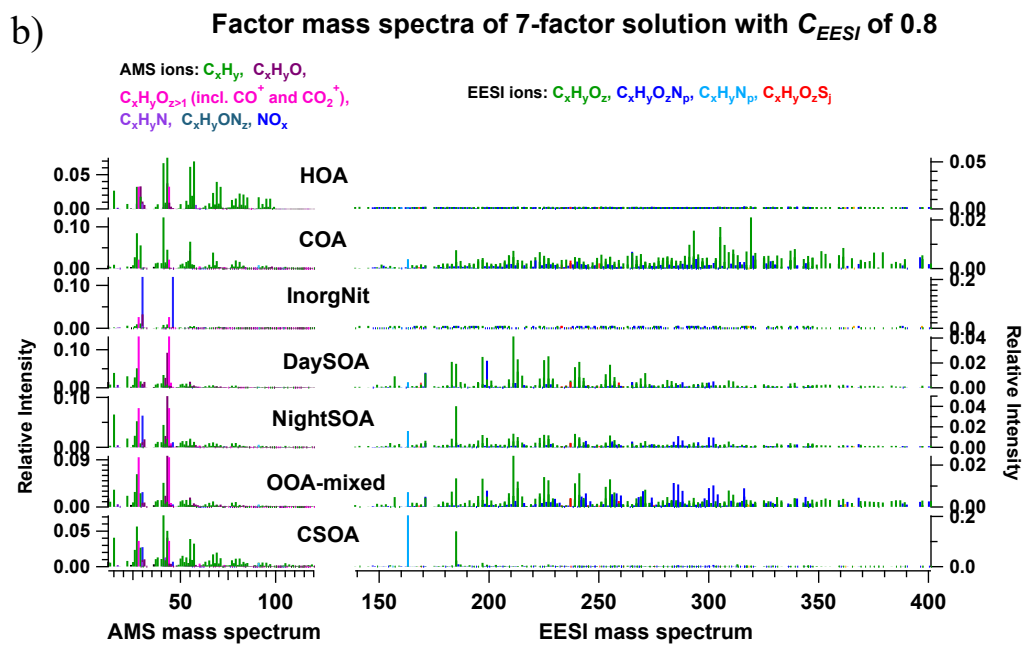
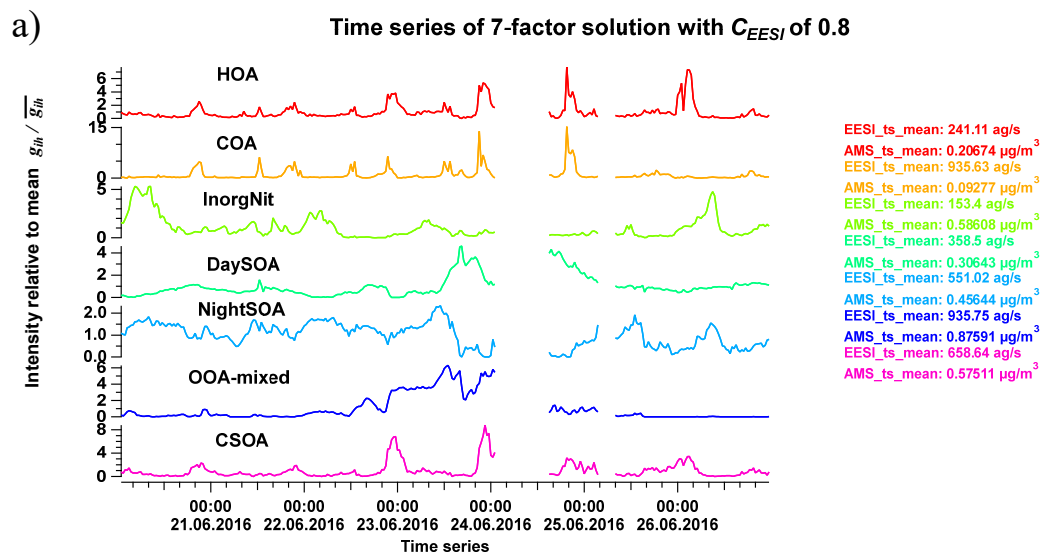


Figure S9. Factor time series in a) and mass spectra in b) for 7-factor solution with C_{EESI} of 0.8 for Zurich summer dataset.

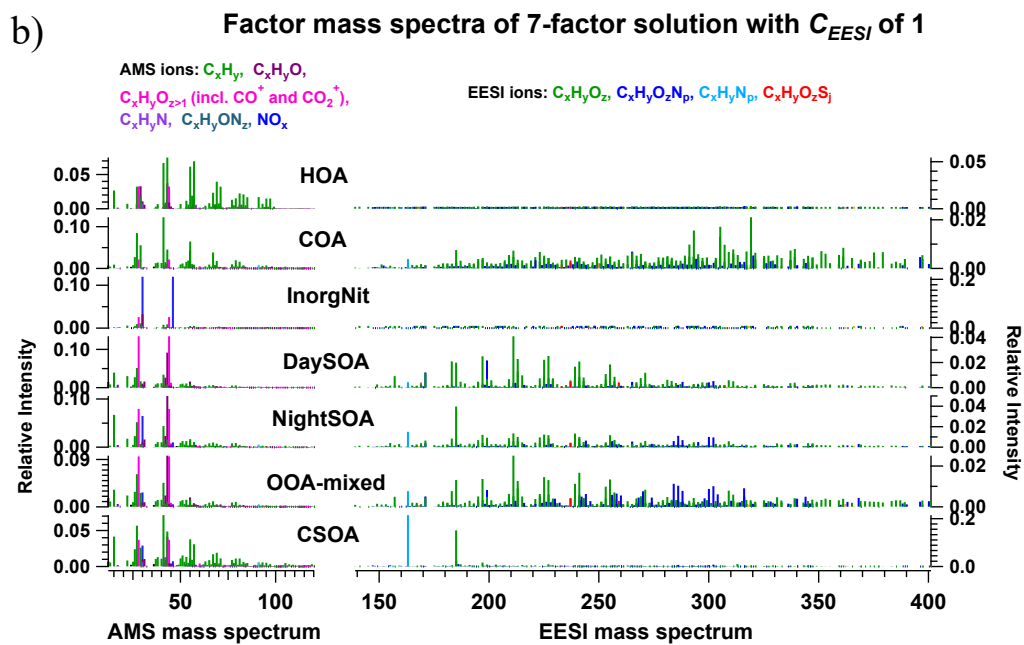
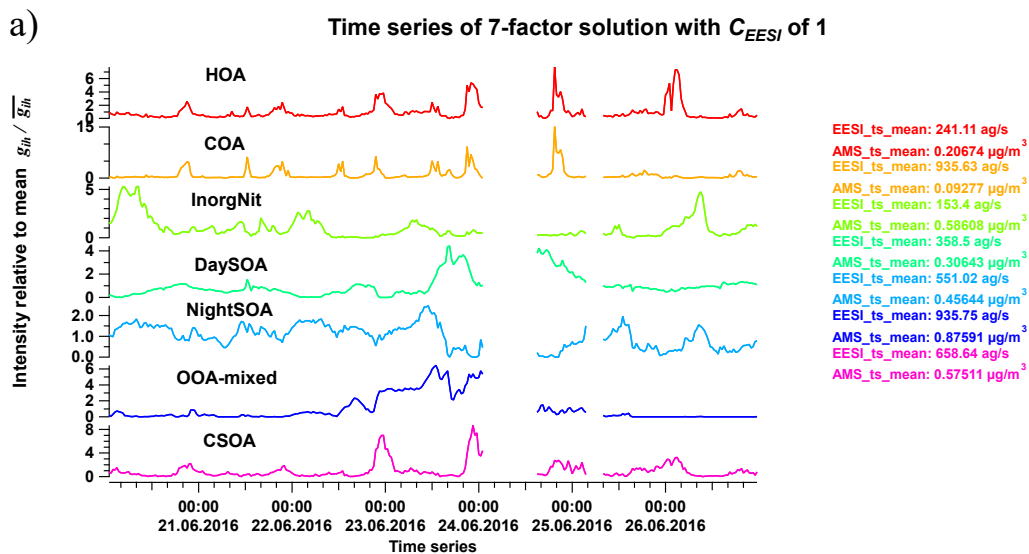


Figure S10. Factor time series in a) and mass spectra in b) for 7-factor solution with C_{EESI} of 1 for Zurich summer dataset.

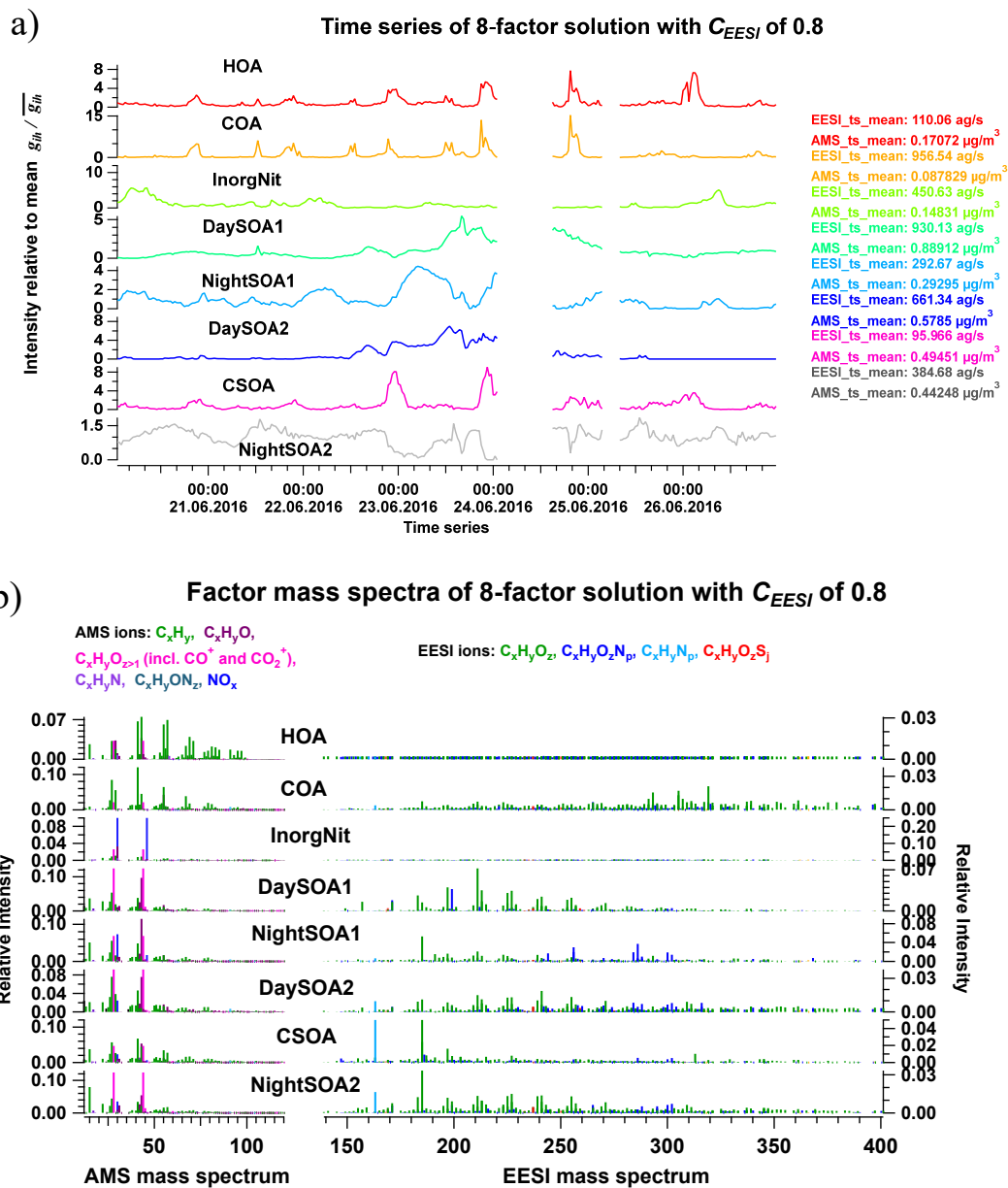


Figure S11. Factor time series in a) and mass spectra in b) for 8-factor solution with C_{EESI} of 0.8 for Zurich summer dataset.

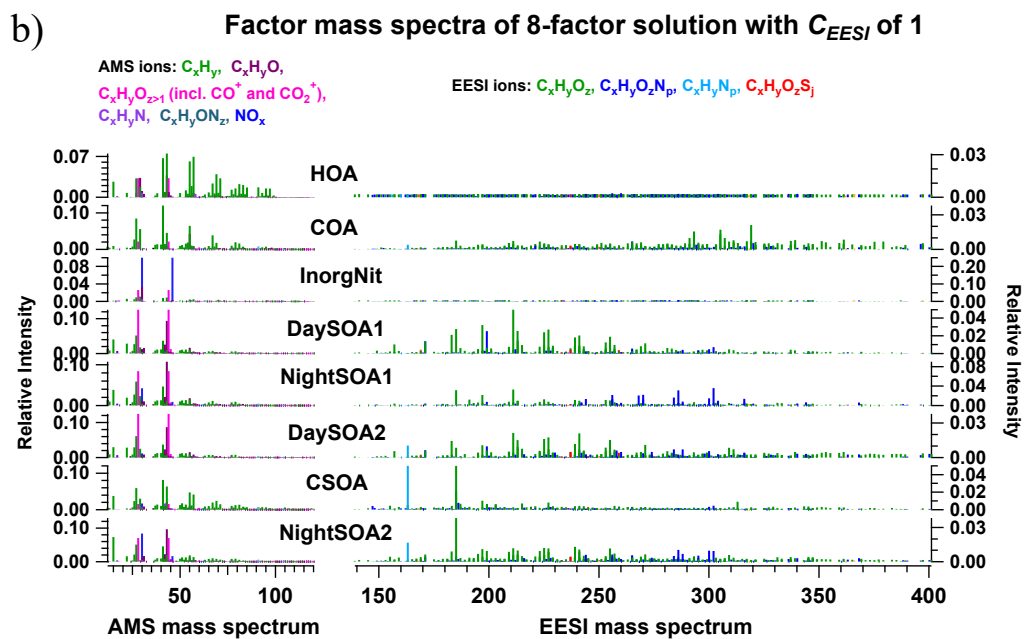
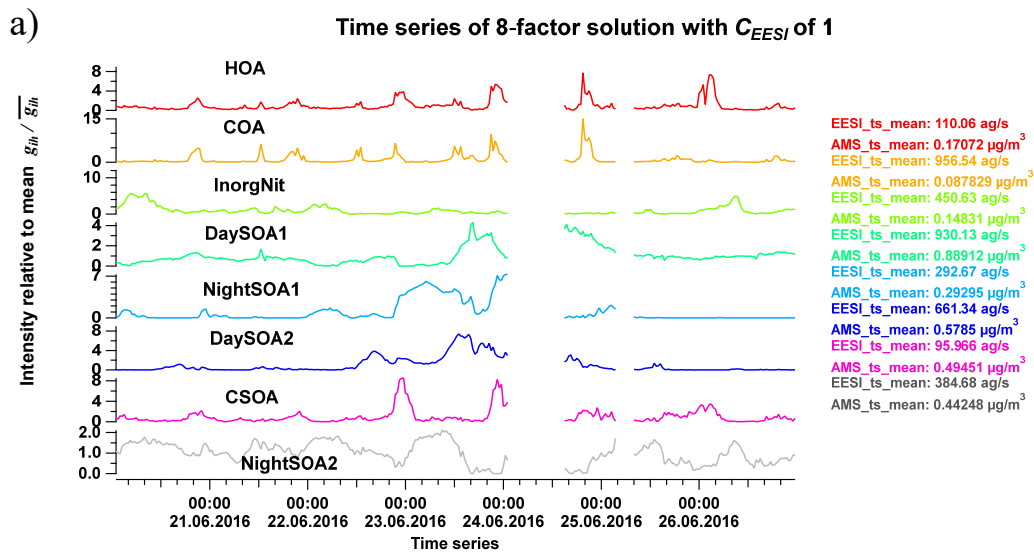


Figure S12. Factor time series in a) and mass spectra in b) for 8-factor solution with C_{EESI} of 1 for Zurich summer dataset.

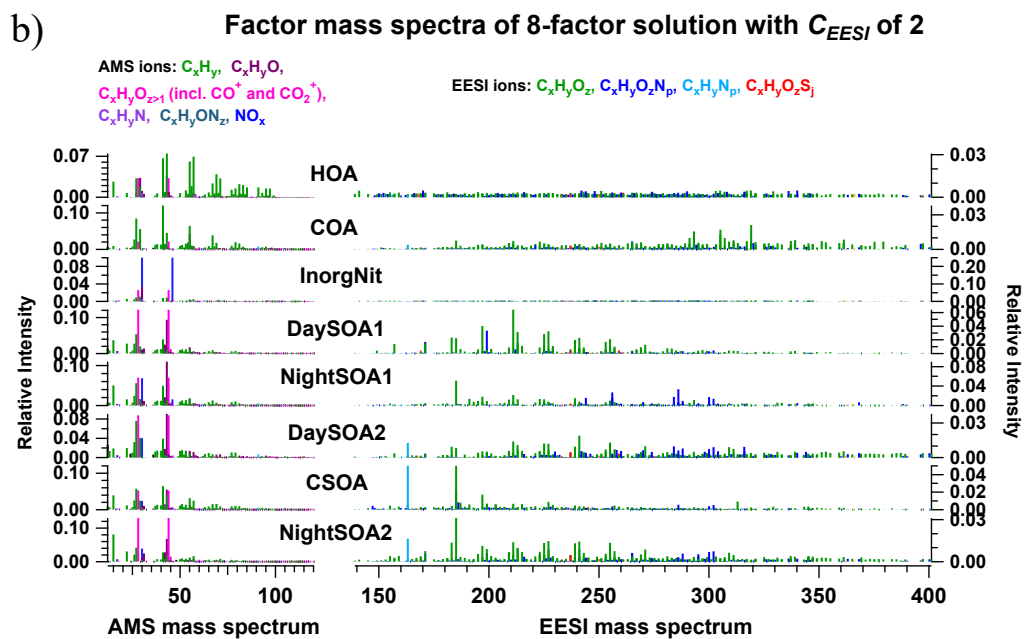
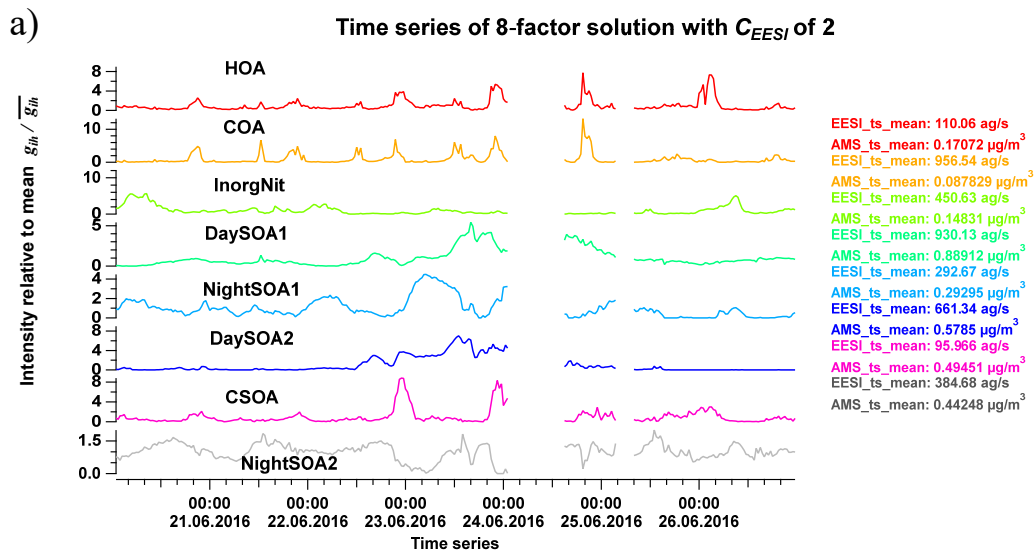


Figure S13. Factor time series in a) and mass spectra in b) for 8-factor solution with C_{EESI} of 2 for Zurich summer dataset.

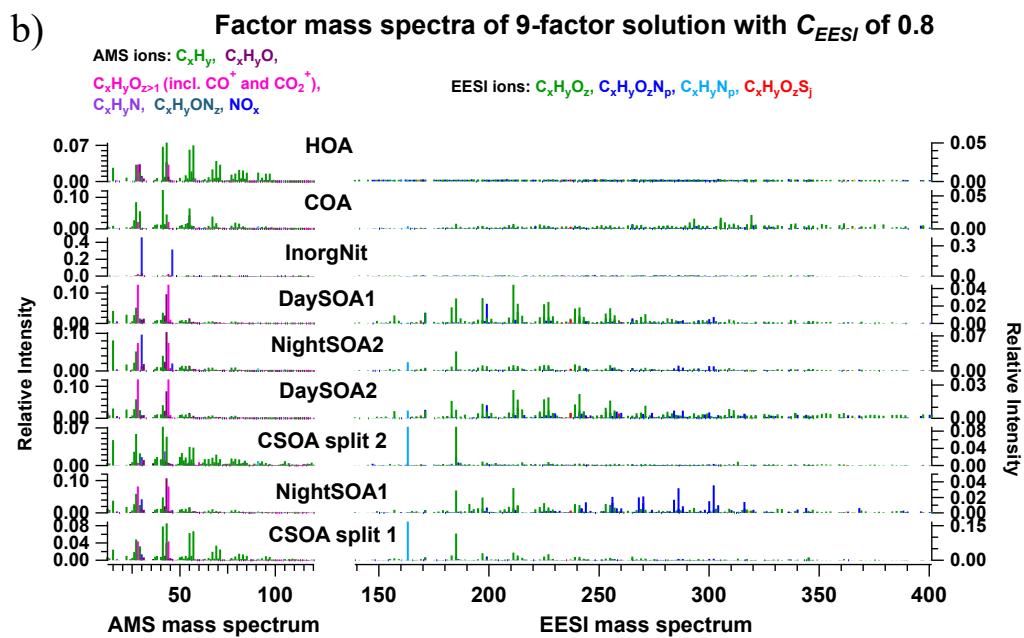
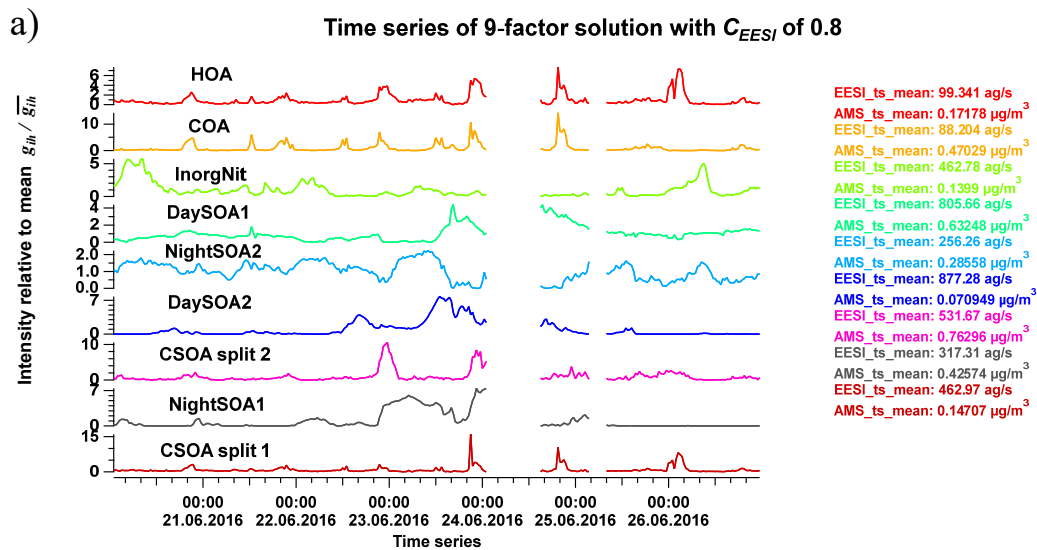


Figure S14. Factor time series in a) and mass spectra in b) for 9-factor solution with C_{EESI} of 0.8 for Zurich summer dataset.

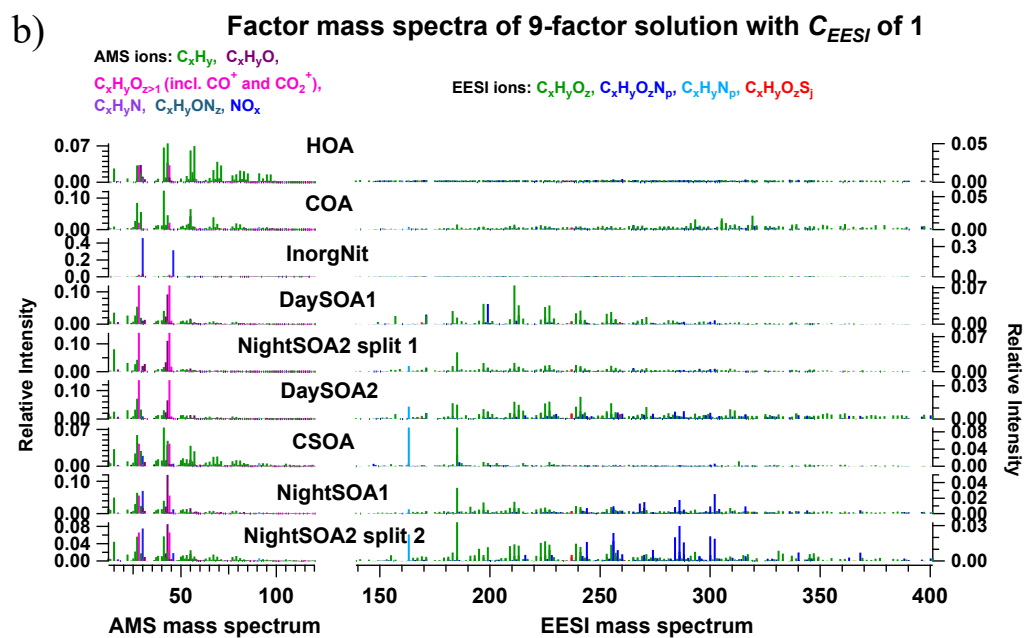
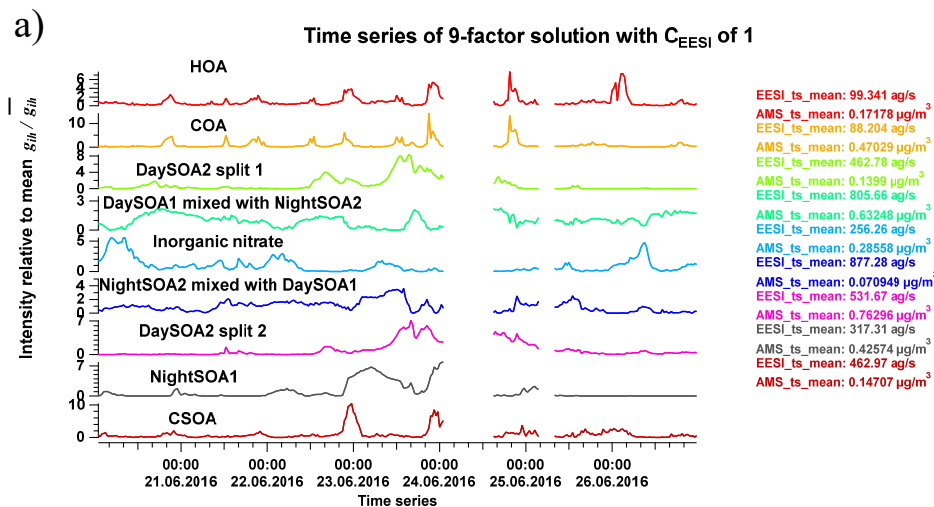


Figure S15. Factor time series in a) and mass spectra in b) for 9-factor solution with C_{EESI} of 1 for Zurich summer dataset.

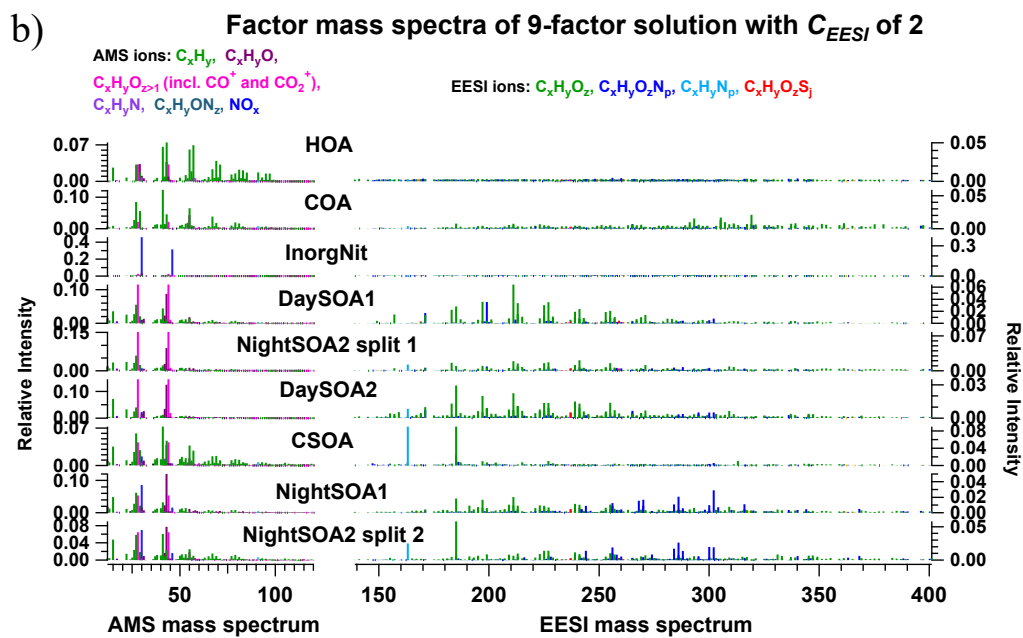
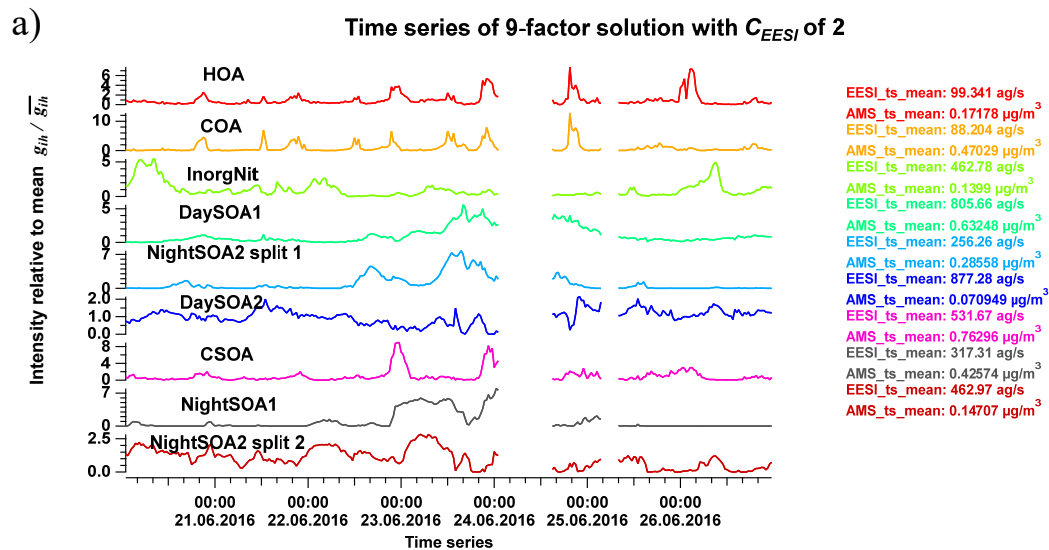


Figure S16. Factor time series in a) and mass spectra in b) for 9-factor solution with C_{EESI} of 2 for Zurich summer dataset.

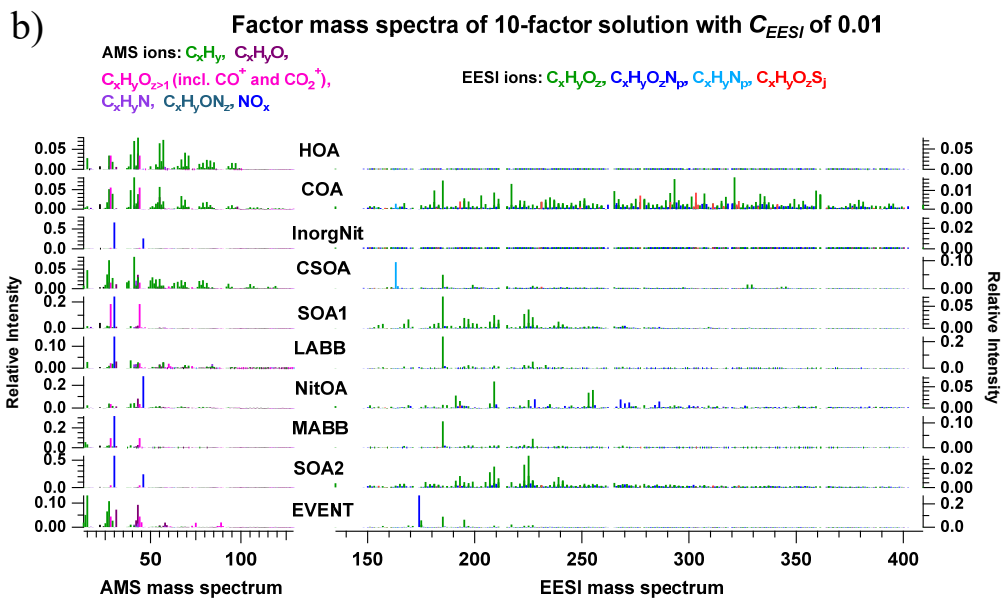
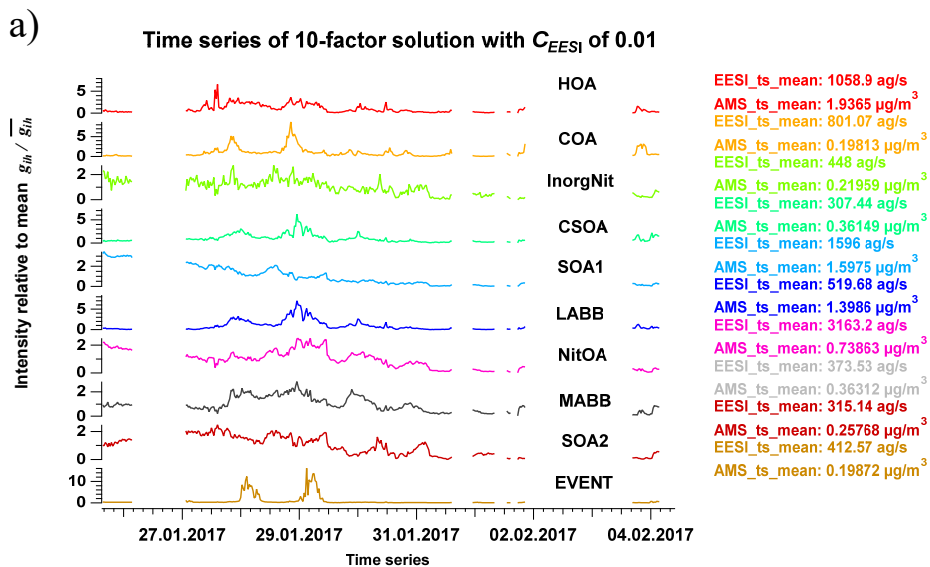


Figure S17. Factor time series in a) and mass spectra in b) for 10-factor solution with C_{EESI} of 0.01 for Zurich winter dataset.

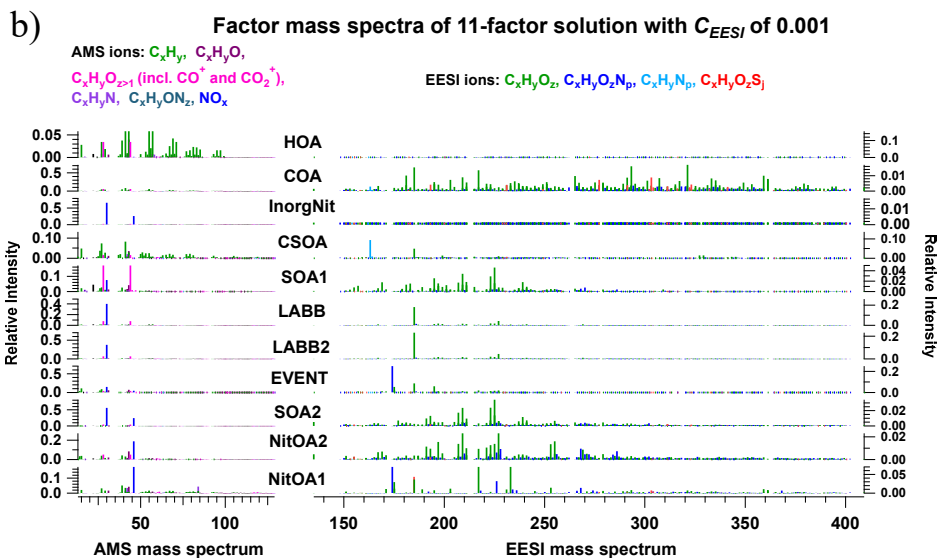
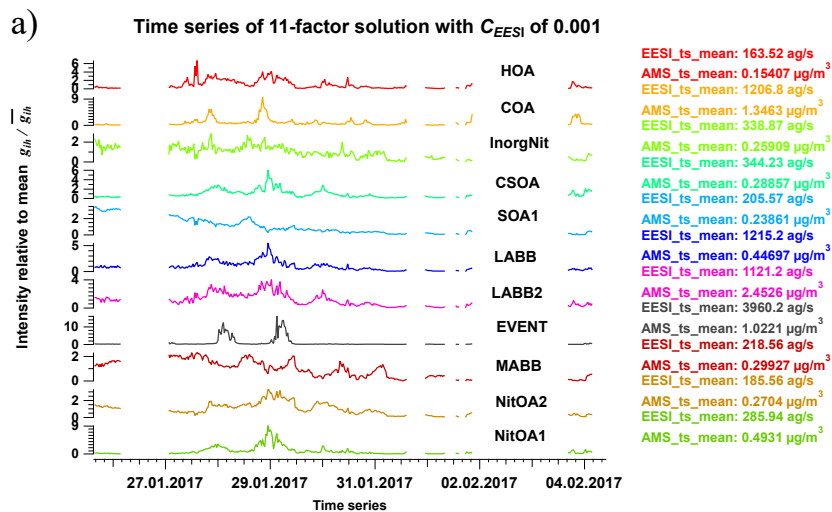


Figure S18. Factor time series in a) and mass spectra in b) for 11-factor solution with C_{EESI} of 0.001 for Zurich winter dataset.

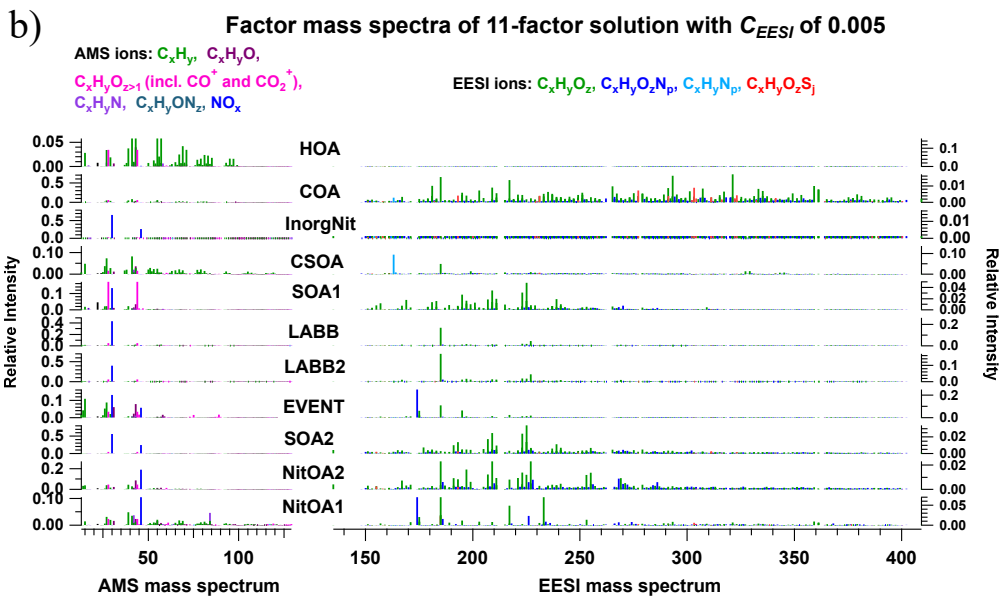
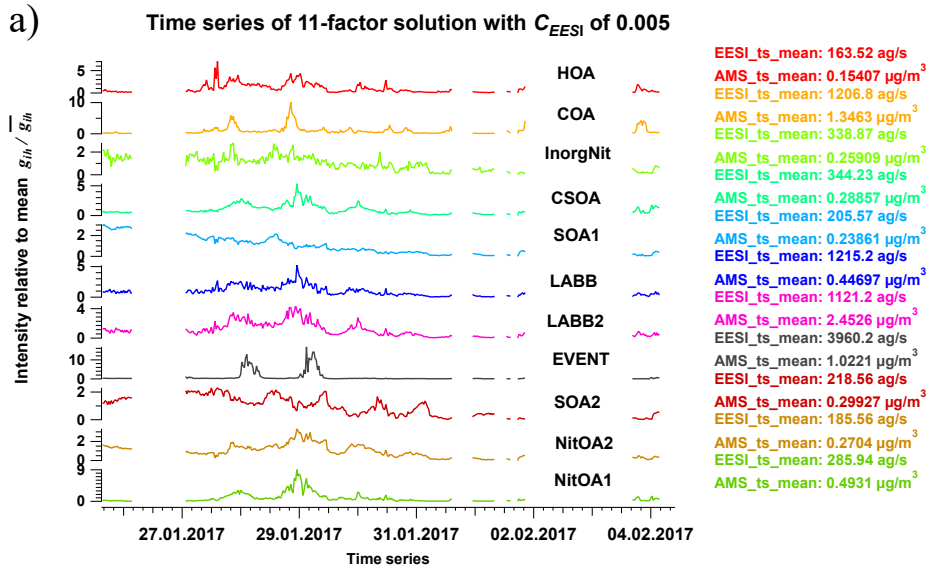


Figure S19. Factor time series in a) and mass spectra in b) for 11-factor solution with C_{EESI} of 0.005 for Zurich winter dataset.

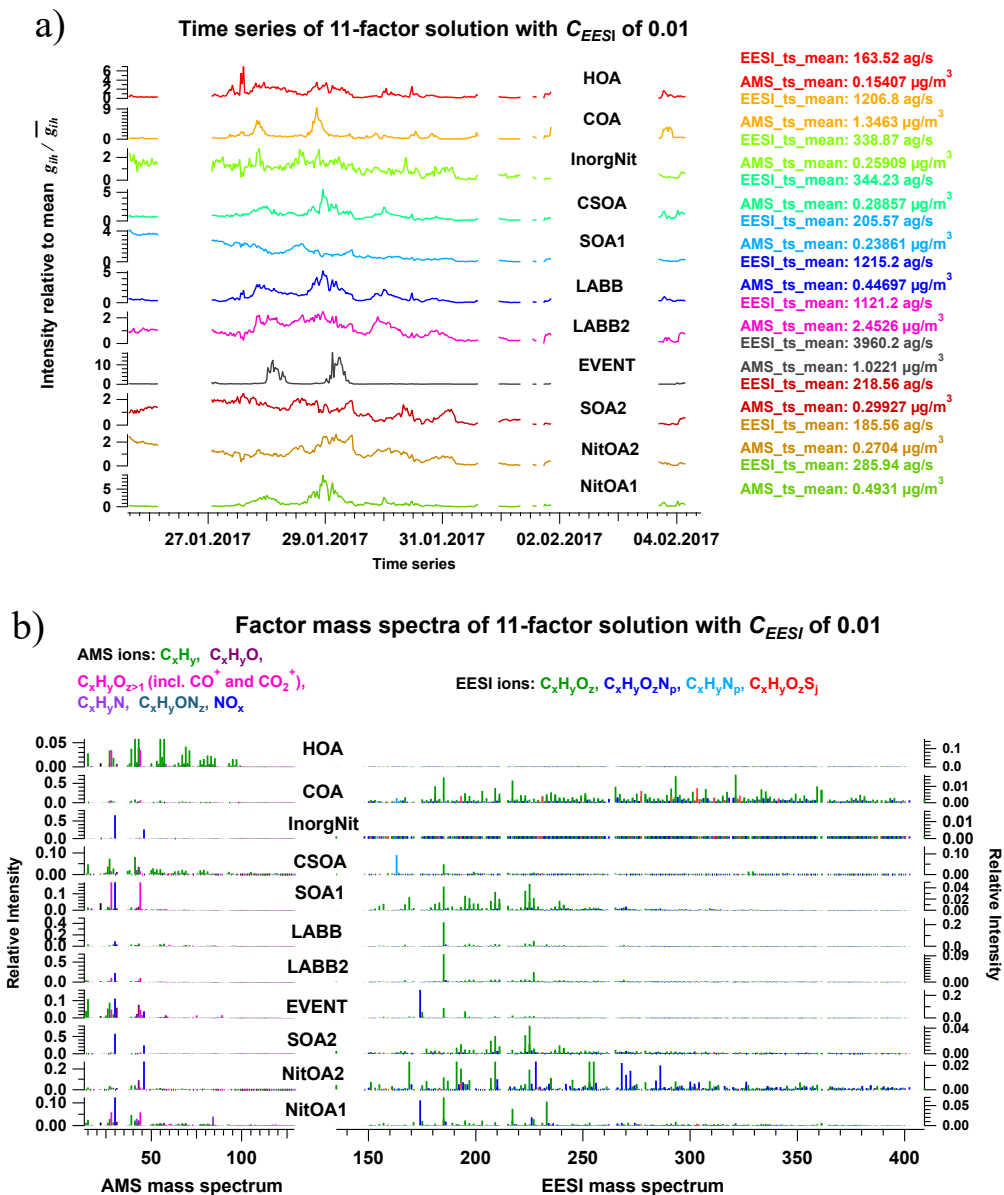


Figure S20. Factor time series in a) and mass spectra in b) for 11-factor solution with C_{EESI} of 0.01 for Zurich winter dataset.

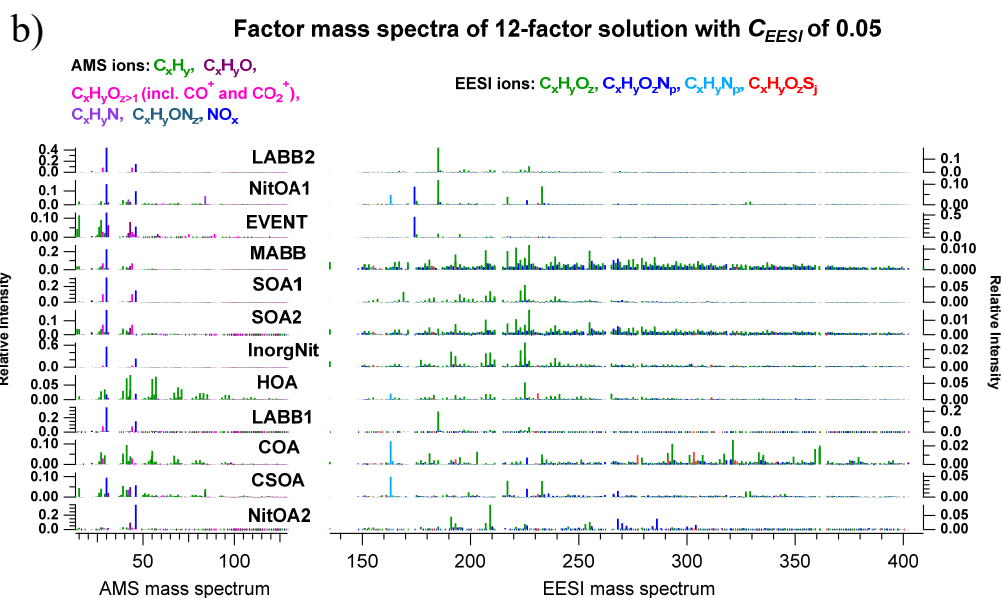
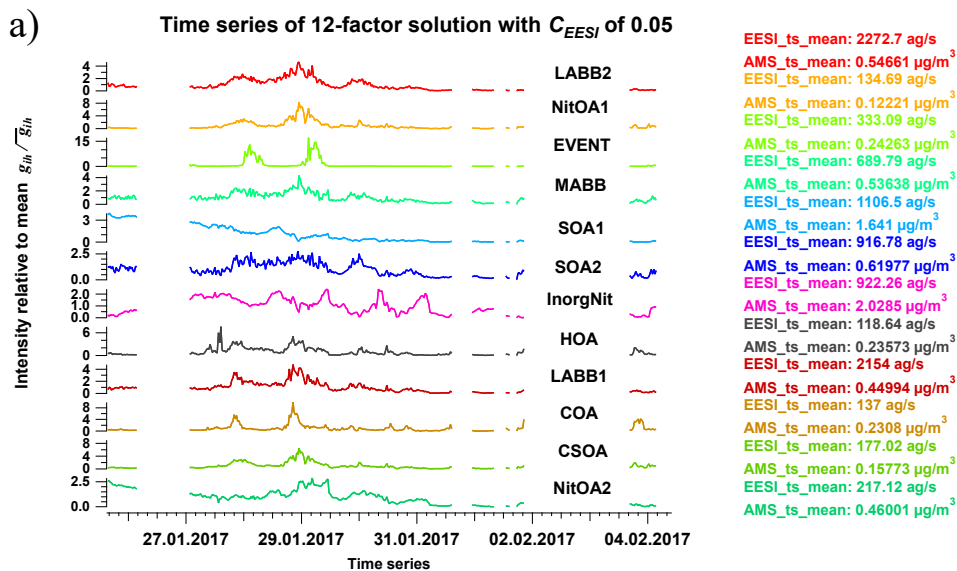


Figure S21. Factor time series in a) and mass spectra in b) for 12-factor solution with C_{EESI} of 0.05 for Zurich winter dataset.

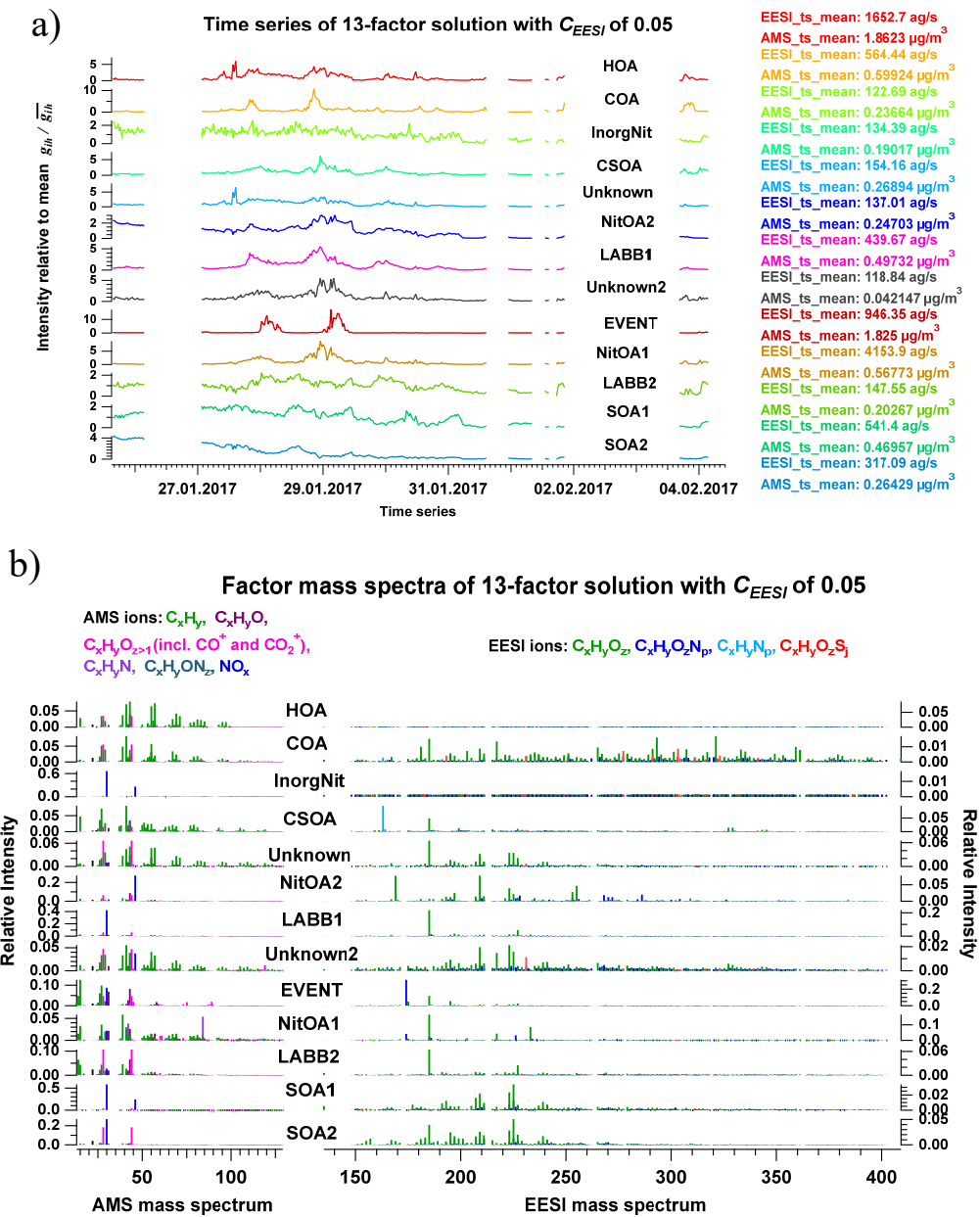
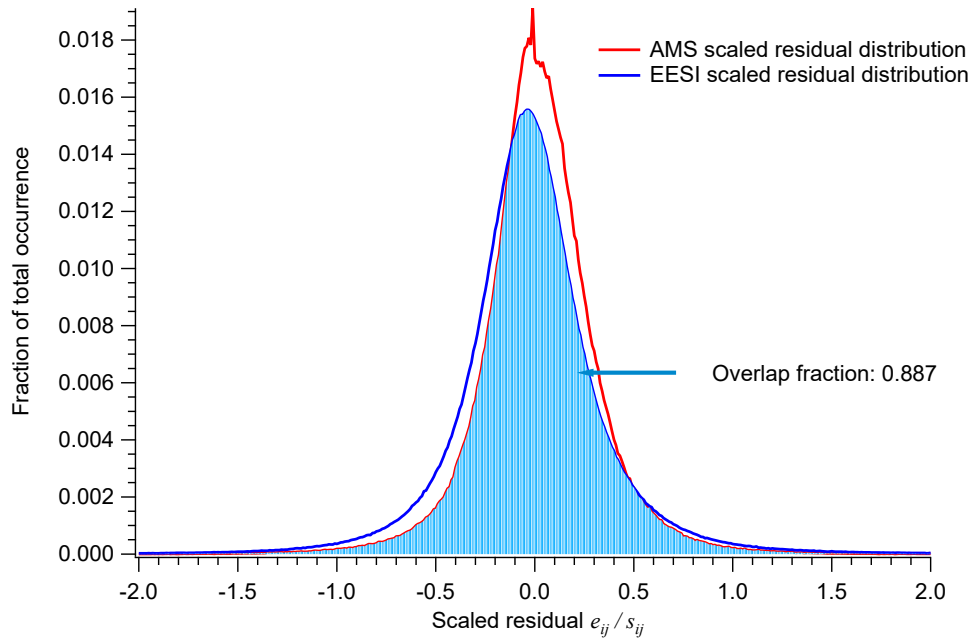


Figure S22. Factor time series in a) and mass spectra in b) for 13-factor solution with C_{EESI} of 0.05 for Zurich winter dataset.

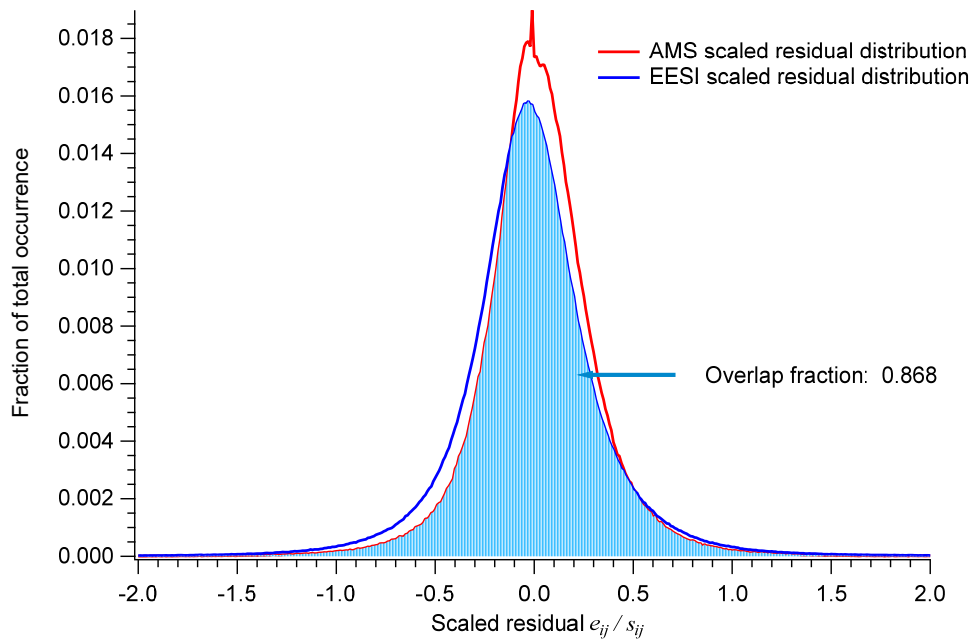
a)

Scaled residual of 12-factor solution with C_{EESI} of 0.005



b)

Scaled residual of 12-factor solution with C_{EESI} of 0.05



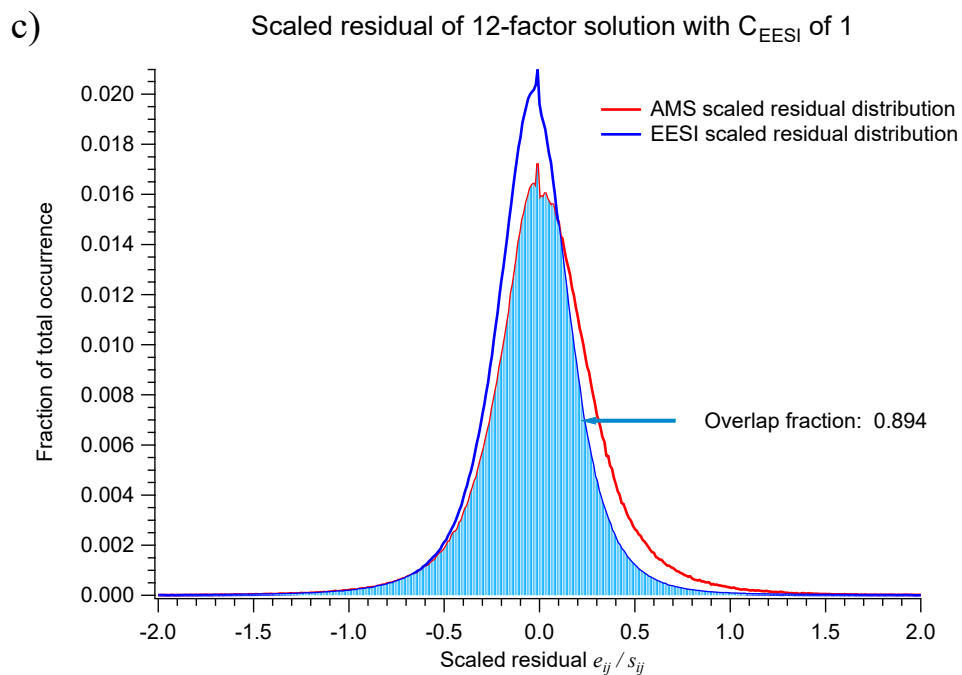


Figure S23. Scaled residual distribution of AMS (red line) and EESI (blue line) in a 12-factor solution from joint dataset in Zurich winter and corresponding overlap fractions when C_{EESI} is equal to 0.005 in a), 0.005 in b), and 1 in c), respectively. Balanced solution is shown in b), whereas in a) and c), AMS and EESI is overweighted, respectively.

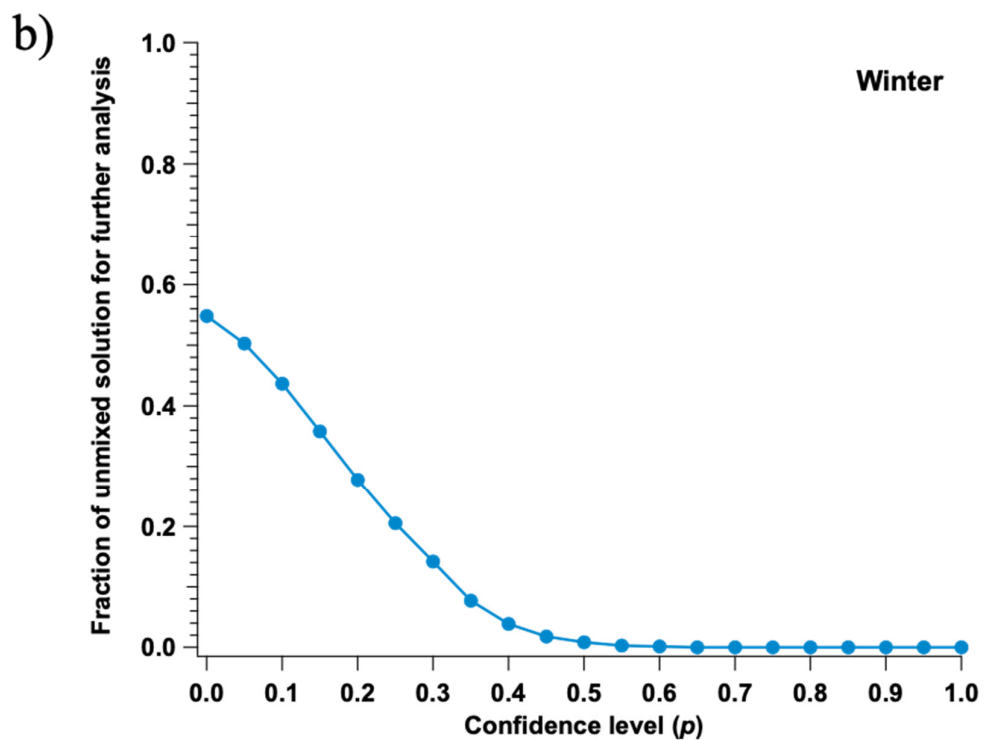
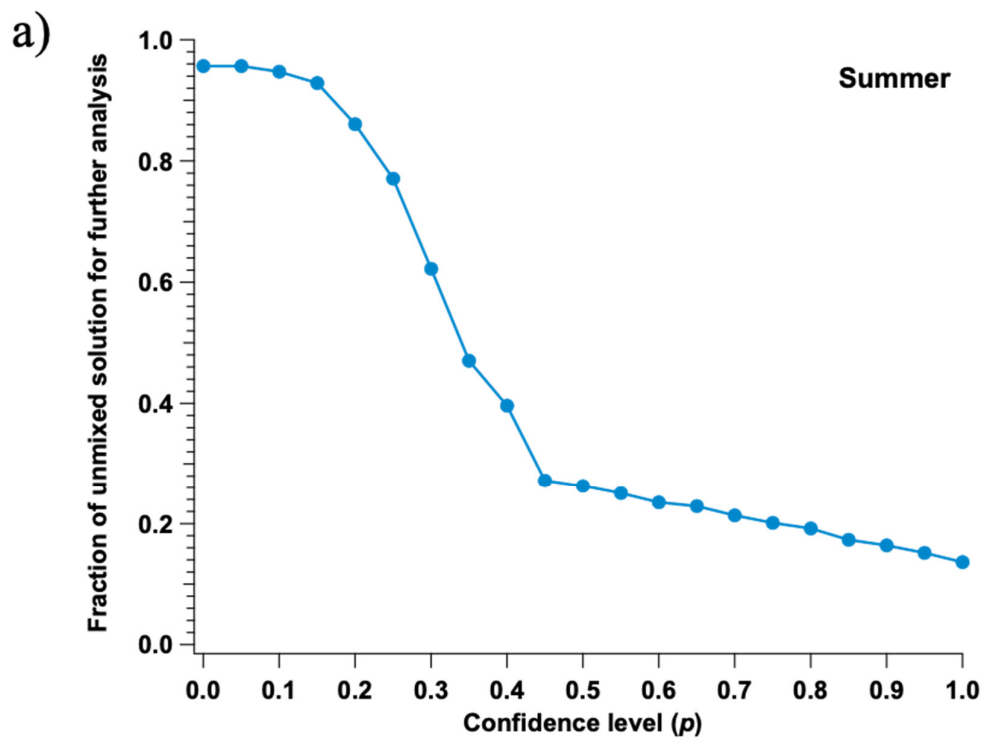
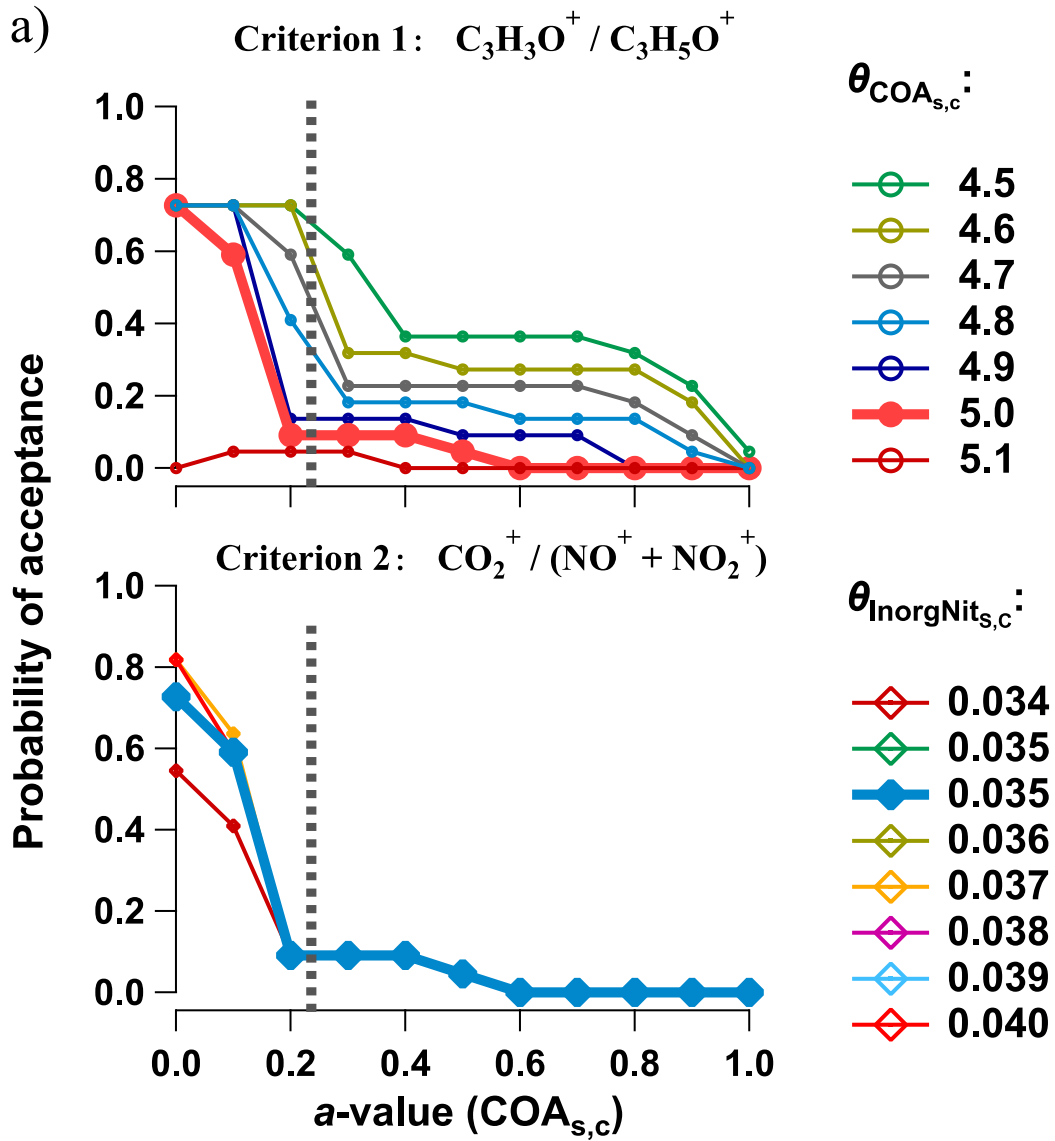
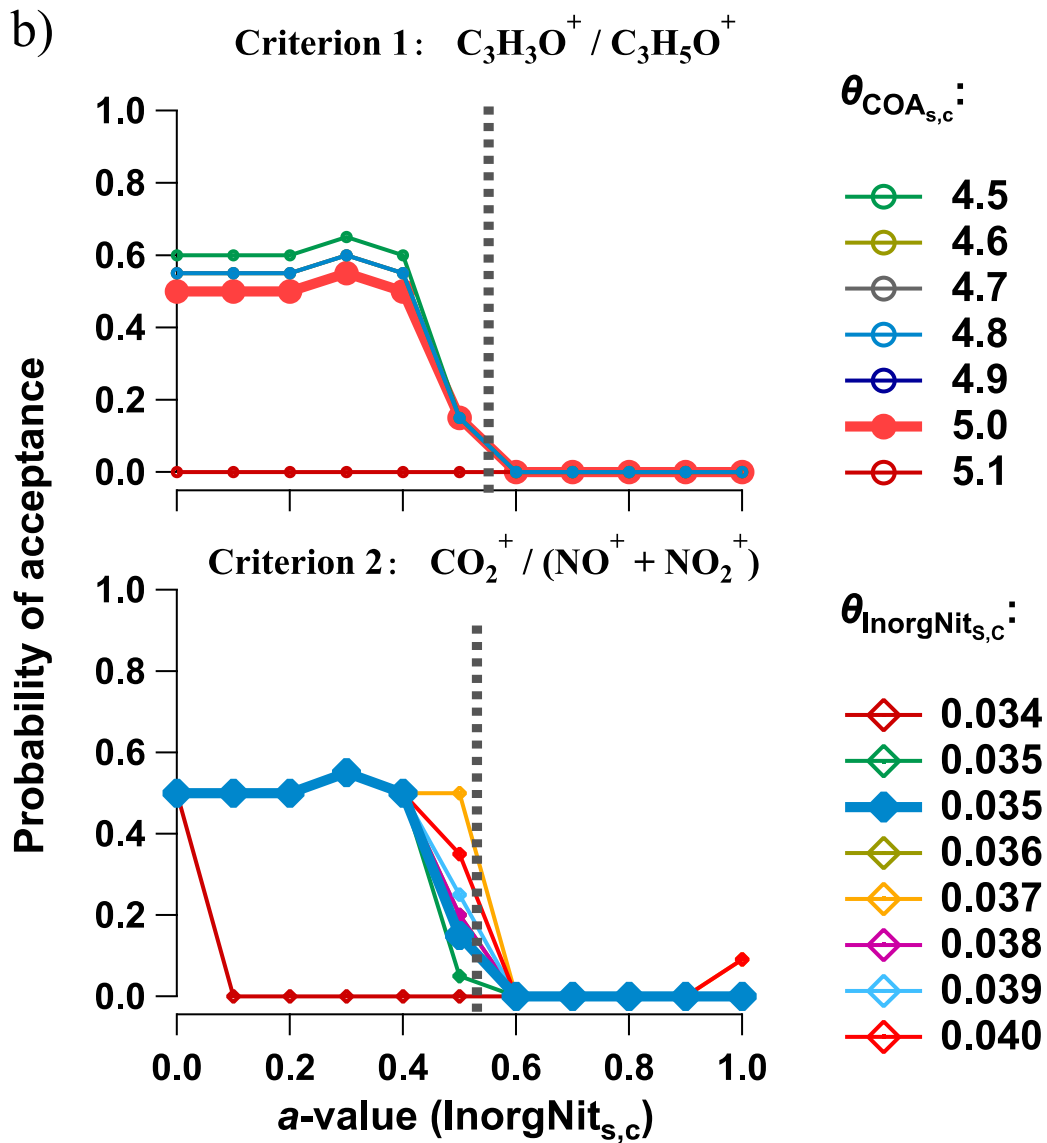


Figure S24. Fraction of unmixed solution selected for further analysis as a function of confidence level (p) for summer dataset in a) and winter dataset in b).



b)



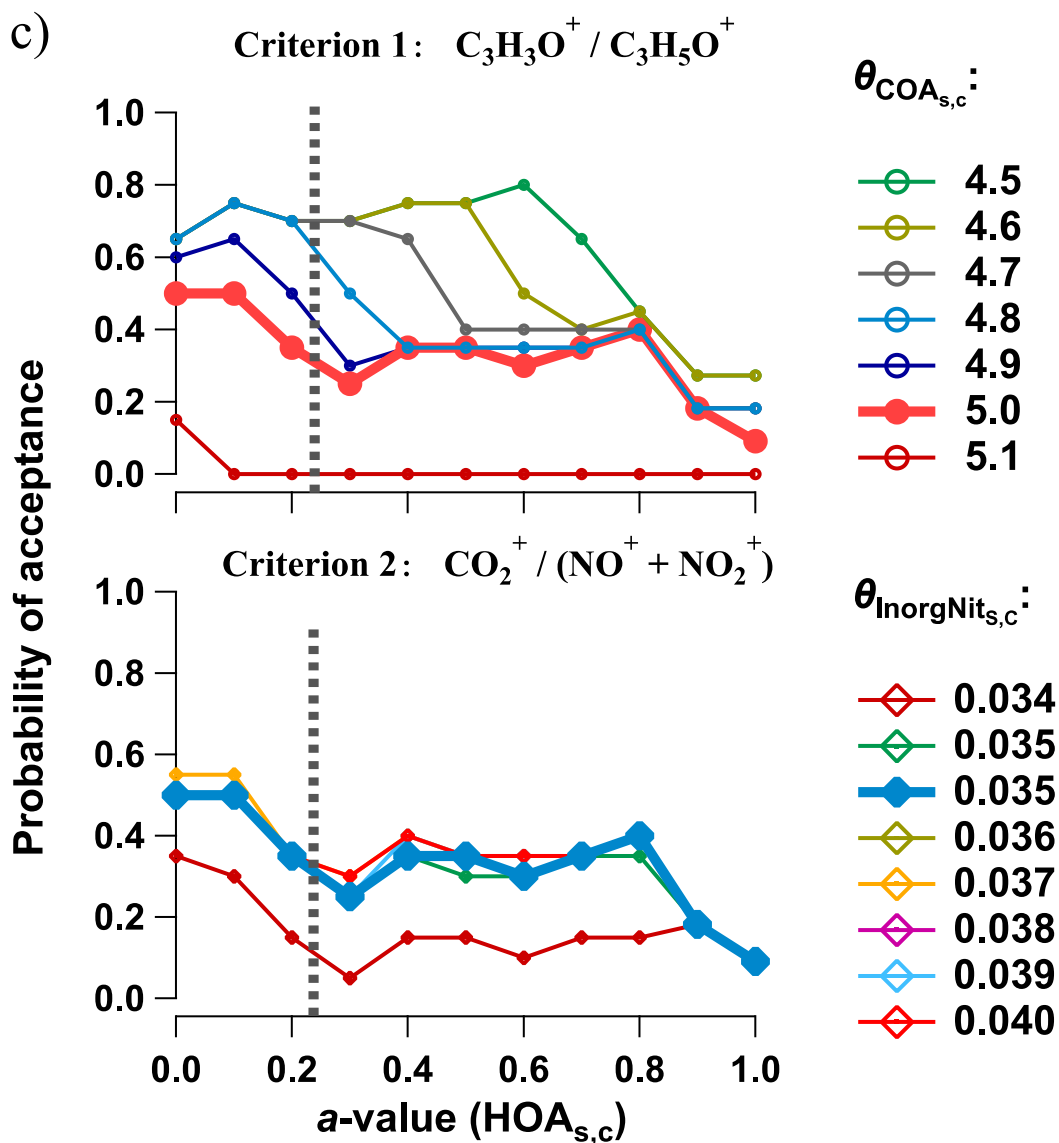


Figure S25. Acceptance probability (i.e., all criteria satisfied simultaneously) calculated from all runs in multi-2D scans as a function of a value of a) $COA_{s,c}$, b) $InorgNit_{s,c}$ and c) $HOA_{s,c}$. To maintain consistency with $a=0.1$ to $a=1.0$, the $a=0$ point considers only runs in which the factor in question is being scanned against a single other factor, discarding runs for which the factor in question is fixed at $a=0$ while two other factors are scanned. Within each sub-figure, the response to different criteria thresholds are shown. Final selected values for criteria thresholds are displayed as a thicker line, while vertical dashed lines denote the final selected upper limit for a -value randomisation in the subsequent bootstrap analysis. Note that due to the requirement that all criteria be satisfied simultaneously, the thicker lines (and only the thicker lines) are identical across all panels in a sub-figure. Acceptance requires that a run fulfil all criteria simultaneously.

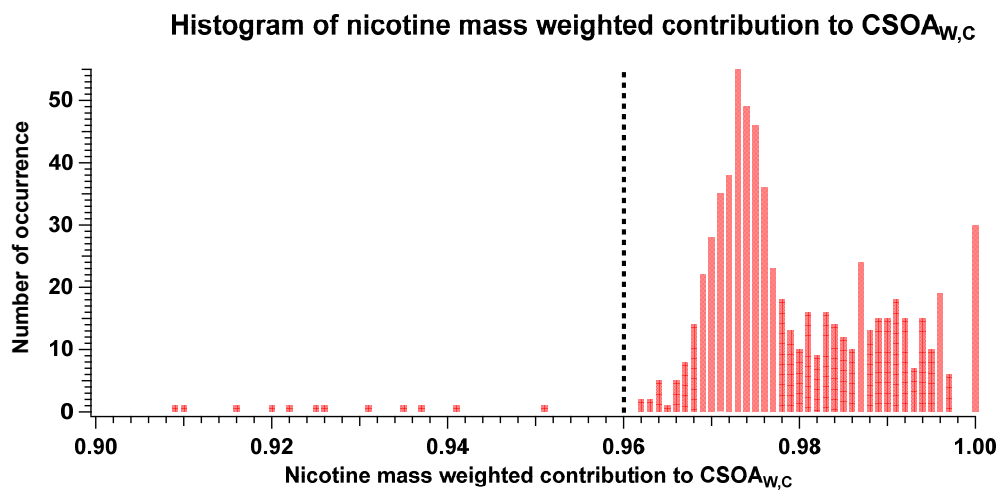
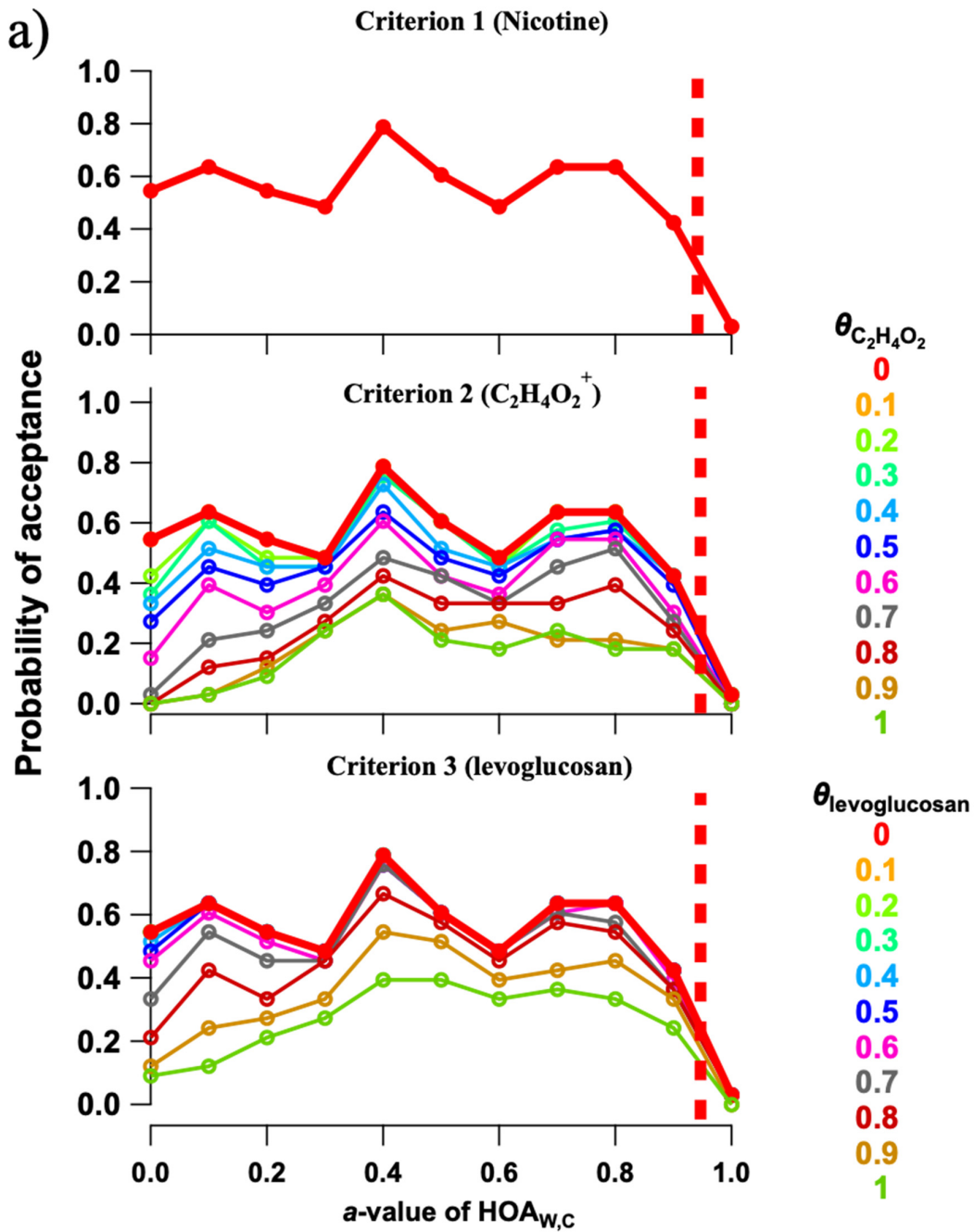
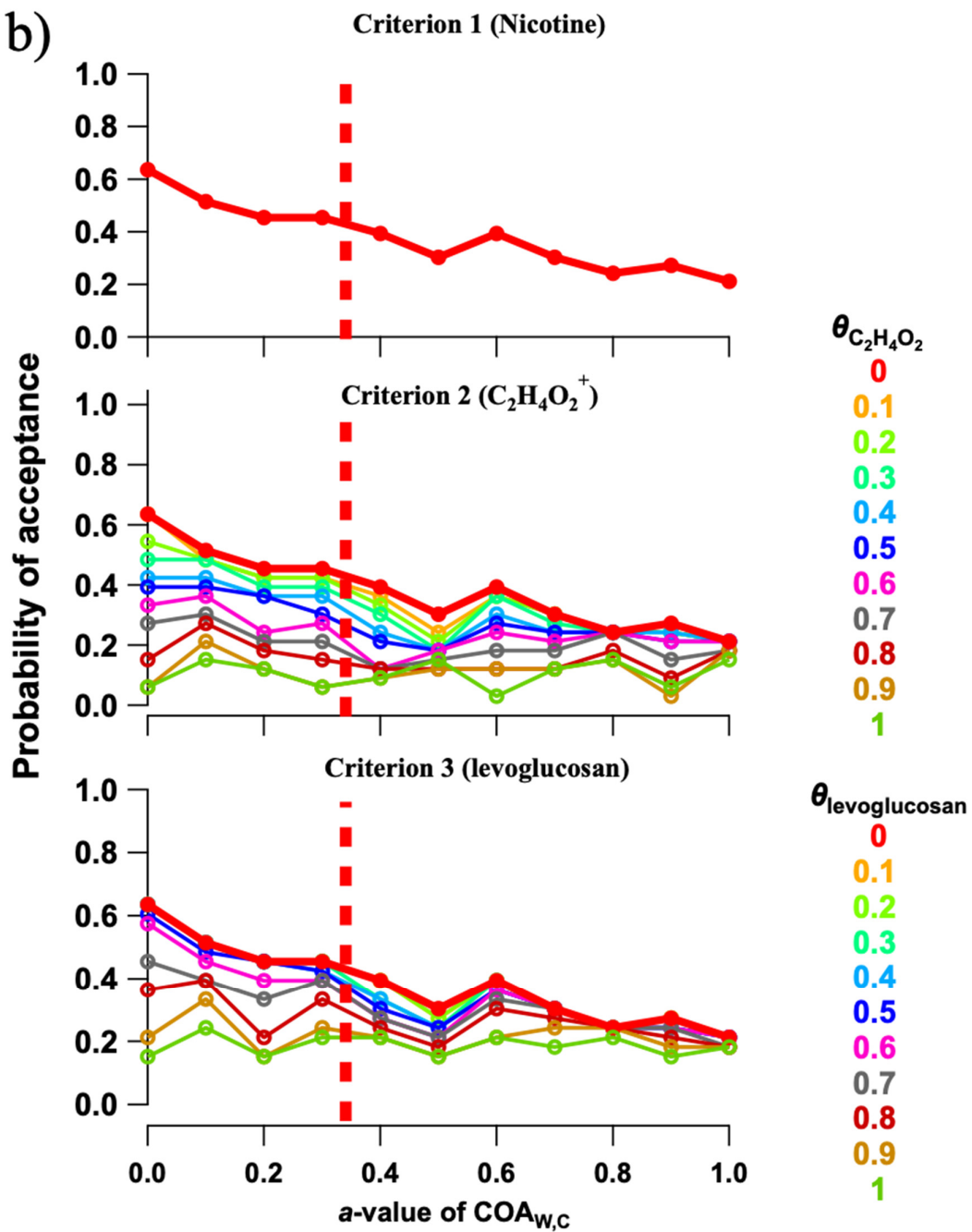
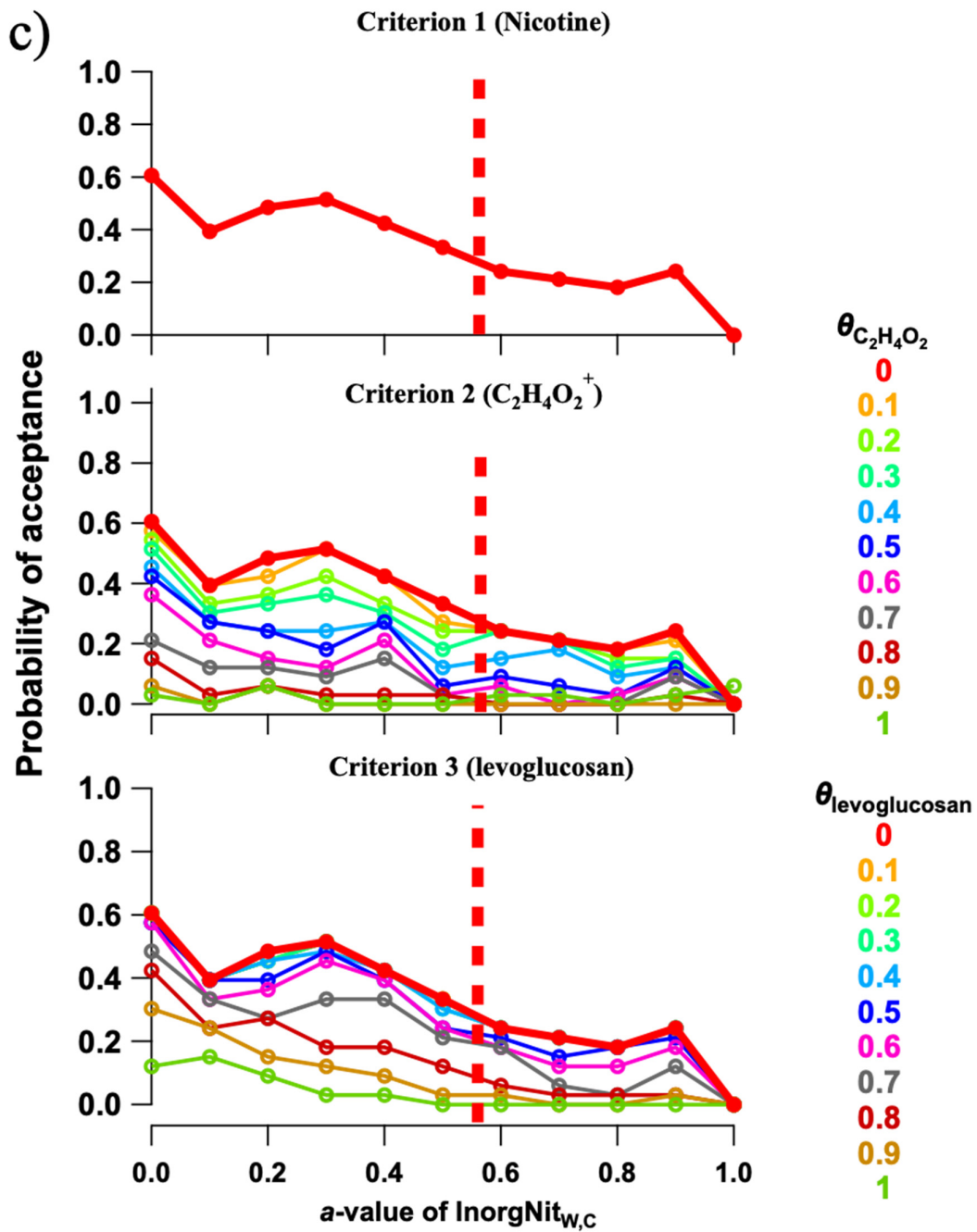


Figure S26. Criteria to select a value range for CSOA_{w,c} factor in Zurich winter dataset. Distribution of mass weighted fraction of nicotine in CSOA_{w,c} for 726 runs, with 396 runs with a value of 0 and 33 runs for each a value from 0.1 to 1. The mass weighted fraction of nicotine apportioned to CSOA_{w,c} in most runs are higher in 0.96.



b)





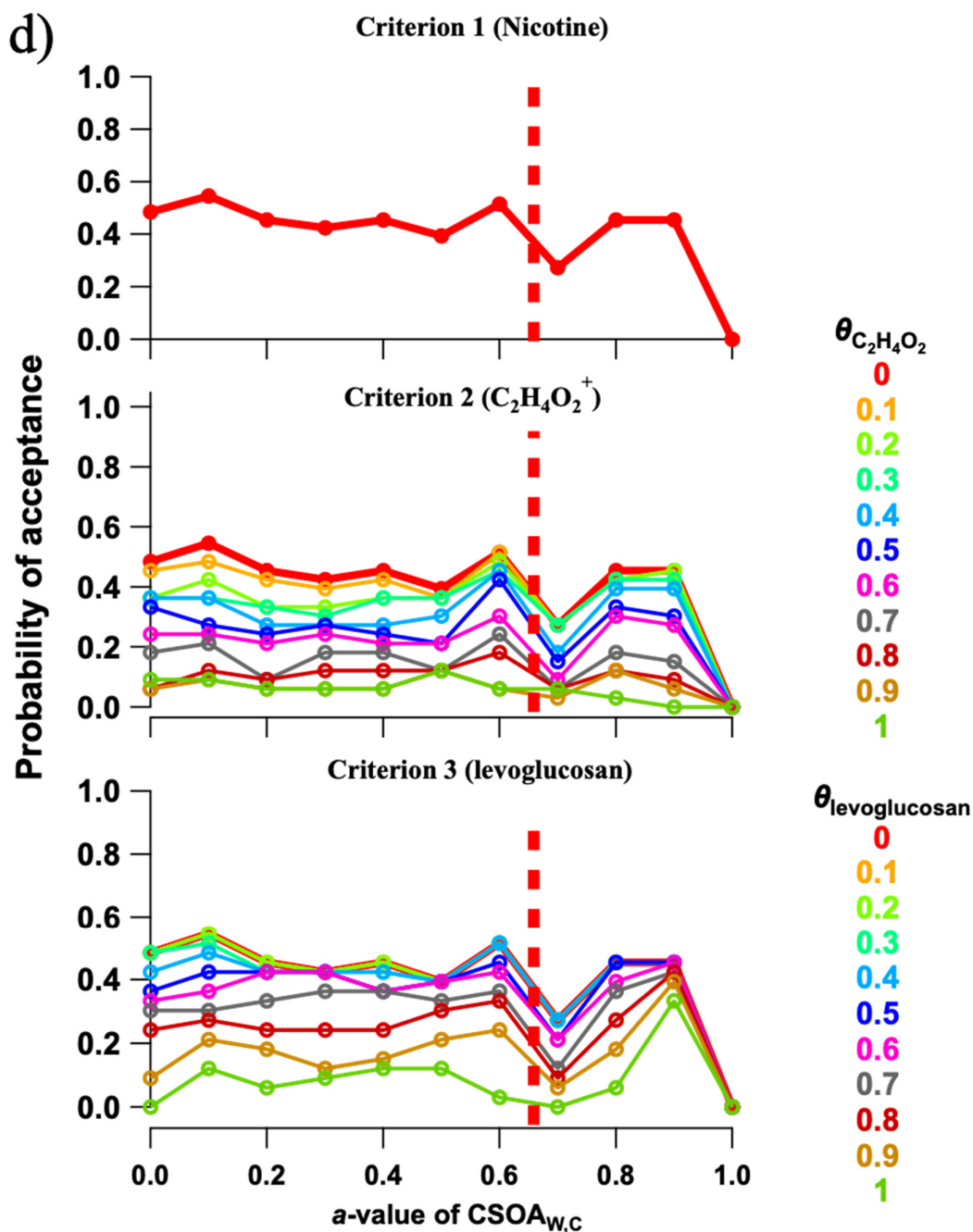


Figure S27. Acceptance probability (i.e., all criteria satisfied simultaneously) calculated from all runs in multi-2D scans as a function of a value of a) $HOA_{w,C}$, b) $COA_{w,C}$, c) $InorgNit_{w,C}$ and d) $CSOA_{w,C}$. To maintain consistency with $a=0.1$ to $a=1.0$, the $a=0$ point considers only runs in which the factor in question is being scanned against a single other factor, discarding runs for which the factor in question is fixed at $a=0$ while two other factors are scanned. Within each sub-figure, the response to different criteria thresholds are shown. Final selected values for criteria thresholds are displayed as a thicker line, while vertical dashed lines denote the final selected upper limit for a -value randomisation in the subsequent bootstrap analysis. Note that due to the requirement that all criteria be satisfied

simultaneously, the thicker lines (and only the thicker lines) are identical across all panels in a sub-figure. Acceptance requires that a run fulfil all criteria simultaneously.

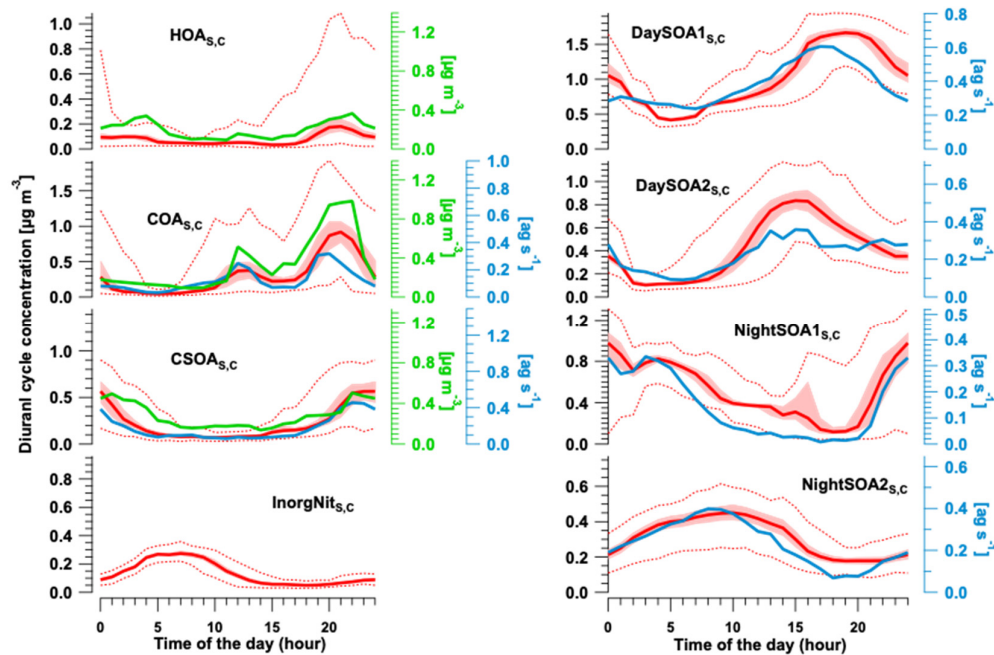


Figure S28. Diurnal cycle of median accepted 764 runs in Zurich Summer dataset, represented in red lines, shaded area indicates the interquartile range, dashed lines are the maximum and minimum value of diurnal cycle calculation.

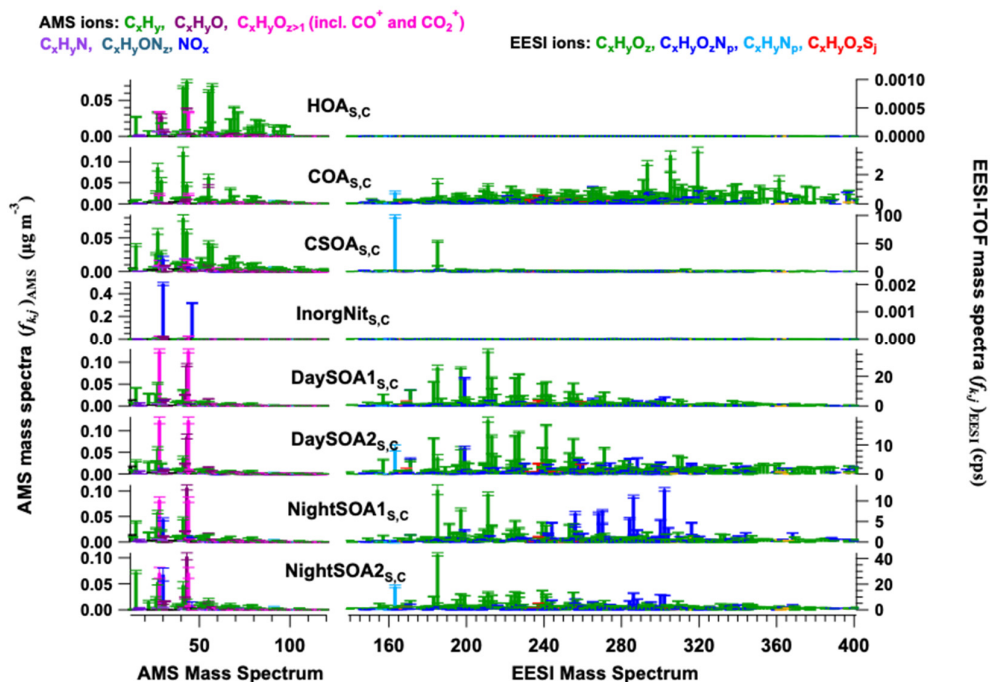


Figure S29. Average factor profiles of 764 accepted bootstrap runs in Zurich Summer dataset, coloured by different ion families, with error bars of mean \pm standard deviation. Note, both AMS and EESI-TOF factor profiles are normalised, according to Eq. (9).

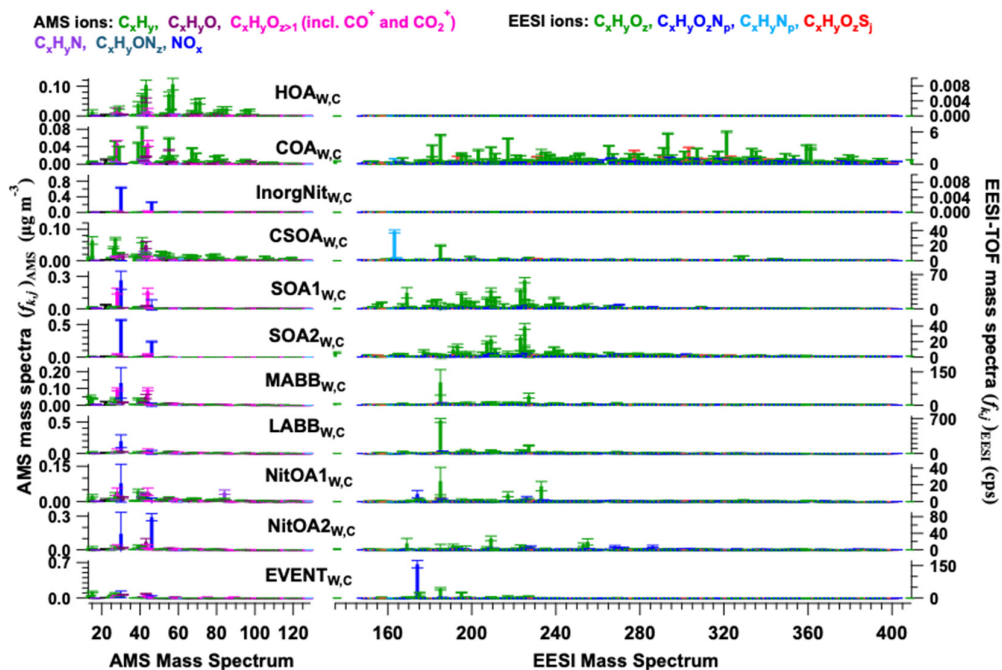


Figure S30. Average factor profiles of 308 accepted bootstrap runs in Zurich winter dataset, coloured by different ion families, with error bars of mean \pm standard deviation. Note, both AMS and EESI-TOF factor profiles are normalised, according to Eq. (9).

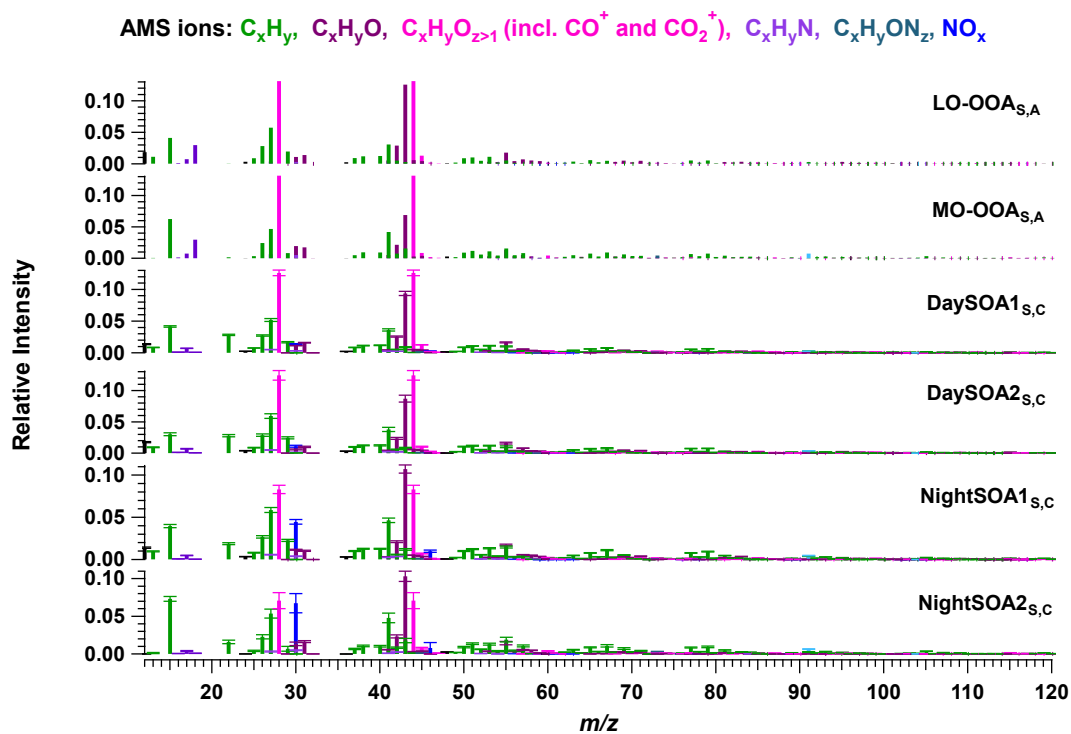
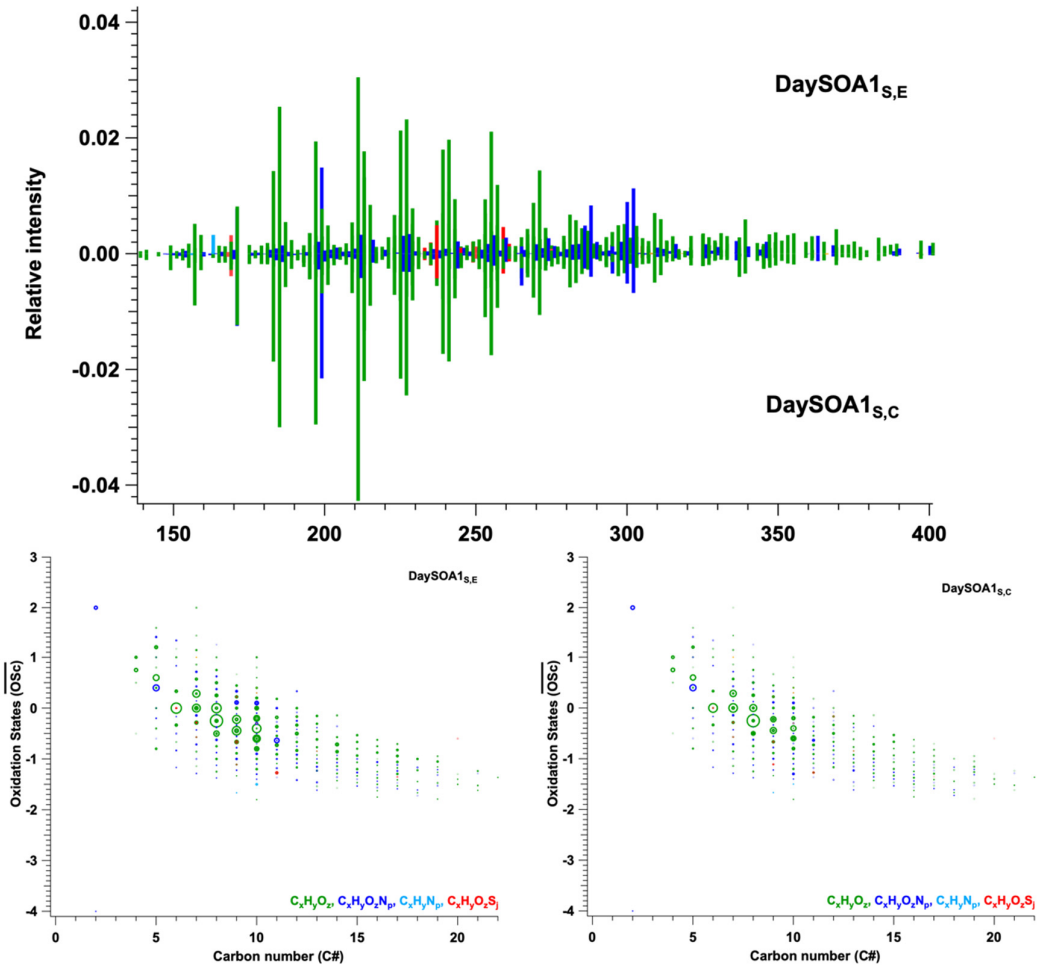
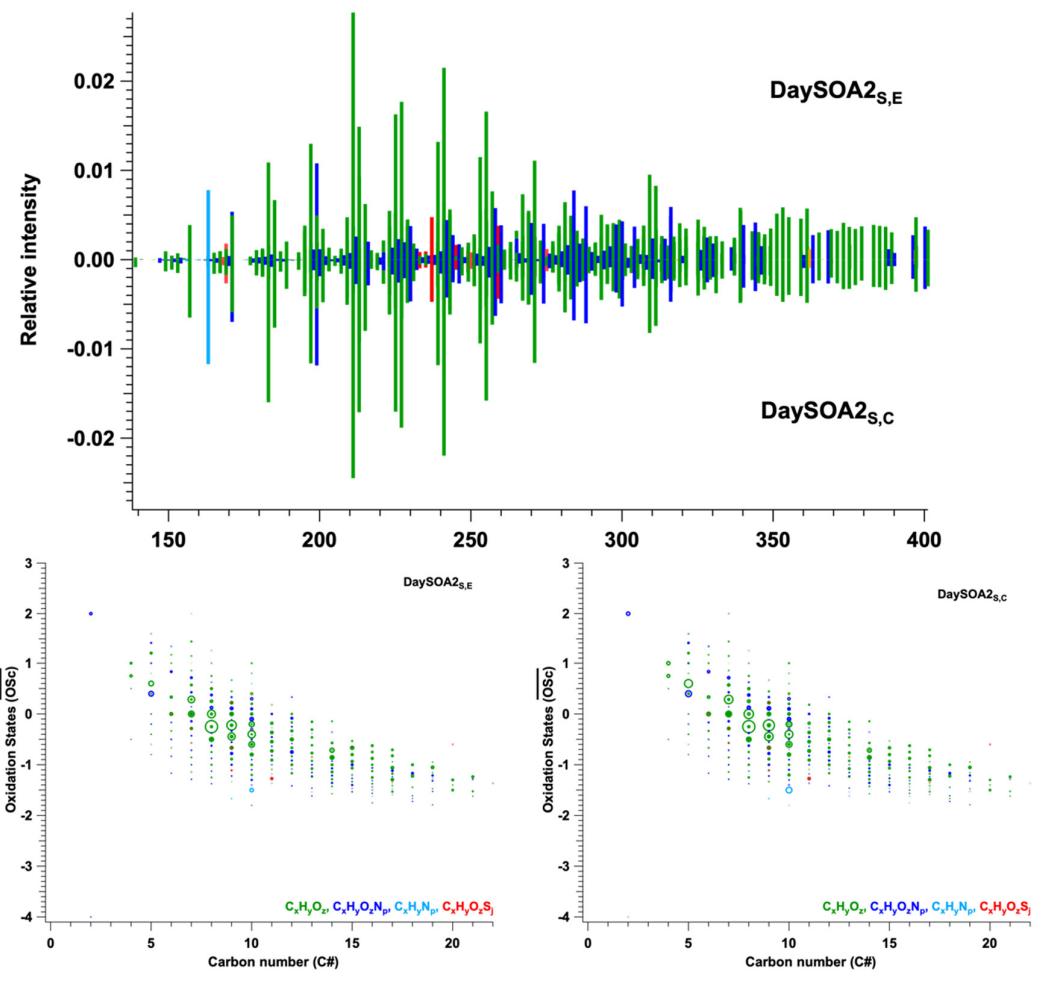


Figure S31. Factor profiles of LO- $OOA_{S,A}$ and MO- $OOA_{S,A}$ from AMS-only PMF analysis and four SOAs (DaySOA1 $_{S,A}$, DaySOA2 $_{S,A}$, NightSOA1 $_{S,A}$ and NightSOA2 $_{S,A}$) resolved from combined PMF analysis for summer.

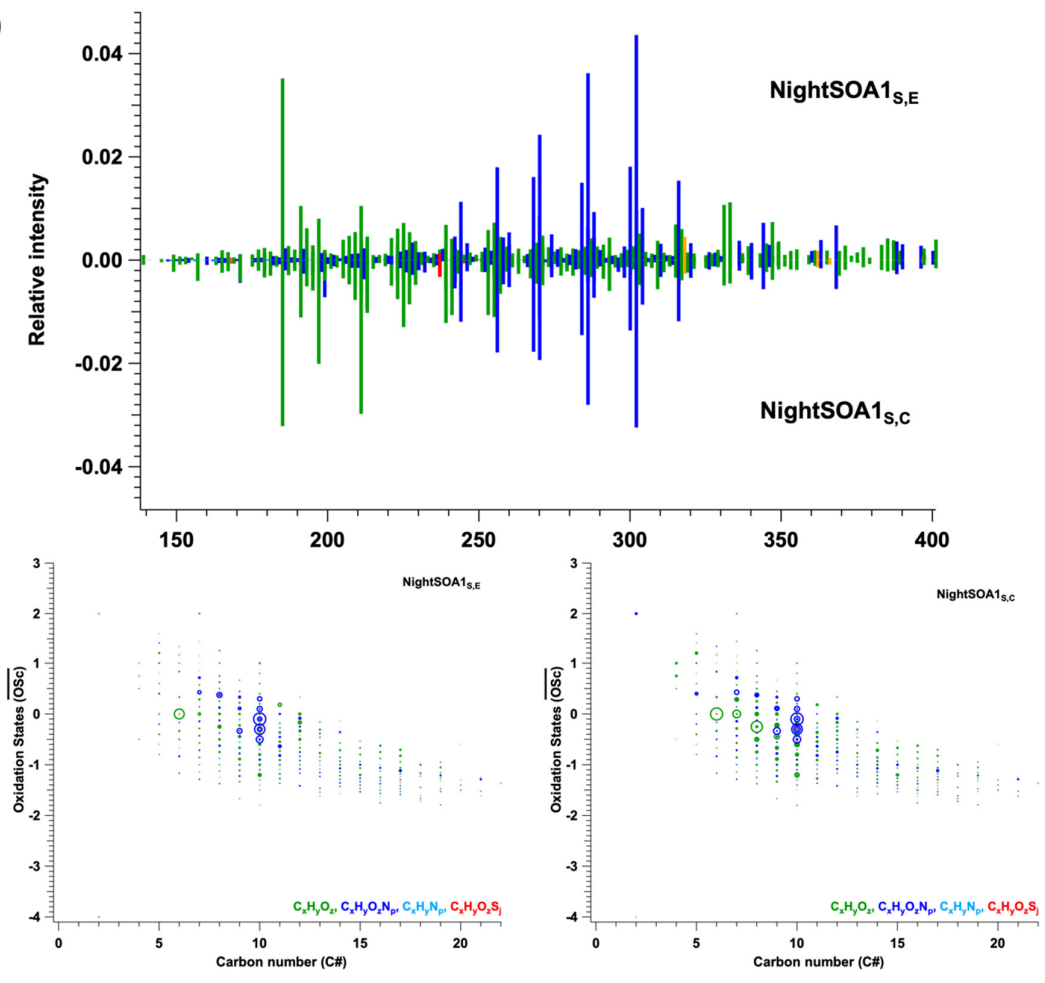
a)



b)



c)



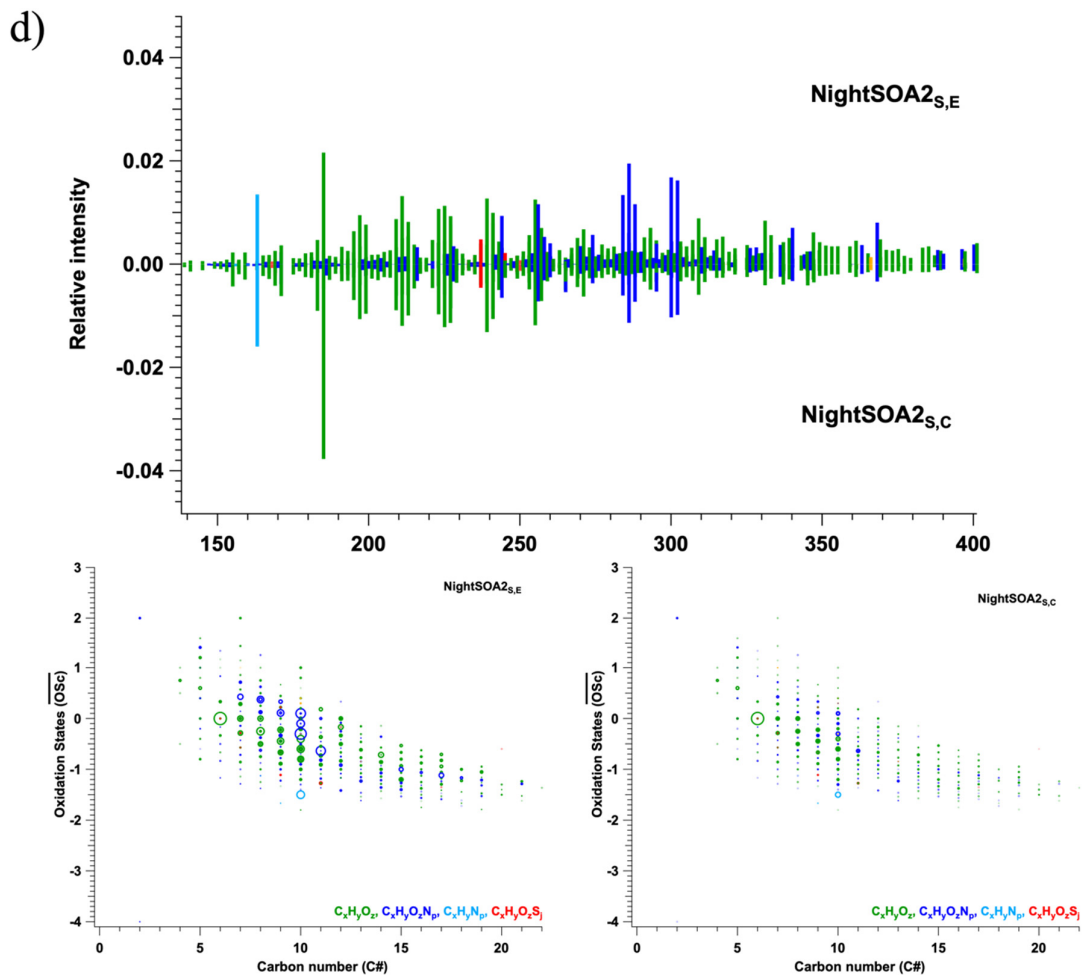
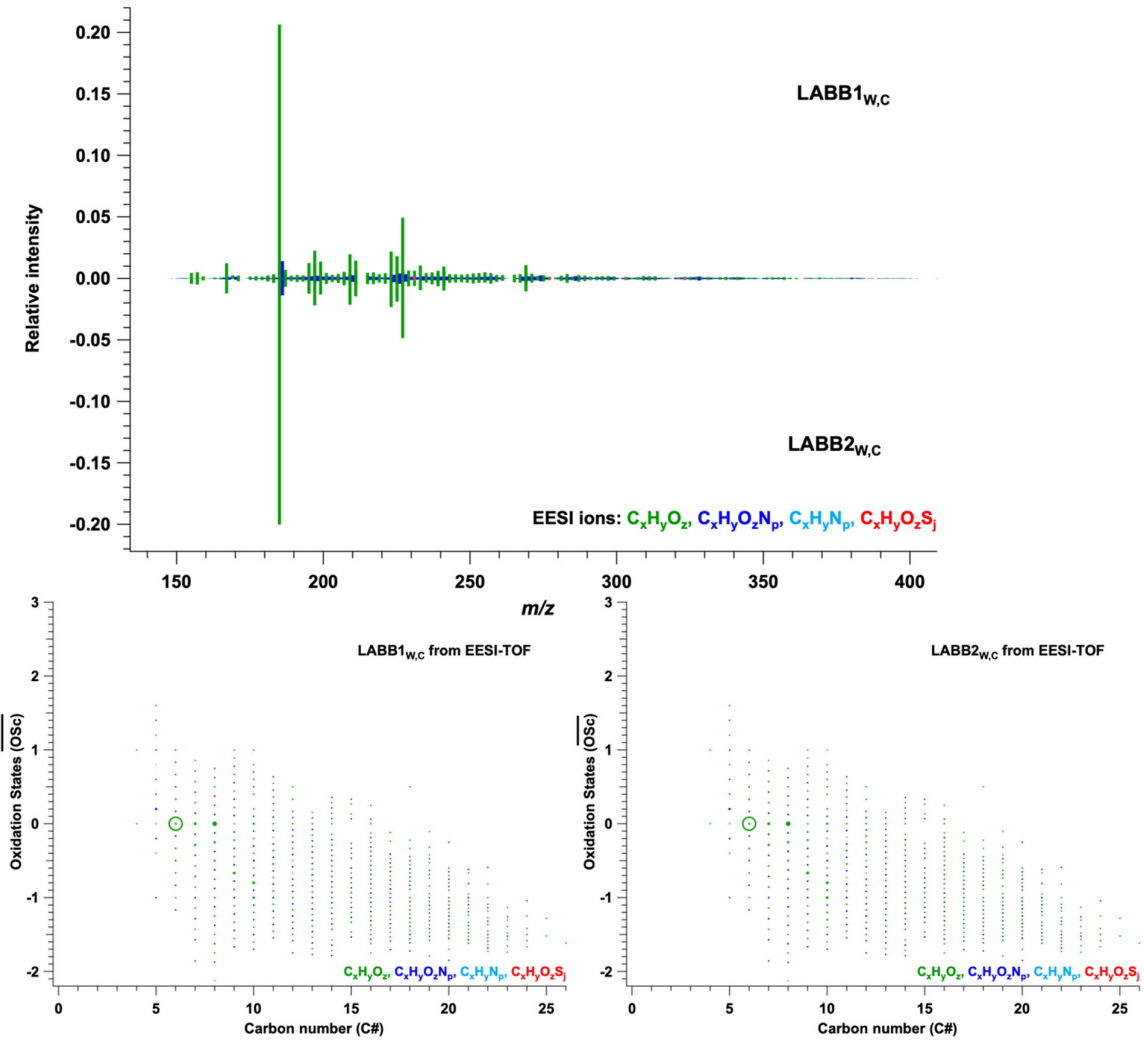


Figure S32. Comparison of four summer SOA factors (DaySOA1_{S,E}, DaySOA2_{S,E}, NightSOA1_{S,E} and NightSOA2_{S,E}) resolved from EESI-TOF-only PMF analysis to the corresponding factors (DaySOA1_{S,C}, DaySOA2_{S,C}, NightSOA1_{S,C} and NightSOA2_{S,C}) resolved from the combined PMF analysis, shown in a), b), c) and d), respectively. Each subfigure contains the direct comparison of corresponding factors, and modified Kroll diagram sized by the ion intensities of the corresponding factor.

a)



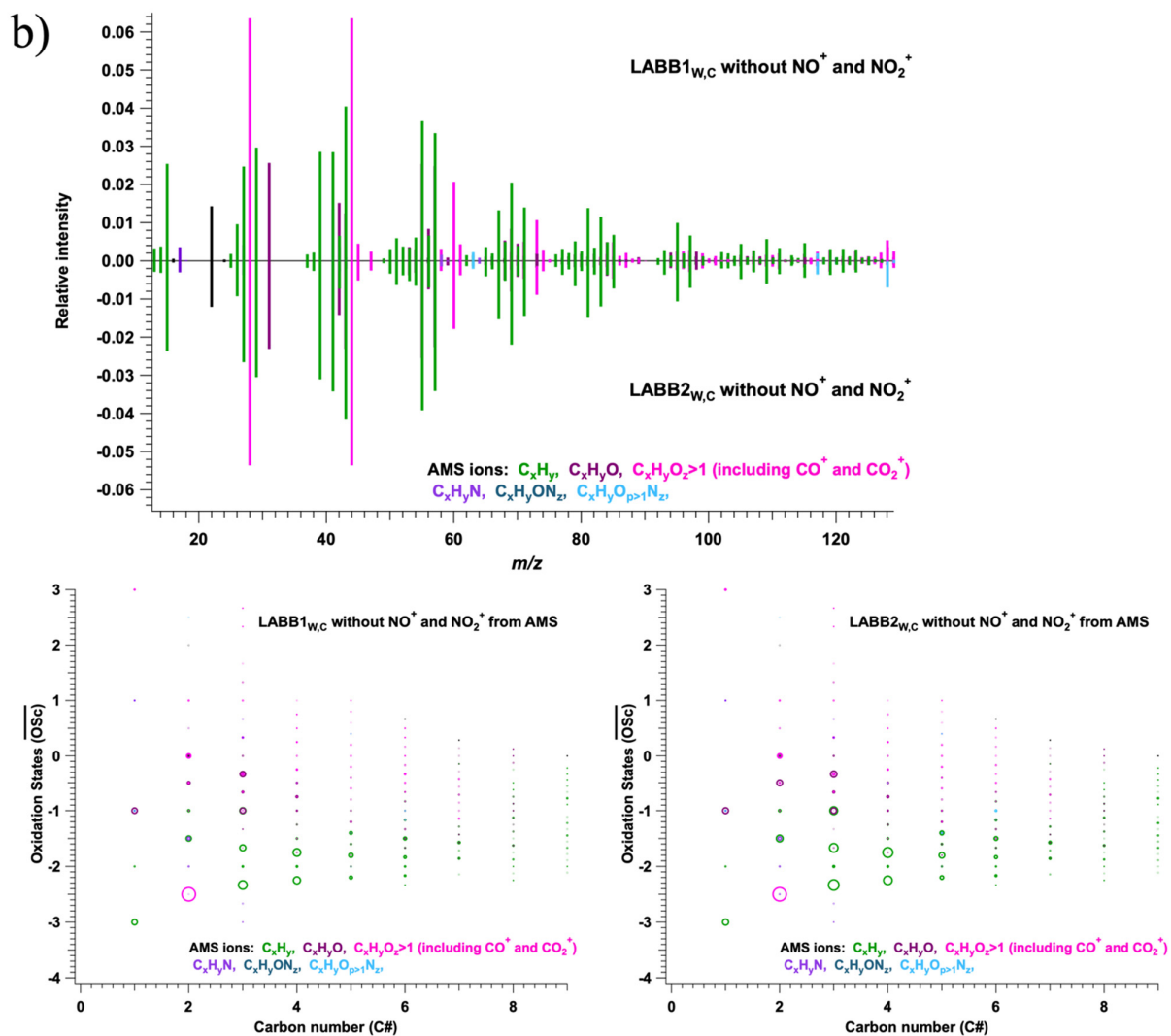


Figure S33. Comparison of two LABB_{W,C} factors resolved from combined dataset in Zurich winter. Direct EESI part mass spectra comparison and modified Kroll diagram sized by the ion intensities are shown in a) and direct AMS part mass spectra comparison and modified Kroll diagram sized by the ion intensities without NO⁺ and NO₂⁺ are shown in b).

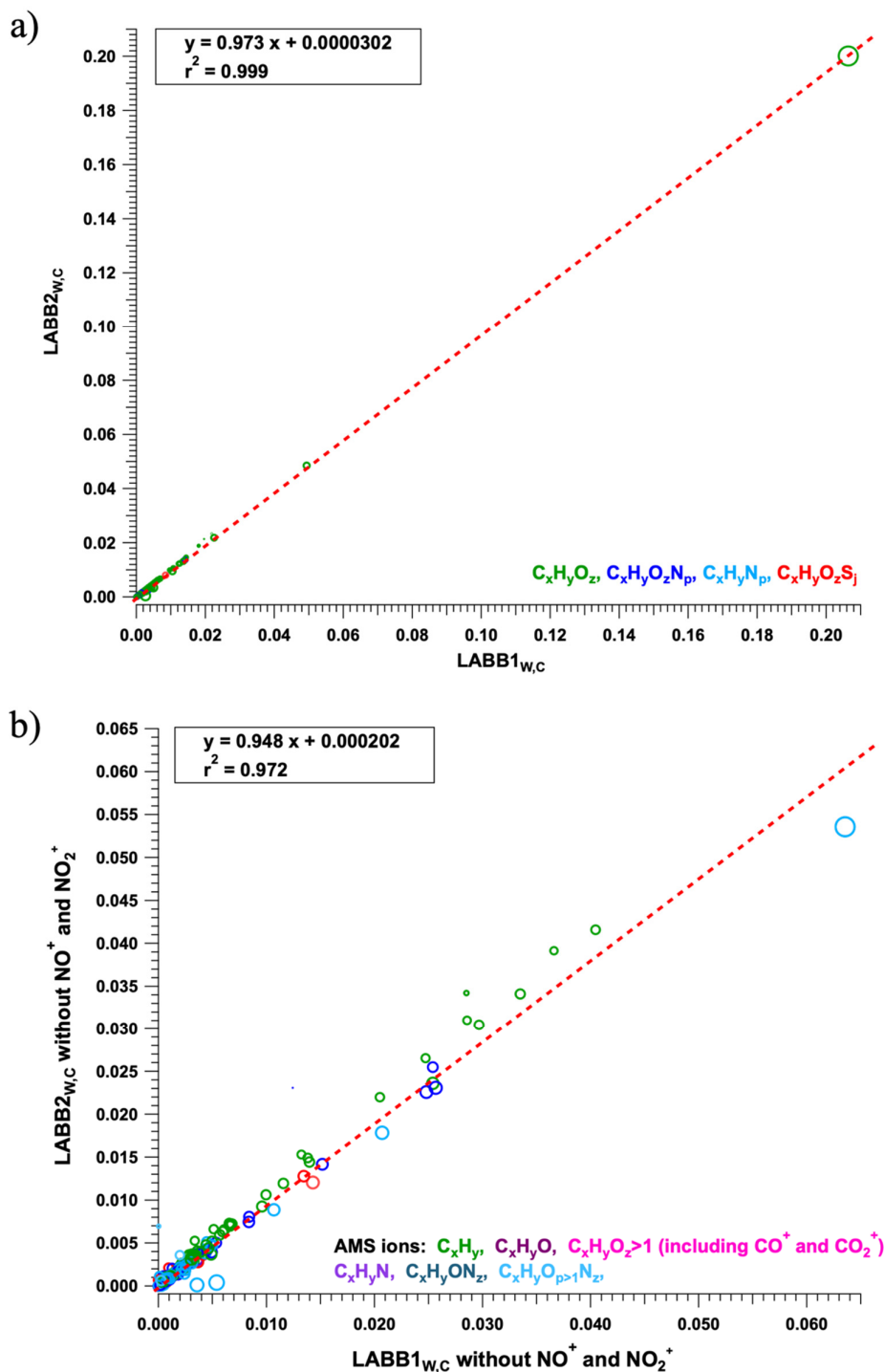


Figure S34. Comparison of two $LABB_{w,c}$ factors resolved from the combined dataset in Zurich winter. Scatter plot of AMS ions without NO^+ and NO_2^+ is shown in a), and scatter plot of EESI ions is shown in b). In both figures, correlation of ion intensity of $LABB1_{w,c}$ and $LABB2_{w,c}$ is higher than 0.97 with slope close to 1.

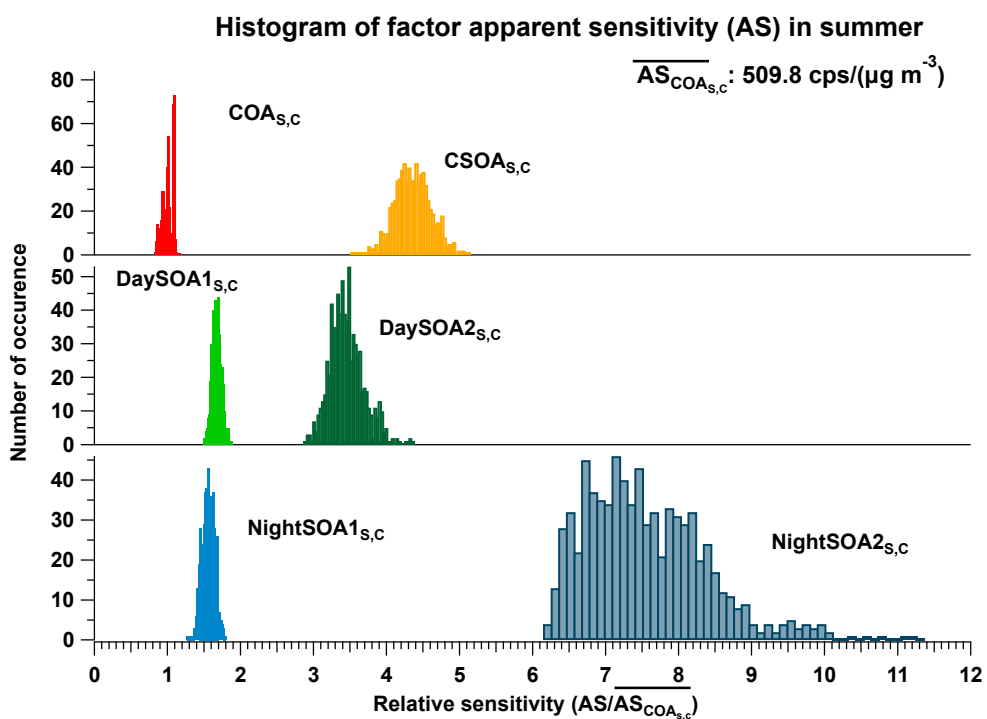


Figure S35. Histogram of factor EESI-TOF relative sensitivity to two primary sources and four secondary sources normalised by EESI-TOF sensitivity to $COA_{s,c}$ in Zurich summer campaign. Relative sensitivity is calculated as apparent sensitivity (AS_k) to a factor over mean apparent sensitivity to COA.

Histogram of factor apparent sensitivity (AS) in winter

$$\overline{AS}_{COA_{w,c}}: 1104.2 \text{ cps}/(\mu\text{g m}^{-3})$$

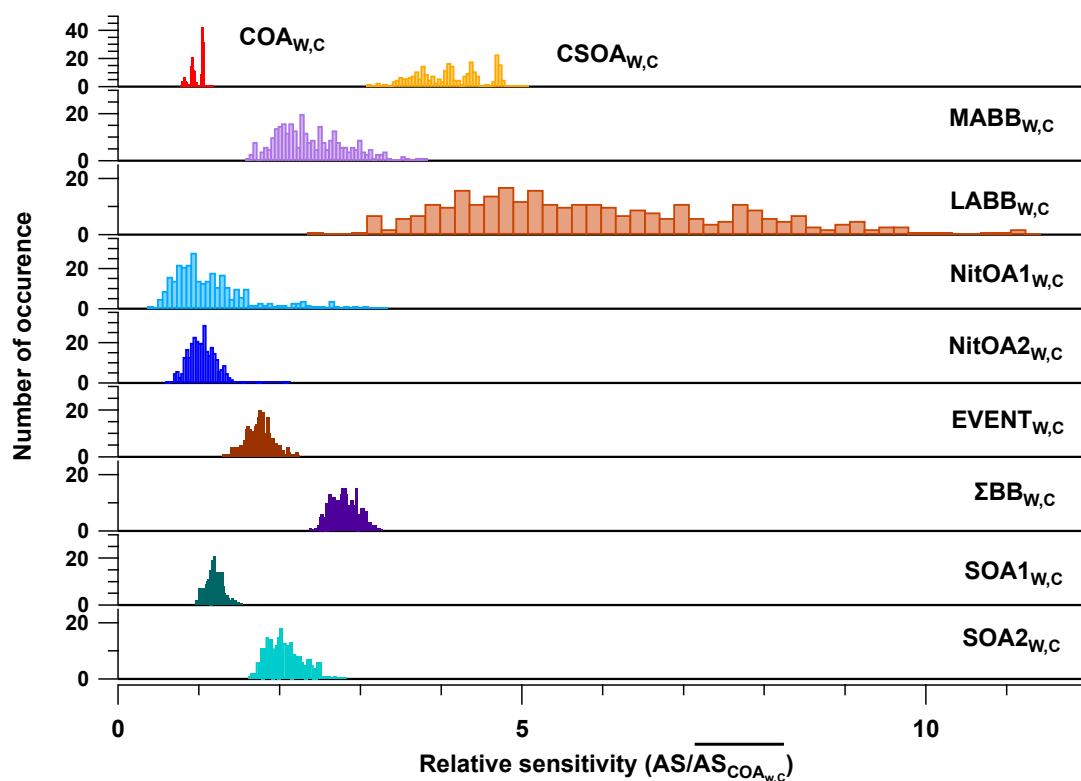


Figure S36. Histogram of factor relative sensitivity to two primary sources, two aged-biomass burning factors, two nitrogen-related sources, one event-specific factor, two secondary sources, and the sum of biomass burning related factors. Relative sensitivity is calculated as the apparent sensitivity (AS_k) to a factor over the mean apparent sensitivity to COA_{w,c}.

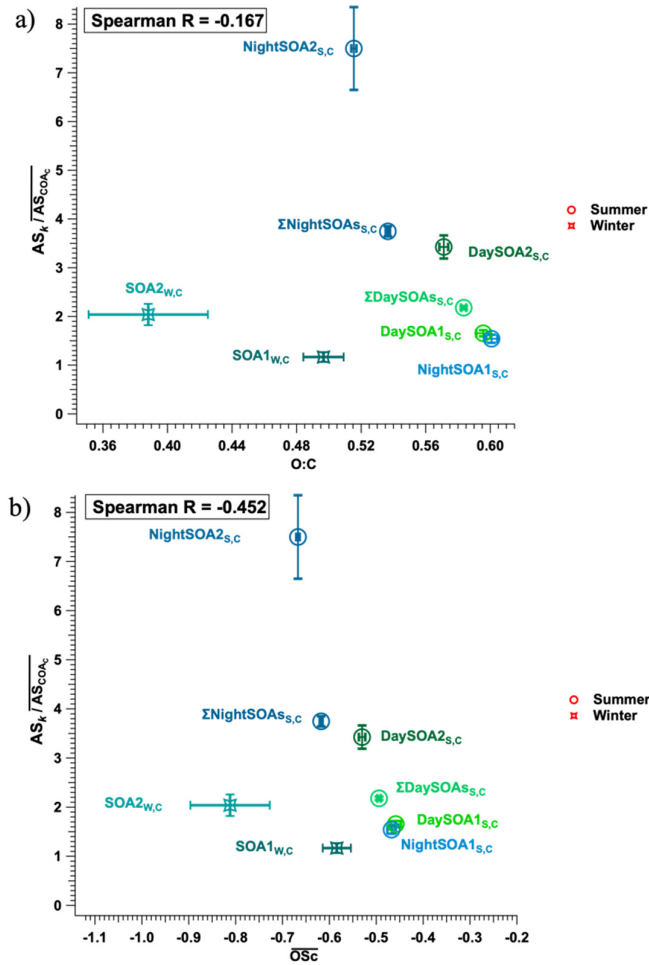


Figure S37. AS_k / AS_{COAc} of SOA factors retrieved from the summer and winter datasets as a function of the a) O:C ratio and b) OSc. Error bars denote standard deviation across all accepted runs. Spearman correlation for a) and b) is -0.167 and -0.452, as indicated in the top-left corner, respectively.

Table S1. Summary of relevant quantities to estimate $frac_{ON,k}$ and corresponding $\sum_j(f_{k,j})_{AMS,k}$, with different R_{ON} for each unconstrained factor from combined PMF analysis for summer and winter. Note that the HOA, COA, and CSOA in both factors are constrained to have zero contribution from NO^+ and NO_2^+ .

Summer									
NH ₄ NO ₃ reference:			$f_{NO^+} = 0.487,$			$f_{NO_2^+} = 0.318,$			$R_{cal} = 0.688$
			$R_{ON} = 0.08$		$R_{ON} = 0.14$		$R_{ON} = 0.20$		
Factor	f_{NO^+}	$f_{NO_2^+}$	$frac_{ON}$	$\frac{\sum_j(f_{k,j})_{AMS,OA}}{\sum_j(f_{k,j})_{AMS,all}}$	$frac_{ON}$	$\frac{\sum_j(f_{k,j})_{AMS,OA}}{\sum_j(f_{k,j})_{AMS,all}}$	$frac_{ON}$	$\frac{\sum_j(f_{k,j})_{AMS,OA}}{\sum_j(f_{k,j})_{AMS,all}}$	
HOA _{s,c}	0	0	0	1	0	1	0	1	
COA _{s,c}	0	0	0	1	0	1	0	1	
InorgNits _{s,c} ^{1*}	0.486	0.318	0.0358	0.225	0.0420	0.230	0.0496	0.236	
CSOA _{s,c}	0	0	0	1	0	0.995	0	1	
DaySOA1 _{s,c}	0.0137	0.00262	0.742	0.996	0.869	0.998	1.000	1.000	
DaySOA2 _{s,c}	0.0111	0.00103	0.969	1.000	1.000	1.000	1.000	1.000	
NightSOA1 _{s,c}	0.0445	0.00979	0.682	0.983	0.798	0.989	0.944	0.997	
NightSOA2 _{s,c}	0.0679	0.00824	0.897	0.993	1	1	1	1	
Winter									
NH ₄ NO ₃ reference:			$f_{NO^+} = 0.630,$			$f_{NO_2^+} = 0.248,$			$R_{cal} = 0.394$
			$R_{ON} = 0.08$		$R_{ON} = 0.14$		$R_{ON} = 0.20$		
Factor	f_{NO^+}	$f_{NO_2^+}$	$frac_{ON}$	$\frac{\sum_j(f_{k,j})_{AMS,OA}}{\sum_j(f_{k,j})_{AMS,all}}$	$frac_{ON}$	$\frac{\sum_j(f_{k,j})_{AMS,OA}}{\sum_j(f_{k,j})_{AMS,all}}$	$frac_{ON}$	$\frac{\sum_j(f_{k,j})_{AMS,OA}}{\sum_j(f_{k,j})_{AMS,all}}$	
HOA _{w,c}	0	0	0	1	0	1	0	1	
COA _{w,c}	0	0	0	1	0	1	0	1	
InorgNit _{w,c} ^{1*}	0.636	0.263	0	0.101	0	0.101	0	0.101	
CSOA _{w,c}	0	0	0	1	0	1	0	1	
SOA1 _{w,c}	0.264	0.0347	0.799	0.940	1	1	1	1	
SOA2 _{w,c}	0.570	0.238	0 ^{2*}	0.192	0 ^{2*}	0.192	0 ^{2*}	0.192	
MABB _{w,c}	0.133	0.00185	1	1	1	1	1	1	
LABB _{w,c}	0.195	0.0176	0.958	0.991	1	1	1	1	
NitOA1 _{w,c}	0.0781	0.00260	1	1	1	1	1	1	
NitOA2 _{w,c}	0.143	0.293	0 ^{2*}	0.564	0 ^{2*}	0.564	0 ^{2*}	0.564	
EVENT _{w,c}	0.0736	0.0203	0.319	0.936	0.416	0.945	0.572	0.960	

Note 1*: The $frac_{ON}$ for InorgNit is not 0 due to the uncertainties in the constraint. $\frac{\sum_j(f_{k,j})_{AMS,OA}}{\sum_j(f_{k,j})_{AMS,all}}$ in this factor is not 0 due to the uncertainties in the constraint and the CO_2^+ resulted from NH_4NO_3 which is also included in the reference profiles (Pieber et al., 2016).

Note 2*: according to Eq. S3, the $frac_{ON}$ is negative, therefore, we regarded all signals from NO^+ and NO_2^+ as inorganics, and set $frac_{ON}$ to be 0.

Table S2. Summary of the median value of the ratio of standard deviation to mean factor concentration over accepted runs at each time point for summer and winter factors.

Factor	(Standard deviation / mean factor concentration) _{median}
HOA _{s,c}	7.4%
COA _{s,c}	4.5%
InorgNits _{s,c}	5.2%
CSOA _{s,c}	3.2%
DaySOA1 _{s,c}	5.4%
DaySOA2 _{s,c}	1.4%
NightSOA1 _{s,c}	0.6%
NightSOA2 _{s,c}	4.3%
HOA _{w,c}	12.8%
COA _{w,c}	14.5%
InorgNit _{w,c}	26.5%
CSOA _{w,c}	13.7%
SOA1 _{w,c}	12.2%
SOA2 _{w,c}	18.5%
MABB _{w,c}	24.1%
LABB _{w,c}	18.1%
NitOA1 _{w,c}	24.3%
NitOA2 _{w,c}	35.1%
EVENT _{w,c}	3.5%

Table S3. Summary of apparent sensitivities for factors retrieved from combined PMF analysis for summer and winter.

Factor	Factor apparent sensitivity (AS_k) (cps / ($\mu\text{g m}^{-3}$))
COA _{s,c}	$5.09 (\pm 0.45) \times 10^2$
CSOA _{s,c}	$22.10 (\pm 1.27) \times 10^2$
DaySOA1 _{s,c}	$8.45 (\pm 0.32) \times 10^2$
DaySOA2 _{s,c}	$17.47 (\pm 1.20) \times 10^2$
NightSOA1 _{s,c}	$7.86 (\pm 0.43) \times 10^2$
NightSOA2 _{s,c}	$38.23 (\pm 4.33) \times 10^2$
Bulk OA_{s,c}	$12.54 (\pm 0.10) \times 10^2$
COA _{w,c}	$1.10 (\pm 0.13) \times 10^3$
CSOA _{w,c}	$4.56 (\pm 0.54) \times 10^3$
SOA1 _{w,c}	$1.29 (\pm 0.11) \times 10^3$
SOA2 _{w,c}	$2.25 (\pm 0.24) \times 10^3$
MABB _{w,c}	$2.62 (\pm 0.49) \times 10^3$
LABB _{w,c}	$6.51 (\pm 2.01) \times 10^3$
NitOA1 _{w,c}	$1.43 (\pm 0.57) \times 10^3$
NitOA2 _{w,c}	$1.12 (\pm 0.21) \times 10^3$
EVENT _{w,c}	$1.93 (\pm 0.18) \times 10^3$
Bulk OA_{w,c}	$2.27 (\pm 0.07) \times 10^3$

Reference

- Alfarra, M. R., Prevot, A. S. H., Szidat, S., Sandradewi, J., Weimer, S., Lanz, V. A., Schreiber, D., Mohr, M., and Baltensperger, U.: Identification of the mass spectral signature of organic aerosols from wood burning emissions, *Environ. Sci. Technol.*, 41, 5770-5777, <https://doi.org/10.1021/es062289b>, 2007.
- Boyd, C. M., Sanchez, J., Xu, L., Eugene, A. J., Nah, T., Tuet, W. Y., Guzman, M. I., and Ng, N. L.: Secondary organic aerosol formation from the β -pinene+NO₃ system: effect of humidity and peroxy radical fate, *Atmos. Chem. Phys.*, 15, 7497-7522, <https://doi.org/10.5194/acp-15-7497-2015>, 2015.
- Bruns, E. A., Perraud, V., Zelenyuk, A., Ezell, M. J., Johnson, S. N., Yu, Y., Imre, D., Finlayson-Pitts, B. J., and Alexander, M. L.: Comparison of FTIR and Particle Mass Spectrometry for the Measurement of Particulate Organic Nitrates, *Environ. Sci. Technol.*, 44, 1056-1061, <https://doi.org/10.1021/es9029864>, 2010.
- Cubison, M. J., and Jimenez, J. L.: Statistical precision of the intensities retrieved from constrained fitting of overlapping peaks in high-resolution mass spectra, *Atmos. Meas. Tech.*, 8, 2333-2345, <https://doi.org/10.5194/amt-8-2333-2015>, 2015.
- Fry, J. L., Kiendler-Scharr, A., Rollins, A. W., Wooldridge, P. J., Brown, S. S., Fuchs, H., Dubé, W., Mensah, A., dal Maso, M., Tillmann, R., Dorn, H. P., Brauers, T., and Cohen, R. C.: Organic nitrate and secondary organic aerosol yield from NO₃ oxidation of β -pinene evaluated using a gas-phase kinetics/aerosol partitioning model, *Atmos. Chem. Phys.*, 9, 1431-1449, <https://doi.org/10.5194/acp-9-1431-2009>, 2009.
- Fry, J. L., Kiendler-Scharr, A., Rollins, A. W., Brauers, T., Brown, S. S., Dorn, H. P., Dubé, W. P., Fuchs, H., Mensah, A., Rohrer, F., Tillmann, R., Wahner, A., Wooldridge, P. J., and Cohen, R. C.: SOA from limonene: role of NO₃ in its generation and degradation, *Atmos. Chem. Phys.*, 11, 3879-3894, <https://doi.org/10.5194/acp-11-3879-2011>, 2011.
- Kiendler-Scharr, A., Mensah, A. A., Friese, E., Topping, D., Nemitz, E., Prevot, A. S. H., Aijala, M., Allan, J., Canonaco, F., Canagaratna, M., Carbone, S., Crippa, M., Dall'Osto, M., Day, D. A., De Carlo, P., Di Marco, C. F., Elbern, H., Eriksson, A., Freney, E., Hao, L., Herrmann, H., Hildebrandt, L., Hillamo, R., Jimenez, J. L., Laaksonen, A., McFiggans, G., Mohr, C., O'Dowd, C., Otjes, R., Ovadnevaite, J., Pandis, S. N., Poulain, L., Schlag, P., Sellegri, K., Swietlicki, E., Tiitta, P., Vermeulen, A., Wahner, A., Worsnop, D., and Wu, H. C.: Ubiquity of organic nitrates from nighttime chemistry in the European submicron aerosol, *Geophys. Res. Lett.*, 43, 7735-7744, <https://doi.org/10.1002/2016gl069239>, 2016.
- Lopez-Hilfiker, F. D., Pospisilova, V., Huang, W., Kalberer, M., Mohr, C., Stefenelli, G., Thornton, J. A., Baltensperger, U., Prevot, A. S. H., and Slowik, J. G.: An extractive electrospray ionization time-of-flight mass spectrometer (EESI-TOF) for online measurement of atmospheric aerosol particles, *Atmos. Meas. Tech.*, 12, 4867-4886, <https://doi.org/10.5194/amt-12-4867-2019>, 2019.
- Mohr, C., DeCarlo, P. F., Heringa, M. F., Chirico, R., Slowik, J. G., Richter, R., Reche, C., Alastuey, A., Querol, X., Seco, R., Penuelas, J., Jimenez, J. L., Crippa, M., Zimmermann, R., Baltensperger, U., and Prevot, A. S. H.: Identification and quantification of organic aerosol from cooking and other sources in Barcelona using aerosol mass spectrometer data, *Atmos. Chem. Phys.*, 12, 1649-1665, <https://doi.org/10.5194/acp-12-1649-2012>, 2012.
- Pieber, S. M., El Haddad, I., Slowik, J. G., Canagaratna, M. R., Jayne, J. T., Platt, S. M., Bozzetti, C., Daellenbach, K. R., Frohlich, R., Vlachou, A., Klein, F., Dommen, J., Miljevic, B., Jimenez, J. L., Worsnop, D. R., Baltensperger, U., and Prevot, A. S. H.: Inorganic Salt Interference on CO₂ in Aerodyne AMS and ACSM Organic Aerosol Composition Studies, *Environ. Sci. Technol.*, 50, 10494-10503, <https://doi.org/10.1021/acs.est.6b01035>, 2016.
- Qi, L., Chen, M. D., Stefenelli, G., Pospisilova, V., Tong, Y. D., Bertrand, A., Hueglin, C., Ge, X. L., Baltensperger, U., Prevot, A. S. H., and Slowik, J. G.: Organic aerosol source apportionment in Zurich using an extractive electrospray ionization time-of-flight mass spectrometer (EESI-TOF-MS) - Part 2: Biomass burning influences in winter, *Atmos. Chem. Phys.*, 19, 8037-8062, <https://doi.org/10.5194/acp-19-8037-2019>, 2019.
- Rollins, A. W., Kiendler-Scharr, A., Fry, J. L., Brauers, T., Brown, S. S., Dorn, H. P., Dubé, W. P., Fuchs, H., Mensah, A., Mentel, T. F., Rohrer, F., Tillmann, R., Wegener, R., Wooldridge, P. J., and

Cohen, R. C.: Isoprene oxidation by nitrate radical: alkyl nitrate and secondary organic aerosol yields, *Atmos. Chem. Phys.*, 9, 6685-6703, <https://doi.org/10.5194/acp-9-6685-2009>, 2009.

Stefenelli, G., Pospisilova, V., Lopez-Hilfiker, F. D., Daellenbach, K. R., Hüglin, C., Tong, Y., Baltensperger, U., Prévôt, A. S. H., and Slowik, J. G.: Organic aerosol source apportionment in Zurich using an extractive electrospray ionization time-of-flight mass spectrometer (EESI-TOF-MS) – Part 1: Biogenic influences and day–night chemistry in summer, *Atmos. Chem. Phys.*, 19, 14825-14848, <https://doi.org/10.5194/acp-19-14825-2019>, 2019.

Tong, Y., Pospisilova, V., Qi, L., Duan, J., Gu, Y., Kumar, V., Rai, P., Stefenelli, G., Wang, L., Wang, Y., Zhong, H., Baltensperger, U., Cao, J., Huang, R. J., Prévôt, A. S. H., and Slowik, J. G.: Quantification of solid fuel combustion and aqueous chemistry contributions to secondary organic aerosol during wintertime haze events in Beijing, *Atmos. Chem. Phys.*, 21, 9859-9886, <https://doi.org/10.5194/acp-21-9859-2021>, 2021.